Engineering
Library

OCT 13 '49

Journal of Research

of the

U.S. National Bureau of Standards

AUGUST 1949

VOLUME 43 NUMBER 2

UNIV. OF MICH.

PERIODICALS OF THE NATIONAL BUREAU OF STANDARDS

Journal of Research

The National Bureau of Standards is the principal agency of the Federal Government for fundamental research in physics, chemistry, and engineering. It has the custody of the national standards of physical measurement in terms of which all working standards in research laboratories and industry are calibrated, and carries on necessary research leading to improvement in such standards and methods of measurement. It also has a general responsibility for basic research in physics, chemistry, and engineering, and for development of improved methods for testing materials and equipment. It determines physical constants and properties of materials, tests and calibrates standard measuring apparatus and reference standards, and studies technical processes. The results of the Bureau's research and investigations are published in the JOURNAL OF RESEARCH.

Research Papers

Reprints of individual articles appearing in the JOURNAL OF RESEARCH. They are made available to serve the needs of research workers, technical groups, and others for the separate papers relating to the special subjects in which they are interested.

Technical News Bulletin

Contains short but complete summaries of research, development, and testing in progress at the Bureau, accounts of the Bureau's national and international activities, scientific and technical announcements of new plans and programs, and a list of publications by members of the staff. It is a prompt and reliable source of official information of value to those who desire to keep in touch with the general activities of the Bureau.

Basic Radio Propagation Predictions

The CRPL–D series, Basic Radio Propagation Predictions, is issued as a monthly publication for those concerned with radio communication in determining the best sky-wave frequencies over any path at any time of day for average conditions for the month of prediction, which is made 3 months in advance. Charts of extraordinary-wave critical frequency for the F2 layer, of maximum usable frequency for a transmission distance of 4,000 km, and of percentage of time occurrence for transmission by sporadic E in excess of 15 Mc, for a distance of 2,000 km, are included.

ANNUAL SUBSCRIPTION Send order, with remittance, to Superintendent of Documents U. S. Government Printing Office, Washington 25, D. C.	United States, Canada, Cuba, Mexico, Newfoundland, Republic of Panama	Other countries
JOURNAL OF RESEARCH of the National Bureau of Standards:		
12 monthly issues (2 volumes), paper covers	$4.50	$5.50
Bound volume (½ year, 1 volume), blue buckram	3.00	3.50
RESEARCH PAPERS	(*)	(*)
TECHNICAL NEWS BULLETIN, 12 monthly issues	1.00	1.25
BASIC RADIO PROPAGATION PREDICTIONS, 12 monthly issues	1.00	1.25

*The prices of the separate Research Papers appearing in this JOURNAL are given in the Contents. If 100 or more copies of any separate are ordered, a discount of 25 percent is allowed. Those who desire copies of separate Research Papers should send their orders and remittances without delay to the Superintendent of Documents, U. S. Government Printing Office, Washington 25, D. C. This will aid him to determine the number of copies to be printed for sale. Research Papers are not printed from electrotypes and usually no more reprints can be had when the first and only printing is exhausted.

The printing of this publication has been approved by the Director of the Bureau of the Budget, April 23, 1947.

U. S. DEPARTMENT OF COMMERCE
Charles Sawyer, Secretary
NATIONAL BUREAU OF STANDARDS
E. U. Condon, Director

AUGUST 1949
VOLUME • 43
NUMBER 2

JOURNAL OF RESEARCH

of the

NATIONAL BUREAU OF STANDARDS

Contents

RP		Page
2010.	Mass spectrum of pentaborane (B_5H_9). Vernon H. Dibeler, Fred L. Mohler, Laura Williamson, and Robert M. Reese. (Price 5 cents)	97
2011.	Effect of chromium plating on the endurance limit of steels used in aircraft. Hugh L. Logan. (Price 10 cents)	101
2012.	Heats of combustion and formation of cyclopropane. John W. Knowlton and Frederick D. Rossini. (Price 5 cents)	113
2013.	Influence of strain rate and temperature on the creep of cold-drawn ingot iron. William D. Jenkins and Thomas G. Digges. (Price 10 cents)	117
2014.	Differences between the International Temperature Scales of 1948 and 1927. Robert J. Corruccini. (Price 5 cents)	133
2015.	An instrument for measuring longitudinal spherical aberration of lenses. Francis E. Washer. (Price 10 cents)	137
2016.	Volume dilatometry. Norman Bekkedahl. (Price 10 cents)	145
2017.	Relation between entrance and exit pupils of telescopic systems. Irvine C. Gardner. (Price 5 cents)	157
2018.	Mechanisms for the formation of acetylglycosides and orthoesters from acetylglycosyl halides. Horace S. Isbell and Harriet L. Frush. (Price 10 cents)	161
2019.	Studies on the flame photometer for the determination of Na_2O and K_2O in portland cement. William R. Eubank and Robert H. Bogue. (Price 10 cents)	173

For sale by the Superintendent of Documents, U. S. Government Printing Office, Washington 25, D. C. • Price 50 cents
$4.50 per year on subscription

UNITED STATES GOVERNMENT PRINTING OFFICE, WASHINGTON : 1949

UNIV. OF MICH.

U. S. Department of Commerce
National Bureau of Standards

Research Paper RP2010
Volume 43, August 1949

Part of the Journal of Research of the National Bureau of Standards

Mass Spectrum of Pentaborane (B_5H_9)

By Vernon H. Dibeler, Fred L. Mohler, Laura Williamson, and Robert M. Reese

The mass spectrum of B_5H_9 has been measured, and the monoisotopic spectrum has been computed using the isotope abundance $B^{10}=0.200$ and $B^{11}=0.800$. The mass spectrum shows that the molecule has a marked tendency for ionization with loss of either two or four hydrogen atoms, but little tendency to lose one or three. The high yield of ions containing five boron atoms and the tendency to give up either two or four hydrogen atoms suggests a five-membered ring structure with two pairs of loosely bound hydrogen atoms. Since the spectrum is quite different from that of C_5 ring compounds, however, no definite conclusion concerning the structure is drawn at present.

I. Introduction

The Mass Spectrometry Section has had an opportunity to run mass spectra of some very pure pentaborane, B_5H_9, prepared by the Naval Research Laboratory. This compound is considered by Pitzer [1] to be a five membered ring compound, B_5H_5, with two additional pairs of hydrogen atoms attached to two of the bonds to form protonated double bonds.

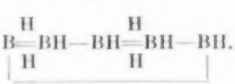

Bauer and Pauling had previously suggested a methylcyclobutane-like structure.[2]

An interpretation of hydroboron mass spectra is complicated by the fact that boron has two isotopes of masses 10 and 11 in the relative amounts 0.20 and 0.80. Consequently, in polyatomic ions many different combinations of boron isotopes and hydrogen atoms contribute to the spectrum. The monoisotopic spectrum of each isotopic configuration must first be evaluated and then all contributions with like numbers of hydrogen atoms summed to give the spectrum that one would obtain if there were only one isotope. To do this an accurate value of the isotope ratio must be found by trial that will give self-consistent results. Another paper on the mass spectrum of diborane has applied this method of analysis.[3]

[1] K. S. Pitzer, J. Am. Chem. Soc. **67**, 1126 (1945).
[2] S. H. Bauer, Chem. Rev. **31**, 43 (1942).
[3] V. H. Dibeler and F. L. Mohler, J. Am. Chem. Soc. **70**, 987 (1948).

II. Experimental Details

The mass spectra were obtained with a 180° Consolidated mass spectrometer using automatic emission control and thermostatic control of the ionization chamber temperature at 245° C. Mass spectra have been measured at 50 and 70 v ionizing voltage. Spectra were obtained with constant magnetic field for the mass range 10 to 64 and a lower field for 1 and 2.

The B_5H_9 was prepared under the direction of Roman R. Miller of the U. S. Naval Research Laboratory. A freezing point determination by J. T. Clarke and H. L. Johnston of Ohio State University indicates a purity of 99.97 percent (informal communication). The material was stored at −78° C until it was used. The sample was held at liquid nitrogen temperature, and any volatile gas pumped off before admitting to the mass spectrometer.

III. Results

Table 1 gives the mass spectrum of B_5H_9 at 50 and at 70v ionizing voltage. Ion intensities are relative to the maximum peak at mass 59 taken as 100. Four of the mass peaks come from doubly charged ions, and all the other peaks are due to singly charged ions. There are no metastable transition peaks.

From statistical considerations, the relative abundances of ions having various combinations of B^{10} and B^{11} atoms in radicals containing from 1 to 5 boron atoms are given by the separate

TABLE 1. *Mass spectrum of B_5H_9*

m/e	Relative intensities		m/e	Relative intensities	
	50 volts	70 volts		50 volts	70 volts
1	4.12	5.71	37	3.39	3.22
2	10.4	15.8	38	1.26	1.24
			39	0.83	0.78
10	6.12	8.24	40	.03	.05
11	23.4	32.3	41	.26	.29
12	7.17	9.26	42	1.45	1.72
13	16.2	18.6	43	5.56	6.03
			44	13.2	13.7
20	--------	0.08	45	22.0	21.5
21	0.20	.41	46	32.0	31.0
22	.86	1.47	47	39.7	39.0
23	2.98	3.56	48	32.6	32.3
24	3.79	4.10	49	8.56	8.58
25	2.28	2.25	50	3.26	3.33
26	1.14	1.14	51	0.31	0.44
27	1.75	1.80	52	2.31	2.52
* 27.5	0.05	0.08	53	9.92	9.85
28	.38	.47	54	25.1	24.1
* 28.5	.29	.31	55	37.0	34.9
* 29	.33	.39	56	38.9	35.7
* 29.5	.12	.17	57	47.1	44.1
30	.03	.13	58	68.6	66.7
31	.17	.24	59	100	100
32	.86	1.23	60	97.0	98.2
33	3.06	3.66	61	67.8	69.1
34	7.42	7.60	62	76.4	77.8
35	10.9	10.6	63	61.5	61.1
36	7.44	6.99	64	49.1	48.7

* Doubly charged ions.

terms in the binomial expansions of $(x+y)^n$, where "n" takes integral values from 1 to 5, and x and y are the fractions of B^{10} and B^{11}.[4] Table 2 lists the terms in the expansions for $n=1$ to 5, and for $x=0.20$ and $y=0.80$. The numbers 0.20 and 0.80 were found by trial to give the best fit. Ions containing the same number of boron atoms will have the relative abundances given along the diagonals running from lower left to upper right. It is possible with the aid of table 2 to calculate the monoisotopic spectra from the mixture spectrum by starting at the heavy mass end and computing the contribution of each ion to each value of m/e.

TABLE 2. *Statistical distribution for B^{10} and B^{11} atoms in ions containing one to five boron atoms* *

B^{11} \ B^{10}	0	1	2	3	4	5
0	-----	20.00	4.00	0.80	0.16	0.032
1	80.00	32.00	9.60	2.56	.64	-----
2	64.00	38.40	15.36	5.12	-----	-----
3	51.20	40.96	20.48	-----	-----	-----
4	40.96	40.96	-----	-----	-----	-----
5	32.77	-----	-----	-----	-----	-----

* The first row gives the number of B^{10} atoms in a molecule, and the first column gives the number of B^{11} atoms. Diagonals from lower left to upper right give the distribution of B^{10} and B^{11} in molecules containing five, four, three, etc., boron atoms.

Table 3 gives in the first and second columns the B_5 part of the 50-v mass spectrum of B_5H_9 and illustrates the computation of the monoisotopic spectrum. The peak at 64 comes entirely from the molecule ion $B_5^{11}H_9^+$. From the lower diagonal of table 2, the six B_5H_9 isotopes have the relative abundance 64=1.0, 63=1.25, 62=0.625, 61=0.156, 60=0.0195, 59=0.001. Multiplying 49.1 by these ratios gives the contribution of B_5H_9 to the mass peaks 64 to 59 shown on the lower diagonal of table 3. Subtracting the B_5H_9 contribution from the 63 peak gives the $B_5^{11}H_8$ contribution as 0.12, and multiplying this by the above ratio gives the B_5H_8 contributions to peaks from 63 to 58. Subtracting $B_2^{10}B_3^{11}H_9+B^{10}B_4^{11}H_8$ contributions from the 62 peak gives the value 45.56 for the ion $B_5^{11}H_7$, etc. When this computation is repeated for each peak down to 55, the complete B_5 spectrum should be accounted for and the residuals on peaks 51, 52, 53, and 54 afford a check on whether the correct isotope ratio has been used. These are all less than the experimental uncertainty. Contributions of all isotopes along each diagonal are then added to give the monoisotopic spectrum in the last column. A large residual, 3.25, on the mass 50 peak is assumed to be $B_4^{11}H_6$, and starting with this value the contributions of the various B_4 ions are computed in the same way as for B_5 ions using the values of table 2 along the second diagonal from the bottom for the relative isotopic abundances of ions containing four boron atoms. Similarly, the entire spectrum omitting doubly charged ions can be computed. Each group of ions with one, two, three, four, and five boron atoms affords one or more checks on the correctness of the analysis, and these check values are tabulated in table 4 for the mass spectrum at 50 volts ionizing voltage. An agreement within 0.2 percent of the maximum peak is entirely within experimental error, and it is only on the mass 10 peak that the discrepancy seems to be definitely greater than the experimental uncertainty. This is discussed in the following section.

[4] The small correction due to hydrogen isotopes is omitted.

TABLE 3. *The B_5 portion of the B_5H_x spectrum at 50 volts illustrating computation of the monoisotopic spectrum*

m/e	Mixture spectrum	Monoisotopic spectra *						ΣB_5H_x
		$B_5^{11}H_x$	$B^{10}B_4^{11}H_x$	$B_2^{10}B_3^{11}H_x$	$B_3^{10}B_2^{11}H_x$	$B_4^{10}B^{11}H_x$	$B_5^{10}H_x$	
50	3.26	.....	.....	.....	.....	.....	0.012	38.7
51	0.31	.....	.....	.....	.....	0.25	.010	33.2
52	2.31	.....	.....	.....	1.98	.21	.013	40.8
53	9.92	.....	.....	7.93	1.70	.26	.013	40.5
54	25.1	.....	15.87	6.80	2.09	.26	.011	34.6
55	37.0	12.70	13.60	8.35	2.07	.22	.062	194.2
56	38.9	10.88	16.71	8.30	1.77	1.24	.003	9.5
57	47.1	13.37	16.61	7.08	9.94	0.06	.044	139.0
58	68.6	13.29	14.16	39.78	0.48	.89	.....	0.4
59	100.	11.33	79.57	1.93	7.12	.003	.048	149.9
60	97.0	63.66	3.87	28.49	0.02	.96	.....	.....
61	67.8	3.10	56.95	0.08	7.67	.....	.....	.....
62	76.4	45.56	0.15	30.69	.....	.....	.....	.....
63	61.5	0.12	61.38	.....	.....	.....	.....	.....
64	49.1	49.1	.....	.....	.....	.....	.....	.....

* "x" assumes integral values from zero to nine, reading down the column.

The four peaks of table 1 ascribed to doubly charged ions come from ions of masses 55, 57, 58, and 59. The small residual on the mass 30 peak (table 4) indicates that ions $B_5H_5^{++}$ are absent or very improbable and that the peak at 29.5 is largely $B_5^{11}H_4^{++}$. On this basis one can compute the monoisotopic doubly charged spectrum. The computations indicate that the 29 peak is entirely composed of doubly charged ions and the 28 peak is largely singly charged. The 27.5 peak can be either B_5^{11++} or $B_4^{11}B^{10}H^{++}$, but the absence of a 26.5 peak favors the latter possibility.

Table 5 gives the monoisotopic spectra of B_5H_9 computed as illustrated in table 3, on the basis of the B_5H_5 ion equal to 100 and includes the doubly charged ions. The B_5H_8 contribution is too small to be significant. If the ratio B^{10}/B^{11} were taken as 0.2505 instead of 0.2500, the computations would give $B_5H_8=0$ at 50 v with no significant change in the residuals used to check the computations. The $B_2H_6^+$ peak is not negligible but

TABLE 4. *Summary of check points for the mass spectrum of B_5H_9 at 50 volts ionizing voltage*

Group	Mixture peak		
	m/e	Observed	Calculated *
B_1	10	6.12	5.65
B_2	20	0	0.04
	21	0.20	.11
	30	0.03	.01
B_3	31	.17	.13
	32	.86	.64
	40	.03	.01
B_4	41	.26	.20
	42	1.45	1.48
	43	5.56	5.64
	51	0.31	0.26
B_5	52	2.31	2.20
	53	9.92	9.90
	54	25.1	25.0

* Calculated for the isotope abundances $B^{10}=0.20$, $B^{11}=0.80$.

TABLE 5. *Monoisotopic mass spectra of B_5H_9*

Ion	Relative intensities		Ion	Relative intensities	
	50 volts	70 volts		50 volts	70 volts
H	2.05	3.00	B_4	3.61	4.35
H_2	5.16	8.28	B_4H	6.96	7.37
			B_4H_2	13.2	12.8
B	14.8	20.7	B_4H_3	14.4	14.1
BH	2.01	3.03	B_4H_4	32.8	33.0
BH_2	10.5	12.2	B_4H_5	6.69	6.74
			B_4H_6	4.07	4.25
B_2	.....	0.27			
B_2H	1.18	1.54	B_5	20.0	20.4
B_2H_2	2.22	2.54	B_5H	17.1	15.6
B_2H_3	1.62	1.64	B_5H_2	21.0	20.2
B_2H_4	0.27	0.27	B_5H_3	20.9	18.5
B_2H_5	1.26	1.28	B_5H_4	17.8	18.4
B_2H_6	0.31	0.39	B_5H_5	100.	100.
			B_5H_6	5.04	8.66
B_3	.61	.87	B_5H_7	71.4	71.7
B_3H	1.55	2.19	B_5H_8	0.25	0.36
B_3H_2	6.52	6.36	B_5H_9	77.2	78.0
B_3H_3	5.27	5.04			
B_3H_4	2.78	2.65	Doubly-charged ions		
B_3H_5	0.64	0.41			
B_3H_6	.83	.81	B_5H^{++}	0.03	0.06
			$B_5H_2^{++}$	0	0
			$B_5H_3^{++}$	0.28	0.28
			$B_5H_4^{++}$	.19	.26

could be ascribed to a trace of nitrogen in the pentaborane. In view of the precautions taken to pump out noncondensible gases, the evidence for $B_2H_6^+$ is considered probable but not certain. It is not diborane, as this would give a much larger $B_2H_5^+$ peak.

The H_2^+ ion is much more abundant than in hydrocarbons, but it definitely does not come from hydrogen in the sample. Thermal dissociation in the ionization chamber may account for a small part of this, but much less H_2^+ was found in the less stable compound, diborane.

IV. Discussion

The mass spectrum of B_5H_9 gives no definite information concerning the structure of the molecule. The high probability of ionization with loss of 2H or 4H is consistent with the view that four hydrogen atoms are loosely bound in "protonated double bonds", and the relative abundance of B_5 ions is suggestive of a stable 5-membered ring structure. However, there is no sound basis of comparison, as the spectrum is unlike that of C_5 ring compounds and also unlike that of diborane, the only other hydroboron that has been studied. In contrast to B_5H_9, diborane gives a very small molecule ion peak, and loss of H to give $B_2H_5^+$ is the most probable ionization product. The very small probability of losing one or three hydrogen atoms from B_5H_9 compared with loss of any other number from two to nine is an unusual feature. Also, the absence of a $B_2H_2^{++}$ ion is quite unlike all C_5 hydrocarbons. In most hydrocarbons ionization with loss of hydrogen atoms is more of a random process with certain processes favored but not to the extent of almost complete exclusion of a particular ion.

The analysis of the polyisotopic spectrum gives a value of the isotope ratio of $B^{10}/B^{11}=0.250\pm 0.002$. This is in very satisfactory agreement with other values obtained in this laboratory. Samples of B_2H_6 from two different sources gave $B^{10}/B^{11}=0.251$ and 0.256, whereas the mass spectrum of BF_3 gave 0.250. These values are not in good agreement with the carefully measured values of Inghram [5] using the BF_3 spectrum and B^+ of $B(OCH_3)_3$, which both give $B^{10}/B^{11}=0.232$. The discrepancy is far beyond any experimental error and indicates a large difference in isotopic abunddances in boron from different samples.

In the summary of check points, table 4, there is a significant discrepancy between the observed and calculated values for the mass 10 peak. This can be explained by the hypothesis that the probability of breaking a bond to B^{10} is slightly different from that for B^{11}. The heights of B, BH, and BH_2 peaks at 50 v give a value of $B^{10}/B^{11}=0.26$ as compared with 0.250 for the rest of the spectrum. This indicates that breaking a B^{10} bond is slightly more probable than breaking a B^{11} bond. A similar effect is well established in the case of C^{12} and C^{13} bonds in hydrocarbons.[6] In propane ionization, breaking a C^{12} bond is 20 percent more probable than breaking a C^{13} bond.

Washington, April 7, 1949.

[5] M. G. Inghram, Phys. Rev. **70,** 653 (1946).
[6] O. Beeck, J. W. Otvos, D. P. Stevenson, and C. D. Wagner, J. Chem. Phys. **16,** 255 (1948).

U. S. Department of Commerce
National Bureau of Standards

Research Paper RP2011
Volume 43, August 1949

Part of the Journal of Research of the National Bureau of Standards

Effect of Chromium Plating on the Endurance Limit of Steels Used in Aircraft

By Hugh L. Logan

Chromium plating reduced the endurance limits of both normalized and hardened (quenched and tempered) SAE X4130 steels; the reduction was larger for the hardened steel. The endurance limits for steel of a given hardness decreased with increased plating bath temperatures. Baking of the plated steel, at temperatures up to 350° C, reduced the endurance limit; baking at 440° C increased the endurance limit of the plated steel. However (for hardened steel) baking did not restore the endurance limit to that of the unplated steel. Damaging effects of chromium on the endurance limits of plated steels are attributed to stresses in the chromium and/or steel, which are increased by low temperature baking but are relieved in part by baking at 400° to 440° C.

I. Introduction

During the period of 1930 to 1936 the Bureau of Aeronautics, Navy Department, submitted for examination a number of chromium-plated hollow-steel airplane propeller blades that had failed by fatigue in service. Preliminary fatigue tests in the laboratory confirmed conclusions, based on the examination of the propeller failures, that the endurance limit of the steel was materially reduced by chromium plating. In addition to the plating of propeller blades and other parts for protective purposes, manufacturers and maintenance shops were exploring the possibilities of reclaiming by chromium plating worn and undersize parts. These considerations prompted the Bureau of Aeronautics to support an extensive investigation conducted by the National Bureau of Standards on the effect of chromium plating on the endurance limits of steels used in aircraft.

Two steels designated SAE X4130 and 6130 were used in the investigation. However, most of the tests were made on X4130 steel, heat treated to a hardness of about Rockwell 40-C, with an ultimate tensile strength of approximately 180,000 lb/in.^{2}

The first phase of this study provided for the determination of the effects of chromium, as plated, on the endurance limit of the steels. The variables studied were: (1) plate thickness, (2) hardness of the steels plated, (3) current densities and temperatures of the plating baths, (4) surface grinding of the chromium after plating, and (5) interruptions of the plating process.

A second phase of the investigation was a systematic study of the effect of heating on the endurance limit of specimens of chromium-plated X4130 steel. If the decrease in the endurance limit of the plated steel is attributable to the large quantities of hydrogen evolved at the cathode during the process of chromium plating, then it appears that the endurance limit may be increased by the removal of hydrogen by heating. However, Swanger and France [1] [1] found that heating the specimens for 5 hours at 350° F (182° C) reduced the endurance limit of the plated steel to about 70 percent of that of the plated but unheated material. Wiegand and Scheinost [2] also reported that heating of chromium plated steel at 250° C decreased its endurance limit. Other workers have spot checked the effect on the endurance limit of heating chromium-plated steel. However, no systematic study of the effect of heating had been made.

A theory has been developed to explain, at least in part, the effects of chromium plating on the endurance limit of the steels studied.

[1] Figures in brackets indicate the literature references at the end of this paper.

Publication of this material, including data circulated during wartime in reports [3] that at that time were restricted but have since been declassified, has been approved by the Bureau of Aeronautics, sponsor of the investigation.

II. Materials

The materials, from which the specimens for this investigation were machined, consisted of three lots of SAE X4130 rod and one lot of 6130 rod. The compositions of these steels, as determined by chemical and spectrochemical analyses, are shown in table 1.

TABLE 1. *Composition of steels*

Element	SAE X4130 Steel			SAE 6130 Steel
	Lot A	Lot B	Lot C	
	Percent	*Percent*	*Percent*	*Percent*
Carbon	0.35	0.29	0.33	0.30
Manganese	.53	.47	.55	.61
Phosphorus	.01	.02	.03	.03
Sulfur	.02	.02	.01	.04
Silicon	.21	.25	.24	.25
Chromium	.95	.96	1.05	1.01
Molybdenum	.19	.24	0.20	(1)
Vanadium	(1)	(1)	(1)	0.22
Nickel	(1)	.15	.17	(1)

[1] Not determined.

Lot A of the X4130 steel was supplied by the Naval Aircraft Factory in two heat-treated conditions, normalized to Rockwell hardness number B–89, and quenched and tempered to Rockwell C–39. The 6130 steel was also supplied by the Naval Aircraft Factory but only in the quenched and tempered condition, Rockwell C–33. The other lots of X4130 rod were heat-treated at the National Bureau of Standards; they were quenched in oil from 1,575° to 1,600° F and subsequently tempered to approximately Rockwell C–40.

Typical microstructures of transverse sections of the steels are shown in figure 1. A longitudinal section of the normalized X4130 steel (not illustrated) showed definite indications of banding and segregation, which are not unusual for this type of steel.

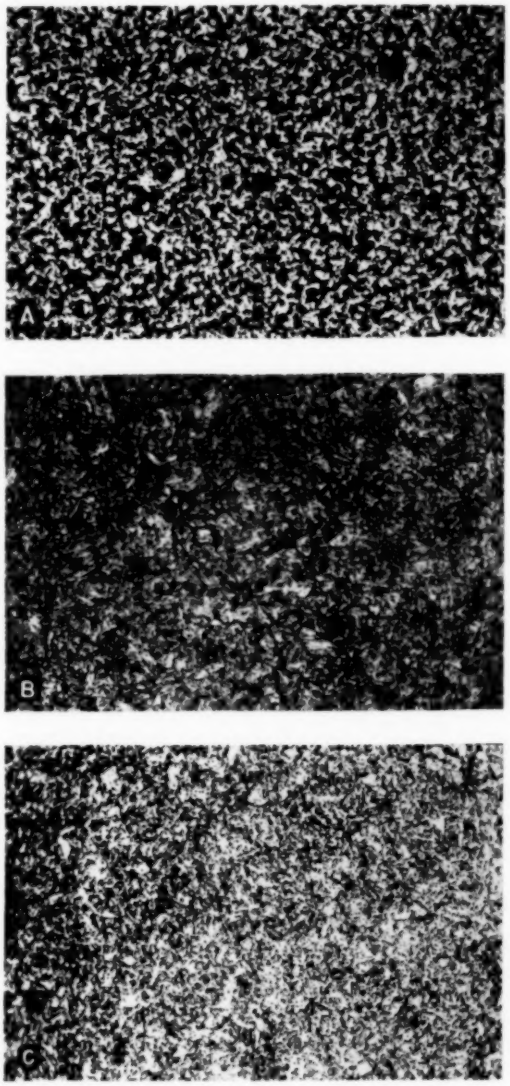

FIGURE 1. *Typical microstructures of transverse sections of steels investigated*

A, normalized X4130 steel, x100; B, Quenched and tempered X4130 steel, x500; C, quenched and tempered 6130 steel, x500. All etched 1 percent Nital.

III. Specimens and Test Methods

1. Preparation and Testing of Specimens

Specimens for the fatigue tests were of the usual "R. R. Moore type" [4] with nominal diameters of 0.30 in. in most cases; however, 0.25-in.-diameter specimens were used in some instances. Computation of the stresses in the outer fibers of the specimens, and hence the endurance limits, were based on the diameters of the specimens prior to plating. Diameters of all specimens machined at this Bureau were determined, before

TABLE 2. *Details of preparation of specimens used in the investigation*

SAE No.	Steel lot	Heat treatment	Rockwell hardness	Specimens prepared for plating by [1]	Specimens chromium plated by	Temperature of plating bath	Plating current density	Nominal thickness of plating
						° C.	*amp/sq. ft.*	*in.*
X4130	A		89–B	NAF	NAF	55	200	0.0001; 0.001; 0.004; 0.009 [2]
X4130	A		89–B	do	do	70	1,000	0.0001; 0.001; 0.004; 0.009 [2]
X4130	A		39–C	do	do	55	200	0.0001; 0.001; 0.004; 0.009 [2]
X4130	A		39–C	do	do	70	1,000	0.0001; 0.001; 0.004; 0.009 [2]
6130	----		33–C	do	do	55	200	0.0001; 0.001; 0.004; 0.009 [2]
6130	----		33–C	do	do	70	1,000	0.0001; 0.001; 0.004; 0.009 [2]
X4130	B	Oil quenched from 1,575 to 1,600° F. drawn at 900 to 925° F.	40–C	NBS	do	70	1,000	0.009
X4130	C		40–C	do	NBS	70	1,000	0.009.
X4130	C		40–C	do	do	55	350	0.001· 0.005; 0.010; 0.017.
X4130	C		40–C	do	do	85	700	0.010.

[1] Includes heat treating, machining, and usually polishing.

[2] Two groups of specimens had been plated to a thickness of about 0.008 in. One of these groups was stated to have been plated to a thickness of 0.010 in. with about 0.001 in. of plate subsequently removed by grinding.

and after plating, with a dial gage comparator reading to 0.0001 in.

Prior to the final polishing, the specimens prepared at this Bureau were ground with a Norton "38" alundum wheel. Subsequently these grinding marks were removed with metallographic polishing papers by one of the following methods: (a) circumferential polishing of specimens in a lathe for fixed periods, determined by experiment to be sufficient to remove grinding marks or marks of coarser papers previously used (papers used were Behr-Manning emery 1, Aloxite 400, Behr-Manning emery 1/0 and 2/0); or (b) longitudinal polishing of specimens using Aloxite 400 paper followed by the Behr-Manning emery 1/0 polishing paper in the form of belts mounted on a rubber-backed wheel. In some instances commercially available coarse and medium emery-impregnated rubber wheels were used in place of the abrasive paper belts.

A few of the mechanically polished specimens were subsequently polished electrolytically as follows: Specimens were made the anodes in a bath containing 50 percent by volume of concentrated H_2SO_4 and 50 percent by volume of 75 percent H_3PO_4; a current density of 250 amp/ft^2 was maintained for 5 minutes; the temperature was 42° C. This reduced the diameters of the specimens by 0.0004 to 0.0006 in. Details regarding the preparation of the fatigue specimens are given in table 2.

Fatigue tests were made in R. R. Moore type rotating beam fatigue testing machines operating at 1,800 or 3,600 revolutions per minute with stresses generally applied in increments of 1,000 lb/in^2. Generally, eight to ten specimens were required to obtain the endurance limit in any one case. Specimens that had run 10,000,000 or more cycles without failure were considered to have been stressed at or below the endurance limit and were removed from the machines.

2. Electroplating of Specimens

Specimens were plated at the National Bureau of Standards by personnel of the Electrodeposition Section. The process prior to plating was as follows: Specimens were cleaned by scrubbing with fine pumice powder and rinsed thoroughly with water. The light oxide film that formed during the time required to assemble the specimens in the plating rack was removed by dipping for a few seconds in 20-percent hydrochloric acid solution. The specimens were again rinsed, placed in the chromium plating solution, and made anodic for 1 minute at the same current density used in plating. After the anodic treatment, full plating current was immediately applied.

The plating electrolyte contained 250 g/liter of CrO_3 and 2.5 g/liter of H_2SO_4. Specimens were plated at three different bath temperatures and current densities. A bath temperature of 55° C and a current density of 350 amp/ft^2 were selected as one condition, because they were within the range (45° to 60° C. and 70 to 450 amp/ft^2) generally used in industrial chromium plating. A temperature of 70° C and a current density of 1,000 amp/ft^2 were employed for the second condition in order to check certain results previously obtained in this investigation on

843576—49——2

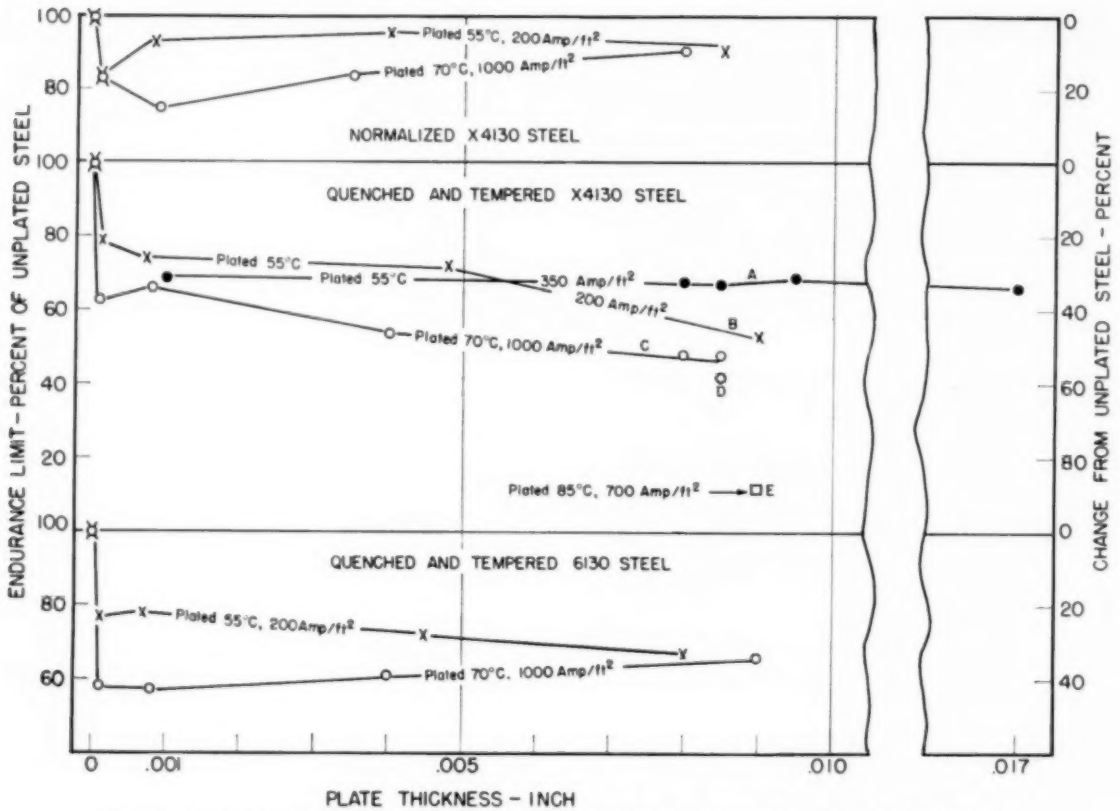

FIGURE 2. *Relationship between the endurance limits and plate thicknesses of X4130 and 6130 steels.*

Data obtained on specimens plated at NBS are shown by curve A and points D and E. All other data were obtained on specimens plated at the NAF.

specimens similarly plated at the Naval Aircraft Factory. A bath temperature of 85° C and a current density of 700 amp/ft² were selected for the third condition, since chromium deposited in this way is supposed to be subject to less contraction when heated than is chromium plated under the other conditions, and it appeared advisable to determine the extent to which this factor might affect the endurance limit of the steel.

In order to determine the effect of interrupted plating on the endurance limit, two sets of specimens were plated to the same final thickness; one set was plated continuously and the other by an interrupted operation. Plating was resumed following the interruption only after the employment of the proper commercial technique for plating chromium on chromium; this involved a short reversal of the current and the gradual increasing of the current from a low value to the plating current.

No information was provided by the Naval Aircraft Factory as to the surface preparation, after the final machining and prior to plating, of fatigue specimens prepared at that agency. The composition of the plating bath used by the Naval Aircraft Factory in plating of fatigue specimens was the same as that used at this Bureau and described above; specimens were stated to have been plated in a bath maintained at 55° C at a current density of 200 amp/ft² and at 70° C and 1,000 amp/ft².

3. Heat Treatment of Chromium-Plated Specimens

Some specimens were heated in oil at about 100° C, in boiling ethylene glycol at 193° C, or in N-butal phthalate at 297° C. Other specimens were heated to temperatures up to 200° C in an electrically heated laboratory oven, with forced air circulation, thermostatically controlled to ±2° C. Temperatures of 300°, 350°, 400°, and

440° C, controlled to ±3° C, were obtained with an electrically heated tempering furnace with forced air circulation.

IV. Results and Discussion

1. Effect of Chromium Plating on the Endurance Limits of SAE X4130 and SAE 6130 Steels

(a) Normalized X4130 Steel

The results of fatigue tests on the normalized X4130 steel (heat A) are given in table 3 and shown graphically in figure 2. The decrease in the endurance limit of the normalized steel caused by chromium plating was generally small; the minimum endurance limit of any group of plated specimens was 75 percent of the endurance limit of the unplated steel. This value was obtained on specimens plated to a thickness of 0.001 in. at a current density of 1,000 amp/ft². Most sets of specimens had endurance limits ranging from 83 to 95.5 percent of that of the unplated steel. Specimens plated in the bath at 55° C and a current density of 200 amp/ft² had endurance limits equal to or greater than those plated at 70° C and 1,000 amp/ft².

(b) Quenched and Tempered SAE X4130 Steel

The results of fatigue tests on quenched and tempered SAE X4130 steel (lots A, B, and C), hardness approximately 40 Rockwell C, bare, and plated to various thicknesses under various plating conditions are given in table 3. Most of the data are also shown graphically in figure 2. The endurance limits of the quenched and tempered steel specimens were reduced much more by chromium plating than were those of the normalized specimens (hardness, Rockwell 89–B). The maximum endurance limits of specimens plated to a thickness of 0.008 to 0.010 inch at a bath temperature of 55° C and tested as plated were 68 to 69 percent of that of the unplated steel. Endurance limits of the specimens in general decreased with increased bath temperatures. Specimens plated at 70° C to the same thickness as those plated at 55° C and discussed above had endurance limits 40 to 48 percent of that of the unplated steel, and

TABLE 3. *Endurance limits of unplated and chromium-plated steels*

Steel	Nominal plating thickness—												
	0 inch	0.0001 inch		0.001 inch		0.004 inch		0.009 inch		Ground to 0.009 inch		0.017 inch	
PLATED AT 70° C—CURRENT DENSITY 1,000 AMP/FT²													
	*lb/in.*²	*lb/in.*²	% [1]	*lb/in.*²	% [1]	*lb/in.*²	% [1]	*lb/in.*²	% [1]	*lb/in.*²	% [1]	*lb/in.*²	% [1]
Normalized X4130. Hardness, Rockwell 89–B	44,000	36,500	83	33,000	75	37,000	84	40,000	91	38,000	86	----	----
Q & T 6130. Hardness, Rockwell 33–C	83,000	48,000	58	47,000	57	51,000	61	55,000	66	55,000	66	----	----
Q & T X4130. Hardness, Rockwell 39–C	93,000	59,000	63	61,000	66	50,000	54	45,000	48	58,000	62	----	----
PLATED AT 55° C—CURRENT DENSITY 200 AMP/FT²													
Normalized X4130. Hardness, Rockwell 89–B	44,000	37,000	84	41,000	93	42,000	95.5	40,000	91	45,000	102	----	----
Q & T 6130. Hardness, Rockwell 33–C	83,000	64,000	77	65,000	78	60,000	72	56,000	67	61,000	74	----	----
Q & T X4130. Hardness, Rockwell 39–C to 40–C	93,000	73,000	79	69,000	74	67,000	62	49,000	53	65,000	70	----	----
PLATED AT 55° C—CURRENT DENSITY 350 AMP/FT²													
Q & T X4130. Hardness, Rockwell 39–C to 40–C	93,000	----	----	66,000	71	----	----	64,000	69	----	----	61,000	66
PLATED AT 85° C—CURRENT DENSITY 700 AMP/FT²													
Q & T X4130. Hardness, Rockwell 39–C to 40–C	93,000	----	----	----	----	----	----	10,000	11	----	----	----	----

[1] Percentage of unplated steel.

those plated at 85° C only 11 percent of that of the unplated steel.

Endurance limits of specimens of the quenched and tempered steel, plated at the Naval Aircraft Factory (table 2), generally decreased with increased plate thickness (fig. 2, curves B and C). There was no significant change in endurance limit with increased plate thickness for specimens plated at 55° C at the NBS (fig. 2, curve A). Plating at this Bureau in the bath at 55° C was at a current density of 350 amp/ft² as compared to a current density of 200 amp/ft² at that temperature at the Naval Aircraft Factory. Specimens plated by the Naval Aircraft Factory to a thickness of approximately 0.009 in. at 70° C, current density 1,000 amp/ft², had a 14-percent higher endurance limit than specimens plated under the same conditions at this Bureau. Curve *C*, fig. 2 represents Naval Aircraft Factory specimens, and point *D*, National Bureau of Standards specimens.

There was no significant difference in the endurance limits of two sets of specimens, both plated to the same final thickness under similar conditions, of which one was plated continuously and the other by an interrupted operation.

(c) Quenched and Tempered SAE 6130 Steel

The results of fatigue tests on the quenched and tempered SAE 6130 steel (hardness Rockwell 33–C), bare and plated to various thicknesses at current densities of 1,000 and 200 amp/ft², are given in table 3 and are shown graphically in figure 2.

Endurance limits of specimens plated at 70° C increased as the plating thickness was increased above 0.001 in.; on the other hand, the endurance limits of specimens plated at 55° C decreased with increased plate thickness above that value. The endurance limits of specimens with 0.009-in. thick plating were approximately the same for both sets of plating conditions and amounted to 66 to 67 percent of that of the unplated steel. Specimens plated to thicknesses of 0.0001 and 0.001 in. had endurance limits of 77 to 78 and 57 to 58 percent of that of the unplated steel for bath temperatures of 55° and 70° C, respectively.

The data obtained on the ground and unground specimens having approximately the same final plate thickness (0.009 in.), in general, indicated that the ground specimens had endurance limits equal to or greater than those of the "as plated" specimens (table 3).

2. Effect of Heating on the Endurance Limit of Chromium-Plated X4130 Steel

The results of fatigue tests on specimens of lots B and C of the SAE X4130 steel, chromium plated to thicknesses of 0.001 to 0.017 in. and subsequently baked at temperatures ranging from 100° C to 440° C, are given in tables 4, 5, and 6; some of the data are shown graphically in figures 3 and 4. The endurance limits of these specimens reached a minimum value for temperatures between 193°

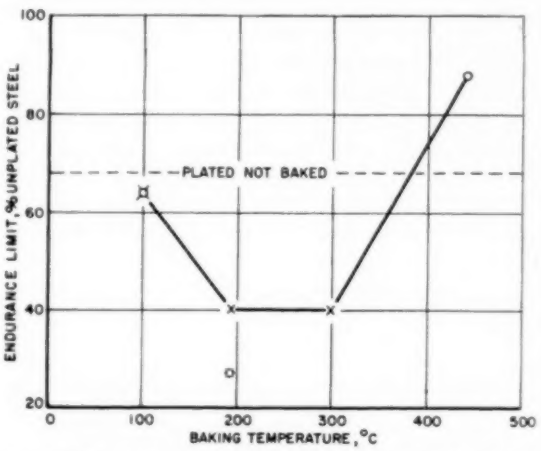

FIGURE 3. *Influence of baking temperatures on the endurance limits of quenched and tempered X4130 steel specimens chromium plated at 55° C and a current density of 350 amp/ft² to a thickness approximately 0.008 in.*

○, Baked in air; X, baked in an organic liquid.

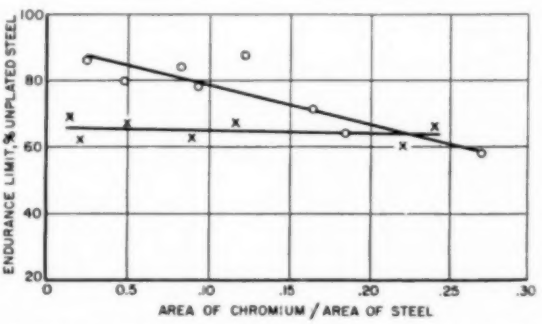

FIGURE 4. *Relationship between endurance limit and ratio of cross-sectional chromium-plated area to steel area for quenched and tempered SAE X4130 steel specimens 0.250 and 0.300 in. in diameter.*

X, As plated; ○, plated and baked 1 hour at 440° C.

TABLE 4. *Endurance properties of SAE X4130 steel specimens (hardness, approximately 40 C scale) chromium plated and subsequently heated*

Nominal thickness of plating	Heat treatment			Endurance limit	
	Temperature	Medium	Time	lb/in.²	Percentage of unplated steel
		LOT C STEEL, PLATING BATH TEMPERATURE 55° C, CURRENT DENSITY 350 AMP/FT²			
in.	*° C*		*hr*		
0.0085	.....	None	.....	64,000	67
.009	100	Oil	1	56,000	64
.010	100	..... do	12	<48,000	<55
.0095	193	Ethylene glycol	1	35,000	40
.0105	193	..... do	6	33,000	37.5
.0100	193	..... do	100	33,000	37.5
.0105	193	Air	1	24,000	27
.0085	200	..... do	6	32,000	34
.0087	296	Butal phthalate	1	35,000	40
.009	440	Air	1	83,000	87.5
		LOT B STEEL, PLATING BATH TEMPERATURE 70° C, CURRENT DENSITY 1,000 AMP/FT²			
.008	.....	None	.....	45,000	51
.008	95.5	Oil	24	39,000	44
.008	95.5	Air	24	35,000	40
.008	200	..... do	6	32,000	36
.008	300	..... do	1	46,000	52
.008	350	..... do	1	51,000	58
.008	400	..... do	1	55,000	63
.008	440	..... do	1	59,000	67
		LOT C STEEL, PLATING BATH TEMPERATURE 70° C, CURRENT DENSITY 1,000 AMP/FT²			
.009	.....	None	.....	40,000	42
.008	200	Air	6	25,000	26
.008	300	..... do	4	28,000	28.5
.008	440	..... do	1	47,000	49.5
		LOT C STEEL, PLATING BATH TEMPERATURE 85° C, CURRENT DENSITY 700 AMP/FT²			
.010	.....	None	.....	10,000	11
.010	193	Ethylene glycol	6	13,000	14.5
.010	440	Air	1	42,000	46.5

and 300° C; at higher baking temperatures the endurance limits increased, and at temperatures of 400° and 440° C exceeded those of the unbaked plated specimens. The endurance limit of one set of specimens heated in air for 1 hour at 193° C was 27 percent of that of the unplated steel (table 4). The endurance limit of specimens heated in ethylene glycol at 193° C was somewhat higher than that of specimens heated in air and was independent of the time specimens were held at the baking temperature. Specimens plated to a thickness of 0.002 in. and heated for 1 hour at 440° C had an endurance limit as high as 87½ percent of that of the unplated steel compared to 68 to 69 percent for unbaked plated specimens. However, the endurance limits of the plated specimens heated 1 hour at 440° C decreased as the ratio of the cross-sectional area of chromium plating to steel

TABLE 5. *Effect of specimen diameter and plating thickness on the endurance limit of quenched and tempered SAE X4130 steel, hardness Rockwell, 40-C, lot C, chromium plated at a current density of 350 amp/ft², bath temperature 55° C*

Specimen diameter	Nominal plate Thickness	Ratio of cross-sectional chromium plate to steel area	Baking treatment		Endurance limit	Percentage of endurance limit of unplated steel
			Time	Temperature		
in.	*in.*		*hr*	*° C.*	*lb/in²*	*Percent*
0.25 to 0.30	.....	0	.....	.....	95,000	100
.30	0.017	0.24	.....	.....	63,000	66
.30	.0085	.116	.....	.....	64,000	67
.30	.001	.014	.....	.....	66,000	69
.25	.0105	.22	.....	.....	57,000	60
.25	.005	.080	.....	.....	59,000	62
.25	.001	.021	.....	.....	59,000	62
.30	.0085	.116	2	200	31,000	33
.30	.0085	.116	6	200	31,000	33
.30	.018	.265	1	440	<55,000	<58
.25	.002	.122	1	440	83,000	87.5
.25	.011	.184	1	440	61,000	64
.25	.010	.164	1	440	67,000	71
.25	.009	.157	2	440	80,000	84
.25	.012	.201	4	440	70,000	74
.25	.005	.082	1	440	80,000	84
.25	.0015	.024	1	440	82,000	86

TABLE 6. *Effect of type of surface preparation of the basis steel prior to plating, on the endurance properties of SAE X4130 steel (lot C) chromium plated to a thickness of 0.008 to 0.009 in. at a current density of 1,000 amp/ft².*

Bath temperature 70° C

Type of surface treatment [1]	Heat treatment		Endurance limit	Percentage of endurance limit of unplated mechanically polished steel
	Time	Temperature		
	hr	*° C*	*lb/in.²*	
Mechanical [2]	.....	.....	95,000	100
Electrochemical [2]	.....	.....	87,000	92
Mechanical	.....	.....	40,000	42
Electrochemical	.....	.....	24,000	25
Mechanical	6	200	25,000	26.5
Electrochemical	6	200	24,000	25
Mechanical	1	440	47,000	49.5
Electrochemical	1	440	45,000	47.5

[1] All specimens were mechanically polished in a longitudinal direction with "400A" Aloxite paper. Subsequently, specimens labeled "Electrochemical" were made anodes in $H_2SO_4+H_3PO_4$ solution and were reduced about 0.0005 in. in diameter by electrochemical means.

[2] Not plated.

increased, reaching values less than for the unbaked steel for very thick plating.

The endurance limit of specimens polished electrolytically prior to plating and tested without subsequent heating was lower than that of mechanically polished specimens (table 6). However, the endurance limits of the plated and heated specimens were independent of the original surface preparation prior to plating.

3. Discussion of Causes of Effects of Chromium Plating on Endurance Limits of Steels

Three possible explanations for the fact that the endurance limits of the steels were reduced by the chromium plate have been proposed: The embrittlement due to hydrogen; cracks in the chromium plate at which stress concentrations occur; and the presence of residual stresses in the chromium or steel or both as the result of the plating. It is of course recognized that these factors may be interrelated and possibly be manifestations of one another.

It is well known that the plating efficiency for depositing chromium is low, approximately 15 to 20 percent of the current being used to deposit chromium. Large quantities of hydrogen are produced at the cathode, and the chromium plate has been shown to contain as much as 128 volumes of hydrogen per volume of chromium [5, 6]. Theories explaining the manner in which the cathodic hydrogen is held in the chromium [7] have been proposed but are not pertinent to the discussion at this point. Zapffe [8] has explained brittleness observed in bend tests on wire plated with chromium as due to hydrogen. Brenner, Burkhead, and Jennings [9] showed that approximately 95 percent of the hydrogen is removed by heating chromium at 450° C. These facts suggest that the improvement in endurance limit of specimens heated at 440° C is due to the expulsion of hydrogen. However, specimens heated at 200° C had in some cases only 50 percent of the endurance limit of unheated specimens, whereas data given by Brenner and coworkers showed that approximately half of the hydrogen was removed from the chromium by heating at 200° C. It is difficult, therefore, to see how the results of the fatigue tests reported here can be attributed directly to hydrogen embrittlement.

At a magnification of 250 diameters, the surfaces of the electroplated chromium samples studied had a pebble-grained appearance. The specimens plated at 55° and 70° C also exhibited surface cracks having the appearance of grain boundaries (figs. 5 and 6). The cracks were less numerous in the specimens plated at 70° C than for those plated at the lower temperature. No cracks were found on specimens plated at 85° C. Metallographic examinations of longitudinal sections of the chromium-plated specimens at distances of 0.01 in. or more from the fatigue fracture failed to reveal cracks penetrating through the chromium, or to reveal cracks extending any appreciable distance into the chromium from the outer surface. There were, however, numerous inclusions and voids in the chromium.

Mehr, Oberg, and Teres [10] reported that, in general, the number of cracks in a given area increased as the chromium plate was heated. Other observers [3] had noted that heating of the chromium plate at a temperature as low as 100° C tended to widen the cracks. The author found this crack-widening tendency to be more pronounced as the temperature of heating was increased (fig. 7).

Bennett [11] has shown that notches reduce the endurance limit of normalized X4130 steel approximately 20 percent and that fine cracks reduce the endurance limit by more than 50 percent. The presence of cracks in the chromium plated at 55° and 70° C might explain the reduction in the endurance limits of steel specimens plated at these temperatures. However, no cracks were found in chromium plated at 85° C, and specimens plated at this temperature had the lowest endurance limit of any specimens tested. Furthermore, preliminary results of an investigation, now in progress, indicate that fatigue damage in chromium-plated steel specimens starts below the surface of the chromium and does not appear to be associated with the surface cracks developed during the plating of the chromium. It must be concluded, therefore, that cracks in the chromium do not have the same effect on the endurance limit of specimens as cracks in the basis steel.

It is well-established that residual stresses in a metal markedly influence its endurance limit. The increased endurance limits, obtained by the shot peening [12] of steel parts, are believed to be the result of residual compressive stresses in the surface of the metal. Conversely, residual ten-

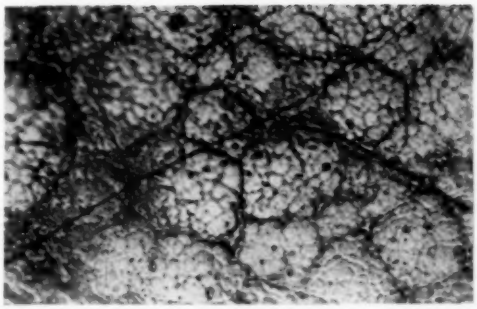

FIGURE 5. *Surface of chromium plated on steel at 70° C (current density 1,000 amp/ft²).*

Areas bounded by sharply defined cracks are larger than those in chromium plated at 55° C (see fig. 6). Unetched, x500.

FIGURE 6. *Surface of chromium plated on steel at 55° C (current density 200 amp/ft²).*

Unetched, x500.

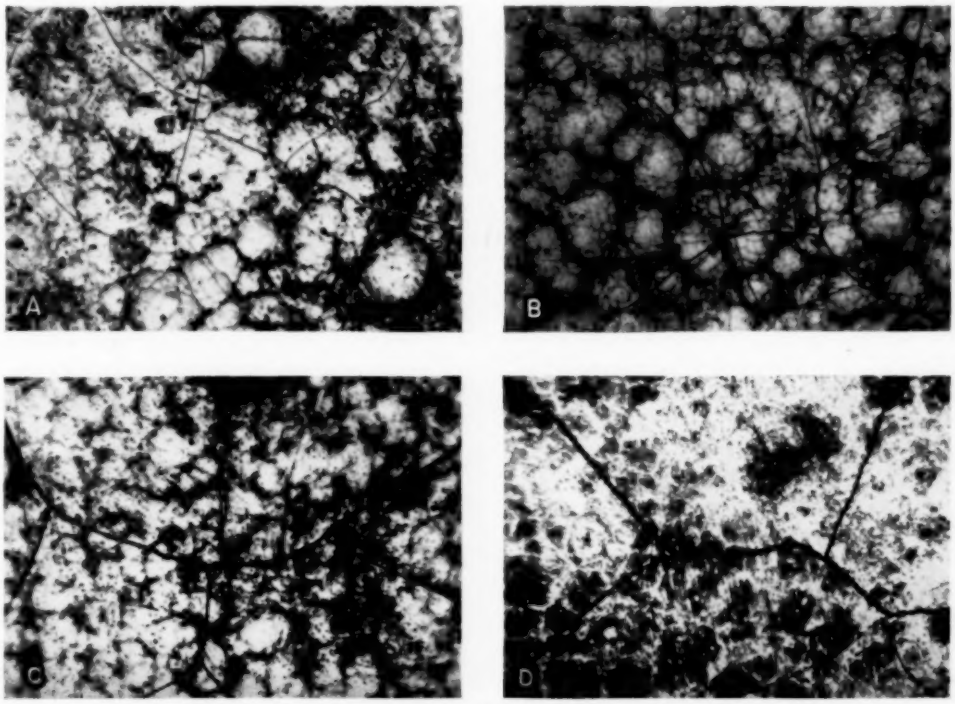

FIGURE 7. *Cracks in chromium plated at 55° C (350 amp/ft²); unetched, x250.*

A, As plated; B, heated 1 hr at 193° C; C, heated 1 hr at 296° C; D, heated 1 hr at 440° C.

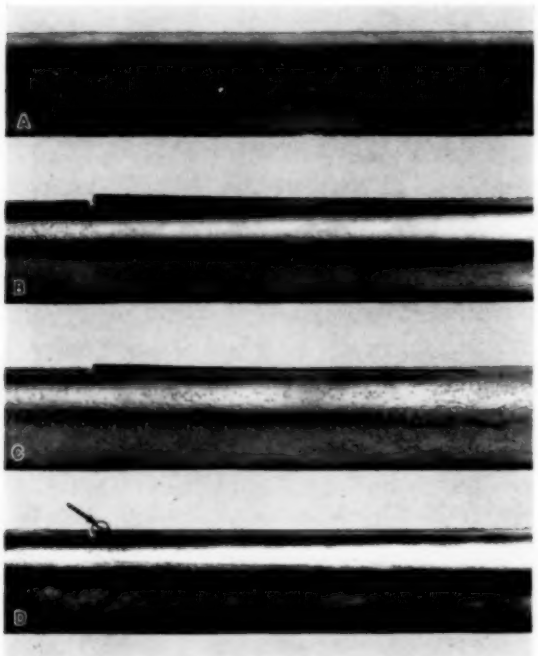

FIGURE 8. *Chromium-plated steel tubes.*

A, Top view of tube showing "tongue;" B, C, and D, side views of tubes showing deflections of "tongue." B, tube plated, heated at 200° C and "tongue" subsequently cut; C, tube plated, "tongue" cut and tube subsequently heated at 200° C; D, tube plated, heated at 440° C and "tongue" cut. A 3/16-in. ball bearing (indicated by arrow) is resting on the depressed "tongue" surface.

sile stresses in the surface layers of the specimens are considered to lower the endurance limit of the material. Hume-Rothery [13] reported tensile stresses as high as 50,000 lb/in.^{2} in electrolytically deposited chromium. Brenner, Burkhead, and Jennings [9] reported that the residual tensile stresses in chromium plated to a thickness of 8×10^{-4} in. increased from approximately 15,000 lb/in.^{2} for a bath temperature of 50° C to over 60,000 lb/in.^{2} for chromium plated from a bath at 85° C. The endurance limit of specimens plated at 55° C was higher than that of specimens plated at 70° C and very much higher than that of specimens plated at 85° C. This is to be expected if the internal stress in the chromium plate increased with the temperature of the plating bath in accordance with Brenner's findings.

The formation of cracks in chromium plating is usually attributed to the rupture of the deposit as the result of high residual tensile stresses [9]. The presence of cracks in the chromium, therefore, indicated at least partial relief of residual stresses. Specimens having the largest number of cracks per unit area, discussed above, would be expected to have the lowest residual stresses, and the residual stresses would be greater as the cracks per unit area decreased (and as the plating temperature increased).

Hidnert [14] showed that an electrodeposited chromium specimen, on the first heating to 500° C, decreased in length and that during the cooling to room temperature it continued to decrease in length. The net decrease in length amounted to 1.1 percent. Hidnert's results showed an inflection in the heating curve at about 300° C. Preliminary results of a current investigation by the author indicate that there is an inflection in the temperature-electrical resistivity curve at about this same temperature. Hidnert did not give any data for specimens heated to 200° C and cooled to room temperature. In the present investigation, the densities of tubes of chromium were determined for each of the following conditions: "as deposited," after heating at 193° C (in boiling ethylene glycol) and after a second heating in helium at 440° C. The densities were 6.95 g/cm^3 as plated, 7.01 g/cm^3 after heating at 193° C, and 7.09 g/cm^3 after heating at 440° C. Brenner [9] indicated that changes in the volume of chromium on heating were isotropic. Hence, heating at 200° C would tend to reduce the volume of the plated chromium. If the chromium was restrained from contracting, as for example by being plated on steel, residual tensile stresses would be set up in the chromium that might be expected to lower the endurance limit. That such stresses do exist in chromium plated on steel is shown in figure 8, B and C. Thin-walled steel tubes were annealed, pickled to remove scale, and chromium plated. Tube B, figure 8, was heated at 200° C for 6 hours, and a "tongue" was subsequently cut in the tube. The deflection shown indicated that there had been residual tensile stresses in the chromium. The tongue was cut in tube C after plating and was deflected only a small amount. Heating at 200° C, however, caused the chromium to contract in volume and produced the deflection shown.

Heating of chromium at a temperature of 440° C produced, as indicated by the density data, more than twice the contraction obtained by heating at 193° C. It is suggested that if a chromium-

plated steel specimen is heated to 440° C, the concurrent expansion of the steel and contraction of the chromium stresses the chromium above its ultimate tensile strength at that temperature, consequently relieving the internal stresses at least in part. This is illustrated on figure 8, tube D, which was heated to 440° C for 1 hour, after plating, but prior to cutting of the tongue. In the figure, a $\frac{3}{16}$-in. ball is resting on the free end of the tongue, which is depressed below the surface of the tube. The tongue deflected so that the chromium was on its convex surface. This indicated that the chromium had been permanently elongated during the heat treatment due to expansion of the steel; there had been either plastic flow or fractures in the chromium or both.

On the basis of the foregoing discussion, it is postulated that the residual tensile stresses in electrodeposited chromium are a major factor in adversely affecting the endurance limits of steel upon which the chromium is plated. Heating at temperatures of 100° to 300° C tends to contract the chromium; the underlying steel resists this contraction, thus producing increased tensile stresses in the chromium and further reducing the endurance limit. Contraction of the chromium during heating at 400° and 440° C, coupled with the expansion of the steel at these temperatures, stressed the chromium beyond its ultimate tensile strength, produced permanent deformation, and hence relieved the stresses in the chromium to some extent with resulting increases in endurance limits of the plated specimens so treated.

V. Summary

1. Chromium plating of SAE X4130 and 6130 steels reduced the endurance limits of these materials, as determined in the rotating-beam type of test.

2. The endurance limits of these steels plated under a given set of conditions generally decreased with increased hardness of the steel. For a steel of a given hardness (Rockwell 40–C), the reductions in endurance limit increased with increased plating bath temperatures.

3. The endurance limits of specimens plated, and subsequently surface ground, were equal to or greater than those of unground specimens having the same final plating thickness. Interruption of the plating process did not affect the endurance limit of the plated specimens, provided that proper precautions for plating chromium on chromium were taken before the plating was resumed.

4. The endurance limits of specimens heated after plating and tested at room temperature reached a minimum value for a baking temperature between 190° and 300° C. Endurance limits of specimens heated for 1 hour at 440° C were significantly higher than those of the "as plated" steel.

5. Reduction of the endurance limits of steel by chromium plating is believed to be due, in part at least, to residual tensile stresses in the chromium. Heating of chromium increased its density and hence decreased its volume. It is postulated that heating at low temperatures increased the residual tensile stresses in the chromium; at sufficiently high temperatures, the concurrent contraction of the chromium and expansion of the steel stressed the chromium above its ultimate tensile strength, thus relieving some of the residual tensile stresses in the chromium and increasing the endurance limit of the plated specimens.

The author gratefully acknowledges the valued advice, aid, and assistance of the following in various phases of this investigation: Naval Aircraft Factory, Philadelphia; N. E. Promisel, Chief Metallurgist, Bureau of Aeronautics, Navy Department, Washington; William Blum and Vernon Lamb of the Bureau's Electrodeposition Section, Harold Hessing, Houston Babb, Thomas P. Royston, Jr., Irene C. Minor, and Lura F. Rochl of the Metallurgy Division of the Bureau. Harold E. Francis, Guy R. McConnell, Richard C. Rohan, and Molly Thompson, formerly of the Metallurgy Division, also assisted in the investigation.

VI. References

[1] W. H. Swanger and R. D. France, National Bureau of Standards. Unpublished.

[2] H. Wiegand and R. Scheinost, Endurance strength of hard chromium plated parts, Z. Ver. deut. Ing. **83,** 655 (1939).

[3] Chromium plating, Bibliography and Correlated Abstract, by M. Kolodney, for War Metallurgy Committee, Information Release No. 4, p. 49 (July 1943).

[4] Metals Handbook (Am. Soc. Metals) p. 120, 1948 ed.

[5] S. P. Makariewe and N. D. Birükoff, The influence of dissolved hydrogen on the hardness of electrolytic chromium, Z. Elektrochem. **41,** 623 (1935).

[6] E. V. Potter and H. C. Lukens, Hydrogen content of electrolytic chromium and its removal, Metals Tech. **15** (January 1948) T. P. 2312.

[7] C. A. Snavely, A theory for the mechanism of chromium plating; a theory for the physical characteristic of chromium plate; Preprint 92–35, Electrochem. Soc. (1947).

[8] C. A. Zapffe and M. E. Haslem, Measurement of embrittlement during chromium and cadmium electroplating and the nature of recovery of plated articles, Trans. Am. Soc. Metals **39,** 241 (1947).

[9] A. Brenner, P. Burkhead, and C. Jennings, Physical properties of electrodeposited chromium, J. Research NBS **40,** 31 (1948) RP1854.

[10] L. Mehr, T. T. Oberg, and J. Teres, Fatigue limit of chromium plated steel, Monthly Rev. Am. Electroplaters Soc. **34,** 1345 (1947).

[11] J. A. Bennett, A study of the damaging effect of fatigue stressing on SAE X4130 steel, J. Research NBS **37,** 123 (1946) RP1733.

[12] J. O. Almen, Shot blasting to increase fatigue resistance, SAE Trans. **51,** 248 (1943).

[13] W. Hume-Rothery and M. R. J. Wyllie, The structure of electrodeposited chromium, Proc. Roy. Soc. (London) [A] **181,** 331 (1943).

[14] P. Hidnert, Thermal expansion of electrolytic chromium, J. Research NBS **26,** 81 (1941) RP1361.

Washington, March 30, 1949.

U. S. Department of Commerce
National Bureau of Standards

Research Paper RP2012
Volume 43, August 1949

Part of the Journal of Research of the National Bureau of Standards

Heats of Combustion and Formation of Cyclopropane[1]

By John W. Knowlton [2] and Frederick D. Rossini

The data of this investigation give $\Delta Hc^\circ = -2091.38 \pm 0.54$ absolute kilojoules (or -499.85 ± 0.13 kcal) per mole, at 25° C for the heat of combustion of gaseous cyclopropane in oxygen to form gaseous carbon dioxide and liquid water. With this value, the heat of formation of gaseous cyclopropane, from solid carbon (graphite) and gaseous hydrogen each in its thermodynamic standard reference state, is calculated to be $\Delta Hf^\circ = +12.74 \pm 0.14$ kcal/mole, at 25° C. The heat of isomerization of gaseous cyclopropane into gaseous propylene is calculated to be $\Delta H^\circ = -7.86 \pm 0.18$ kcal/mole, at 25° C.

I. Introduction

Two determinations of the heat of combustion of cyclopropane are reported in the literature, one by Thomsen [1] [3] in 1886 and one by Berthelot and Matignon [2] in 1893. The values differ by 7.5 kcal/mole or 1.5 percent of the measured value. Because of the increasing importance of cyclopropane in science and industry, it was desirable to determine the heat of combustion of cyclopropane with present-day apparatus and materials. This report gives the results of measurements of the heat of combustion of cyclopropane and calculations of its heat of formation from the elements and its heat of isomerization to propylene.

II. Unit of Energy, Molecular Weights, Uncertainties

The unit of energy upon which values reported in this paper are based is the absolute joule, derived from mean solar seconds and absolute ohms and volts, in terms of which certification of standard resistors and cells is made by this Bureau. For conversion to the conventional thermochemical calorie, the following relation is used [3,4]:

1 calorie = 4.1840 absolute joules.

The molecular weight of water, the mass of which was used to determine the amount of reaction, was taken as 18.0160 from the 1947 table of international atomic weights [5].

The uncertainties assigned to the various quantities dealt with in this paper were derived, where possible, by a method previously described [6].

III. Method, Apparatus, and Materials

The same method and apparatus were used as in the investigation on the heat of combustion of propylene previously reported by the same authors [7].

The cyclopropane was prepared from commercial cyclopropane of anesthetic grade manufactured by the Monsanto Chemical Co. In this laboratory, the cyclopropane was purified by fractional distillation with the same apparatus and procedure as was used for propylene [7]. The center half of the distillate was selected as the "best" portion. The purity of this cyclopropane was determined from measurements of freezing points, according to a procedure previously described [8,9,10], with the following results: freezing point of the actual sample, in air at 1 atmosphere, -127.53 ± 0.01 deg C; calculated freezing point for zero impurity, in air at 1 atmosphere, -127.42 ± 0.04 deg C; calculated amount of impurity, 0.0034 ± 0.0012 mole fraction. It is calculated that the effect on the heat of combustion of this amount of the most probable impurity, propylene, would be 0.005 percent.

In the combustion of cyclopropane, the products contained carbon monoxide in an amount, on the average, corresponding to 0.00028 ± 0.00007

[1] This investigation was completed in 1940, but the preparation of the results for publication was delayed by the transfer of the senior author to work in the U. S. Bureau of Agricultural and Industrial Engineering and the U. S. Bureau of Mines.

[2] Deceased.

[3] Figures in brackets indicate the literature references at the end of this paper.

TABLE 1. *Calorimetric results of the electrical energy experiments for cyclopropane*

Number of experiments	ΔR [1]	k	K	U	Electrical energy [2]	Mass of calorimeter water	Energy equivalent calorimeter system [3]	
							Mean	Standard deviation of the mean
	Ohm	min^{-1}	*Ohm*	*Ohm*	*abs j*	*g*	*abs j/ohm*	*abs j/ohm*
12	0.389772 to 0.413989	0.001949 to 0.002000	0.009928 to 0.010434	0.000234 to 0.001080	57,087.5 to 60,918.3	3542.85 to 3551.41	150,746.2	±9.9

[1] The average temperature of the calorimeter was between 24.97° and 25.03° C in all experiments except one in which the average temperature was 25.09° C.
[2] The time of electrical energy input was 1500.00 sec. in each experiment except one where the time was 1440.00 sec.
[3] Adjusted to 3550.00 g of water and an average temperature of 25.00° C.

TABLE 2. *Calorimetric results of the reaction experiments for cyclopropane*

Number of experiments	ΔR [1]	k	K	U	Electrical energy equivalent of calorimeter system [2]	"Gas" energy [3]	"Vaporization" energy	Mass of water formed in the reaction [4]	Heat of combustion [5] ($-\Delta Hc$)	
									Mean	Standard deviation of the mean
	Ohm	min^{-1}	*Ohm*	*Ohm*	*abs j/Ohm*	*j*	*j*	*g*	*abs kj/mole*	*abs kj/mole*
14	0.395633 to 0.397962	0.001951 to 0.001999	0.009555 to 0.010429	0.000237 to 0.000609	150,453 to 150,833	−5.3 to 11.7	−268.8 to −310.0	1.50845 to 1.51795	2091.33	±0.18

[1] The average temperature of the calorimeter was between 25.01° and 25.02° C in all experiments.
[2] Corrected to the actual mass of water in the calorimeter can in each experiment and including the heat capacity of one-half the mass of water condensed in the reaction.
[3] The "ignition" energy was 22.4 j in each experiment except in two experiments where it was 31.4 j and 33.6 j due to the use of sparking times of 14 and 15 sec, respectively, instead of the usual 10 sec.
[4] The amount of reaction was determined from the mass of water formed in the combustion.
[5] Includes a correction of +0.011±0.003 percent because of the presence of a small amount of carbon monoxide in the exit gases.

mole fraction of the total carbon.[4] This necessitated a correction (see next section) of +0.011 ±0.003 percent to the observed heat evolved in the calorimetric combustion experiments in order to obtain the heat that would have been evolved had all the carbon appeared as carbon dioxide. In eleven experiments in which the masses of water and carbon dioxide formed in the combustion were determined, with correction made for the 0.00028 mole fraction of carbon not formed as carbon dioxide, the mean value of the ratio of the number of moles of carbon dioxide to the number of moles of water was 0.99989 with a standard deviation of ±0.00006.

IV. Results

The experimental results on the determination of the energy equivalent of the calorimeter system are summarized in table 1, which gives the following data: the number of experiments performed; the minimum and maximum values of ΔR, k, K, U, electrical energy, mass of calorimeter water; and the energy equivalent of the calorimeter system, the mean value of the energy equivalent of the calorimeter system and its deviation. The symbols have the same significance as in earlier reports [7, 13].

The "ignition energy" was determined to be 22.4 joules for a time of sparking of 10 sec.

The experimental result of the calorimetric combustion experiments are summarized in table 2, which gives the following data: the number of experiments; the minimum and maximum values of ΔR, k, K, U, energy equivalent of the calorimeter system (calculated from the mean value as given in table 1, corrected to the actual mass of water in the calorimeter can in each experiment, and including one-half the mass of water condensed in the reaction), "gas" energy, "vaporization" energy, mass of water formed; and the mean value of the heat of combustion in absolute kilojoules/mole cyclopropane and its standard deviation.

Conversion of the observed mean value of the

[4] The tests for carbon monoxide were kindly made by E. C. Creitz of the Gas Chemistry Section of this Bureau.

heat of combustion to the value for the standard heat of combustion, with each substance in its thermodynamic standard state, involves addition of 0.05 kilojoules/mole to the mean value of $-\Delta Hc$ given in table 2. This correction is taken to be the same as that for propylene [11]. Accordingly, the present investigation yields for the standard heat of combustion at 25° C:

$$C_3H_6 \text{ (gas, cyclopropane)} + 4\tfrac{1}{2}\ O_2 \text{ (gas)} = 3CO_2 \text{ (gas)} + 3H_2O \text{ (liquid)};$$

$$\Delta Hc^\circ_{298.16} = -2091.38 \pm 0.54 \text{ kilojoules/mole or } -499.85 \pm 0.13 \text{ kcal/mole} \quad (1).$$

Combination of the value in eq 1 with the values for the heats of formation of water and carbon dioxide [12] yields for the standard heat of formation at 25° C:

$$3C \text{ (solid, graphite)} + 3H_2\text{(gas)} = C_3H_6 \text{ (gas, cyclopropane)};$$

$$\Delta Hf^\circ_{298.16} = +12.74 \pm 0.14 \text{ kcal/mole.} \quad (2)$$

Combination of the value in eq 2 with the value for the heat of formation of propylene [11] yields for the heat of isomerization of cyclopropane into propylene:

$$C_3H_6 \text{ (gas, cyclopropane)} = C_3H_6 \text{ (gas, propylene)};$$

$$\Delta H^\circ_{298.16} = -7.86 \pm 0.18 \text{ kcal/mole.} \quad (3)$$

Comparison of the results of the present investigation with the data previously reported by Thomsen [1] and Berthelot and Matignon [2] is given in table 3.

TABLE 3. *Comparison of the present with previous results on cyclopropane*

Investigators	Heat of combustion of cyclopropane, ΔH, at at 25° C	Heat of isomerization of cyclopropane to propylene, ΔH at 25° C
	kcal/mole	*kcal/mole*
Thomsen [1]	−499.2	−7.0
Berthelot and Matignon [2]	−506.7	−7.8
Present	−499.85±0.13	−7.86±0.18

V. References

[1] J. Thomsen, Thermochemische Untersuchungen **IV** (Barth, Leipzig, 1886).

[2] M. Berthelot and C. Matignon, Ann. Chim. Phys. [6] **30,** 561 (1893).

[3] E. F. Mueller and F. D. Rossini, Am. J. Phys. **12,** 1 (1944).

[4] Selected Values of Chemical Thermodynamic Properties. Values of constants (National Bureau of Standards, Dec. 31, 1947).

[5] G. P. Baxter, M. Guichard, and R. Whytlaw-Gray, J. Am. Chem. Soc. **69,** 734 (1947).

[6] F. D. Rossini and W. E. Deming, J. Wash. Acad. Sci. **29,** 416 (1939).

[7] F. D. Rossini and J. W. Knowlton, J. Research NBS **19,** 249 (1937) RP1024.

[8] A. R. Glasgow, Jr., A. J. Streiff, and F. D. Rossini, J. Research NBS **35,** 355 (1945) RP1676.

[9] A. R. Glasgow, Jr., N. C. Krouskop, J. Beadle, G. D. Axilrod, and F. D. Rossini, Anal. Chem. **20,** 410 (1948).

[10] B. J. Mair, A. R. Glasgow, Jr., and F. D. Rossini, J. Research NBS **26,** 591 (1941) RP1397.

[11] E. J. Prosen and F. D. Rossini, J. Research NBS **36,** 269 (1946) RP1702.

[12] D. D. Wagman, J. E. Kilpatrick, W. J. Taylor, K. S. Pitzer, and F. D. Rossini, J. Research NBS **34,** 143 (1945) RP1634.

[13] F. D. Rossini, BS J. Research **6,** 1 (1931) RP 259; **7,** 329 (1931) RP343.

WASHINGTON, March 24, 1949.

U. S. Department of Commerce
National Bureau of Standards

Research Paper RP2013
Volume 43, August 1949

Part of the Journal of Research of the National Bureau of Standards

Influence of Strain Rate and Temperature on the Creep of Cold-Drawn Ingot Iron

By William D. Jenkins and Thomas G. Digges

A study was made of the effects of variations in both strain rate and temperature on the creep characteristics in tension of cold-drawn ingot iron. The third stage of creep began without necking or without the presence of cracks of microscopic dimensions, but considerable necking occurred in all specimens tested to fracture. The resistance to creep in the second stage and the resistance to fracture increased as the test temperature was decreased. The stress required to initiate fracture also increased as the strain rate increased. The general trend was for the ductility at fracture to increase with an increase in the strain rate and the plastic extension at fracture to decrease with an increase in temperature.

The plastic extension at the beginning of the third stage was less than about 1 percent, except in specimens tested at relatively high strain rates or at a low temperature.

I. Introduction

The influence of strain rate and temperature on the mechanical properties of Monel and oxygen-free high-purity copper and the progress of fracture during creep of these metals were discussed in some detail in a previous paper [1].[1] The evidence presented indicated that the ductility of both metals increased with increase in strain rate and with decrease in temperature. The third stage of creep was sometimes initiated by the formation of microscopic cracks and with sufficiently slow strain rates at elevated temperature, specimens of both metals failed without local contraction. Since Monel and copper are face-centered cubic metals, the program on creep testing was extended to include a study of the behavior of body-centered cubic iron as affected by variations in strain rate and in temperature, and the results are given in the present paper.

Jenkins and Mellor [2] determined some properties of ingot and other commercial iron in tension tests made in vacuum at elevated temperatures and with different strain rates. In short-time tests of ingot iron, initially as hot-rolled or normalized, the reduction of area increased from 73 percent at room temperature to 78 percent at 550° C and then decreased with further increase in temperature; the reduction of area at 350° C was less than at room temperature. At 350° C, the reduction of area in a long time test (46 hrs) was greater than in a short time test (75 and 64%, respectively), whereas at all the higher temperatures used the reduction of area of the ingot iron was lower in creep than in the short time test. However, the creep tests were of relatively short duration and the strain rates in the second stage were not given. Tapsell and Clenshaw [3] made a study of the high-temperature properties of normalized ingot iron. Creep tests were made with different strain rates at temperatures ranging from about 450° to 900° F for periods ranging from 2 to 70 days. The investigation with this iron was extended by Tapsell [4] to include creep tests at lower temperatures, Brinell hardness measurements at room temperature, and stress-strain curves at elevated temperatures of some of the specimens previously extended in creep, but the ductility of these specimens was not given.

II. Material and Procedures Used

The chemical composition, ferrite grain size, tensile properties, and hardness at room temperature of the ingot iron used in the initial condition as cold-drawn, approximately 13-percent reduction (in area) are given in table 1.

The apparatus used for carrying out the creep tests was the same as that described in some detail

[1] Figures in brackets indicate the literature references at the end of this paper.

TABLE 1. *Chemical composition and mechanical properties of the ingot iron used*

The iron was initially in the form of a ¾-in. round bar as cold-drawn approximately 13-percent reduction in area

Composition (percentage by weight)	
Carbon	0.019
Manganese	.029
Phosphorus	.005
Sulfur	.018
Silicon	.005
Chromium	Nil
Copper	0.05
Oxygen	.080
Nitrogen	.0004
Hydrogen	Nil
Property [a]	
ASTM Grain No. Avg lower	5
Rockwell Hardness, B scale	77
Tensile strength,[b] 1,000 psi	60.0
Yield strength, 1,000 psi	47.2
Elongation, percent in 2 in.	20.6
Reduction of area, percent	68.2

[a] As determined at room temperature.

[b] Drop of beam.

by Bennett and McAdam [5]. All specimens used for creep testing were prepared from the same bar as cold-drawn, and these specimens were machined to American Society for Testing Materials Standard for 0.505 in. diameter with 2 to 4 in. gage lengths. Each specimen used for determining creep was heated in air (furnace atmosphere not controlled) to the desired temperature and held for 48 hr before loading. The load was applied in selected increments in order to produce an approximate rate of extension of 30 to 50 percent per 1,000 hr until the desired ultimate load for testing was attained; in one test the specimen was intentionally loaded at a relatively slow rate of 3-percent extension in 1,000 hr. Thereafter the load was not changed on any specimen until the test was either completed or the third stage was reached. For specimens tested to fracture, the rate in the third stage was maintained approximately constant and equal to that in the second stage by repeatedly decreasing or adjusting the load. This procedure of maintaining a constant

TABLE 2. *Summary of conditions used and results of creep tests on ingot iron initially as cold-drawn, 13-percent reduction in area*

Temperature	Strain rate [a]	Ultimate stress	Beginning of third stage			End of test							Remarks
			Time	Plastic extension	True stress	Time	Plastic extension	Reduction of area	L/L_0	A_0/A	True stress	Hardness, Rockwell B[b]	
°F	%/1,000 hr	1,000 lb/in.²	hr	%	1,000 lb/in.²	hr	% in 2 in.	%			1,000 lb/in.²		
70	7×10^4	60.0	0.72	8.8	65.2	1.2	20.3	68.9	1.20	3.21	120.0	77	Test made at room temperature on specimens as cold-drawn.
70	6×10^4	60.0	.51	7.0	65.3	1.1	21.0	67.5	1.21	3.08	117.5	77	Do.
Avg				7.9	65.3	1.2	20.6	68.2	1.20	3.15	118.7	77	
500	14.5	42.8	238	3.8	44.5	2,588	[c] 37.3	50.5	1.37	2.0	70.6	69	Test stopped as load dropped sharply, indicating the start of fracture.
600	0.45	30.0	862	0.65	30.2	1,249	1.0	0.91	1.01	1.01	30.3	66	Test stopped after beginning of third stage.
600	1.60	33.3	295	.72	33.6	9,556	[c] 16.5	56.6	1.17	2.30	49.6	65	Tested to fracture.
600	380	37.1	5.6	1.73	37.9	130	50.0	70.7	1.50	4.30	80.8	65	Do.
600	1,340	39.5	5.0	5.60	41.9	46.8	65.1	82.5	1.65	5.72	102.4	65	Do.
700	0.06	20.7	6,500	0.63	20.8	7,727	[c] 0.72	0.08	1.01	1.00	20.7	60	Test stopped after beginning of third stage.
700	.39	22.5	863	.62	22.7	3,350	[c] 1.70	1.29	1.02	1.013	22.1	60	Do.
700	2.63	24.4	171	.65	24.6	5,802	[c] 16.4	44.7	1.16	1.81	30.2	62	Tested to fracture.
[d] 700	3.0	28.5	315	.87	28.7	3,676	[c] 11.2	45.4	1.11	1.83	39.0	62	Tested to fracture; loaded slowly.
700	46.0	28.5	9.4	.66	28.7	590	28.8	45.6	1.29	1.84	36.0	63	Tested to fracture.
800	5.1	18.8	108	.71	18.9	168	1.1	2.0	1.01	1.02	19.2	56	Test stopped after beginning of third stage.
800	17.0	20.5	41	.80	20.7	53.8	1.2	1.0	1.01	1.01	20.7	56	Do.
800	42.0	23.6	8	.50	23.7	225	[c] 9.2	42.3	1.09	1.72	30.9	54	Tested to fracture.

[a] Except for the tension tests made at 70° F (room temperature), the strain rate is the average value obtained during the second stage. The strain rate during the third stage of specimens tested to fracture was maintained nearly constant and equal to that in the second stage by repeatedly decreasing the load during the third stage. The specimens tested at elevated temperatures were loaded at a rate of 30- to 50-percent extension in 1,000 hr in the first stage.

[b] Hardness measurements were made on the undeformed (shoulder) of the specimens after testing in tension.

[c] Plastic extension, percent in 4 in.

[d] The specimen was loaded at a rate of 3-percent extension in 1,000 hr in the first stage.

rate beyond the beginning of the third stage was considered essential in this study for, as pointed by McAdam and coworkers [1], when a creep test is made under a constant load the increasing rate in the third stage tends to cause an increase in ductility at fracture. The conditions used in making the creep tests are given in table 2. Tests were made at 600°, 700°, and 800° F with different strain rates and, in addition, a specimen was tested at 500° F. In some cases, the test was discontinued after the beginning of the third stage of creep, whereas with other specimens the loads were adjusted and maintained until fracture occurred.

Rockwell B hardness (100-Kg load, $\frac{1}{16}$-in. diameter ball) measurements were made on the cross section of the bar initially as cold-drawn and on selected specimens after testing in creep. The amount of plastic deformation of each specimen fractured in creep varied over the "necked" section (local contraction). Two flats 180° apart were prepared parallel to the longitudinal axis of the specimens after fracturing, and Rockwell readings were made at room temperature at various points along the center line of these flats. The diameters of the specimen at the points of indentation were accurately determined by means of a measuring microscope. As the shoulder of the tensile specimen (fig. 7) was not deformed during creep but was exposed to the same temperature for the same time as the plastically deformed section, the hardness value obtained on the shoulder was used as the basis for determining the change in hardness due to plastic deformation and the accompanying strain hardening, aging, and recovery during the creep tests.

In the tension tests made at room temperature, the specimens were extended at a rate of about 6 to 7×10^4 percent per 1,000 hr to the maximum load, after which the load was gradually reduced so as to produce a nearly constant rate of reduction in area during the remainder of the test. The change in diameters of the specimens during the course of the test was followed with a micrometer. Usual procedures were followed in preparing specimens and carrying out the microscopic examination.

III. Results and Discussion

The results obtained in the creep tests are summarized in table 2 and figures 1 to 13.

Representative extension-time curves for some of the specimens tested either to the beginning of the third stage or to complete fracture are reproduced in figures 1 and 2, respectively. As is illustrated by the shape of curves A and B in figure 1, the change in extension with time in the second stage frequently did not occur uniformly but varied in a cyclic manner. During the time of a cycle, the change in extension ranges from relatively high to low or negative values. That is, a period of acceleration in high strain rate was followed by negative creep (contraction of specimen) and vice versa. The frequency and amplitude of these cycles apparently depended upon the temperature, strain rate, and the time elapsed in the second stage of creep. The trend was for both the frequency and amplitude of the cycles to decrease with an increase in either temperature (curves A and B) or strain rate (curves B and C) and also to decrease as the deformation or time approached the beginning of the third stage of creep. It is believed that the cycles result from a combination of strain hardening, strain aging, and recovery (annealing) of the ingot iron. At sufficiently high strain rates and temperatures, strain aging was not manifested in the shape of the extension-time curve, and the creep rate was nearly constant in the second stage (curve C). Because of the described behavior of some of the test specimens, the *average* and not the *minimum* values for creep during the second stage are given in table 2 and the several figures in this report; obviously, in some tests, the miminum creep rate actually was a negative value, and in other tests it corresponded to the average rate.

The time required to complete the third stage of creep under a controlled condition of constant rate was often considerably greater than the total time elapsed during the first and second stages (fig. 2). As is shown by the positions of the points as plotted in figure 2, the rate during the entire third stage could be maintained at a desired and nearly constant value by the procedure of adjusting the load on the specimen; usually the rate increased somewhat just prior to complete fracture of the specimen due to a "rim" effect [1].

The relation between true stress [2] and creep rate in the second stage of tests made at different temperatures is shown in figure 3. With the se-

[2] The "true stress" is that value obtained by dividing the current load by the current minimum area of the specimen.

lected rate of loading (30- to 50-% extension per 1,000 hr in the first stage of creep), the experimental values obtained at test temperatures of 600°, 700° and 800° F do not fall on a straight line when plotted on logarithmic coordinates. The trend was for the curves drawn through the experimental values to deviate from liniarity by bending downward with the slower, and upward with the higher ranges in strain rates used at each temperature; the tests at 800° F were not extended to relatively slow rates, but it would be expected that the results of such tests would also follow the downward path. Although the stress-strain rate curves follow the same general pattern, it is noteworthy that the curves are not parallel, and the relative positions where the bends occurred were influenced by the temperature of testing. Thus, the pronounced downward curvature was shifted to a lower creep rate as the temperature was changed from 600° to 700° F and the upward curvature to higher rates as the temperature decreased. Similar trends are shown in the curves obtained when the experimental values for true stress are plotted against the logarithm of the strain rate. The shape of the stress-strain rate curve was not established at 500° F as only one creep test was made at this temperature. 500° F is within the so-called "blue heat" region where the effects of strain aging attain a maximum, as shown by the results of short-time tensile tests. It is to be expected, however, that this region would shift to a different range in temperature as the amounts of prior cold-working and creep rates are changed. According to Greaves and Jones [6], a maximum in the tensile strength-temperature curve of ingot iron occurred at about 300° F with relatively slow loading and at 700° F with fast loading. The relatively high ductility of the specimen tested at 500° F (fig. 6 and table 2) indicates that the conditions were such as to be above the blue heat range.

The use of a linear relationship in either a log-log or semi-log plot of true stress versus strain rate is not justified for extrapolating for very long service life of the initially cold-worked ingot iron at 600° or 700° F. Such an extrapolation would result in premature failure.

The resistance to creep at 700° F was materially increased by decreasing the rate of extension in the first stage during loading from about 40 to 3 percent per 1,000 hr; the plastic extension of fracture was also affected by variation in rate of loading (fig. 6). In previous investigations but little attention has been given to controlling the rate of extension during the first stage of creep, and this is a factor that merits further study. The results obtained with the two specimens loaded at different rates again serve to emphasize the importance of accurately controlling the conditions encountered in creep testing.

The effect of temperature on the resistance to creep of ingot iron is shown by a comparison of the positions of the stress-strain rate curves (fig. 3) and by the derived stress-temperature curves for creep rates of 1, 5, 10, and 50 percent per 1,000 hr, as given in figure 4. With the semi-log plot used (fig. 4), the curves were not exactly linear, and their slopes varied somewhat with strain rates; the trend was for the family of curves of figure 4 to diverge as the temperature was increased. Obviously, the resistance to creep, that is, the stress required to produce a selected creep rate, increased as the temperature decreased.

As is illustrated in figure 5, the true fracture stress increased with an increase in strain rate (temperature constant) and with a decrease in test temperature (strain rate constant).

The influence of strain rate on the ductility of specimens tested in creep at different temperatures is shown in figure 6. Variations within the range of strain rates used had no significant effect on the plastic extension at the beginning of the third stage of creep of the specimens tested either at 700° or 800° F. Furthermore, the extension at the beginning of the third stage of specimens tested at 600° F with strain rates less than about 2 percent per 1,000 hr was about the same as that obtained in the tests at 700° and at 800° F; the extension of each of these specimens was less than 1 percent. However, the extension at the beginning of the third stage of creep was materially increased in specimens tested at 600° F by increasing the strain rate to relatively high values and also in another specimen tested at a lower temperature (500° F) with a strain rate of only about 15 percent per 1,000 hr. The result of this latter test supports the belief that the relation between strain rate and plastic extension at the beginning of the third stage of creep of specimens tested at 500°, 700°, and 800° F is represented by a family of curves similar in shape to that obtained at 600° F; the start of the bend in these curves is

displaced to a lower strain-rate value at 500° F, and to higher values at 700° and 800° F, than that at 600° F. That is, the point of divergence in the curve is shifted to a lower creep rate as the temperature of the test is decreased, and at 500° F a strain rate of 15 percent per 1,000 hr is considerably above this point.

At 600° F, the ductility at fracture, as determined both by plastic extension and reduction of area, decreased with a decrease in strain rate. At 700° F, the extension also decreased with a decrease in strain rate, whereas the reduction of area was not appreciably affected by this change. At 800° F, the plastic extension at fracture of a specimen tested at a strain rate of about 45 percent per 1,000 hr was considerably less than that of a specimen tested at 700° F at the same rate, but values for the reduction of area of the two specimens at fracture were nearly alike.

For a selected strain rate, the plastic extension at fracture decreased continuously as the temperature of the creep test increased, but no consistent relationship was obtained between temperature and the reduction of area. It is to be expected that the temperature might affect differently the ductility as determined by extension and reduction of area, as the stress during the third stage of creep was not unidirectional. Although the strain rate was controlled and maintained nearly constant in this stage, considerable necking occurred in each specimen tested to fracture. In some cases, the necking was confined principally to a relatively narrow region in the vicinity of the fracture (fig. 7, B), whereas in other specimens there was a more gradual necking over a considerable portion of the gage length (fig. 7, A). Both the extension and reduction of area were affected by the manner in which the specimen necked, but not necessarily to the same degree.

Since the described trends for the ductility to increase with an increase in strain rate and with a decrease in temperature were shown in the creep tests, it is of particular interest to compare some of the values for ductility at 600° F (fig. 6) with that obtained at room temperature in ordinary tension tests (table 2). Although the latter tests were made at a considerably faster rate and lower temperature than the former (both factors tend to cause an increase in ductility in creep), the values for plastic extension and reduction of area at fracture in the room-temperature tests were significantly lower than the maximum attained at 600° F. The combined effects of strain rate, aging, and temperature on the ductility of ingot iron vary appreciably depending on the testing conditions. Evidently the strain rate-temperature and temperature-ductility curves for this material would show a reversal in curvature when the testing conditions are changed from the high strain rates used in creep at elevated temperature to considerably higher strain rates obtained in the tension test at atmospheric temperatures; the reversals may even occur in the low-temperature range used in the creep tests.

The relation of fracture stress to ductility in creep is shown in figure 8. At 600° F, the fracture stress increased continuously with an increase in both plastic extension and reduction of area. This trend for the fracture stress to increase with plastic extension was also obtained in two specimens tested at 700° F (loaded at the same rate), but there was a considerable difference in the stress at fracture of these specimens, although both had approximately the same reduction of area. This latter condition is also attributed to a difference in the manner of necking of the two specimens, as is illustrated by typical photographs given in figure 7. The fracture stress at 700° F of the specimen loaded relatively slowly in the first stage was somewhat higher than that of the specimens loaded at the higher rate; the plastic extension of the former specimen was also lower, but the reduction of area was approximately the same for each specimen. At 800° F, the fracture stress was less than that at 700° F when the specimens were tested at the same strain rate of about 45 percent per 1,000 hr, but it was of the same order of magnitude of that of a specimen tested at 700° F with a slower strain rate (2.6% per 1,000 hr).

As previously pointed out, the final ductility of a specimen of ingot iron tested in creep is affected by the strain rate and the temperature at which the test is made. Both of these factors also influence the stress necessary to cause fracture.

The influence of temperature on the resistance to plastic deformation in the early stage of creep of ingot iron is shown by the relative positions of the curves reproduced in figure 9. At 800° F, plastic deformation commenced with the application of a relatively small stress, whereas at 500° F the extension was elastic with stresses up to about 20,000 lb/in^2. The relation of temperature

TABLE 3. *Tensile properties at room temperature of specimens of ingot iron after extending at different temperatures and strain rates into the beginning of the third stage of creep and of specimens as aged at different temperatures*

All specimens were prepared from the same bar as initially cold-drawn, 13-percent reduction in area and were finally tested in tension at room temperature at an approximate strain rate of 7×10^4 %/1,000 hr

Temperature of creep test	Strain rate	Plastic extension at end of creep test	Yield stress [a]		Ultimate stress	Maximum load		Beginning of fracture		Complete fracture		
			Upper	Lower		Plastic extension	True stress [b]	Reduction of area	True stress [b]	Plastic extension	Reduction of area	True stress [b]
°F	%/1,000 hr	Percent	1,000 lb/in.²	1,000 lb/in.²	1,000 lb/in.²	Percent	1,000 lb/in.²	Percent	1,000 lb/in.²	Percent	Percent	1,000 lb/in.²
None [c]	------	------	47.2	47.1	60.0	7.9	65.3	63.2	103.4	20.6	68.2	118.7
None [d]	------	------	37.3	37.1	50.7	12.6	57.1	68.9	100.0	27.5	73.3	119.8
600	0.45	1.00	42.1	42.0	52.1	10.8	57.8	68.1	100.2	31.0	72.7	117.4
700	.39	1.60	39.1	36.9	48.8	15.8	56.5	69.5	97.7	27.0	73.0	112.2
700	.06	.72	38.6	37.3	48.6	14.3	55.5	69.4	98.2	24.0	72.9	111.0
800	5.10	1.11	40.1	36.3	48.9	16.4	57.0	66.6	98.7	34.5	71.7	114.9
800	17.0	1.20	38.1	36.3	49.1	16.6	57.3	69.4	98.7	34.5	74.0	116.7

[a] Drop of beam.
[b] The true stress is that value obtained by dividing the current load by the current minimum area of the specimen.
[c] Tension tests made in duplicate on specimens aged at room temperature and not tested in creep.
[d] Tension test made on a specimen aged at 800° F for 48 hr and not tested in creep.

to yield stress for 0.2 percent extension is given in figure 10. The yield strength decreases rapidly with increase in temperature used in the creep tests. However, the yield strength at 500° F was only slightly less than that obtained at room temperature in the ordinary tension test, which was also made at a considerably higher strain rate (40% and 7×10^4 % per 1,000 hr, respectively). Tension tests were not made at temperatures between 70° and 500° F, and the exact location of the yield stress-temperature curve was not established through this temperature range. However, according to Carpenter and Robertson [7], the yield (point) strength, in general, should decrease as the temperature of testing is raised. The hardness at room temperature of the specimens as exposed at the temperatures for the time used in the creep tests also decreased with an increase in temperature, and these values were appreciably lower than that of the original cold-worked iron.

The specimens tested into the third stage of creep (not fractured) were unloaded and then cooled in the furnace to room temperature. A summary of the results of measurements made at room temperature for change in diameter over the entire gage length and the determination of extension during creep of these five specimens (one specimen tested at 600°, two at 700°, and two at 800° F, table 2) showed no evidence of local contraction in four and only a very slight indication of necking in the other specimen (800° F with strain rate of 5.1% per 1,000 hr). Actually, a comparison of the values for extension during creep (L/L_0) [3] with comparable values for the reduction of area obtained after cooling to room temperature (A_0/A) indicate that there was a slight increase in volume of four of the specimens during creep. This is to be expected from cold-working, even when carried out under conditions where necking could not possibly occur. An oxide film formed on the specimens during exposure at test temperature, especially those at 800° F, but the change in volume from the presence of this film was negligible. These specimens were then tested in tension at room temperature under controlled conditions, as previously described. Another specimen as cold-drawn was heated at 800° F (highest temperature used in the creep tests) for 48 hr and then cooled to room temperature and tested in tension. The results of these tests are summarized in table 3 and figure 11.

The flow curves at room temperature for the two specimens previously extended at different rates to about 1 percent at 800° F are nearly alike, and the position of these curves was only slightly below that of the specimen aged only at 800° F. As all the specimens tested in creep were aged for this same period (48 hr) before loading, the small differences obtained in the stresses required to produce flow is believed to be due to the additional aging or recovery of the creep specimens during

[3] L_0 and A_0 are the initial gage length and area of cross section, respectively; L and A are the current length and area, respectively.

their longer exposure at 800° F. The results of hardness tests made at room temperature on undeformed sections of these specimens indicate that some additional softening occurred when the aging time exceeded 48 hr. The flow curves at room temperatue for the two specimens extended in creep at 700° F (not shown in fig. 11) were quite similar to that of the curve reproduced for the specimens tested in creep at 800° F; the former fall just below the latter curve. The resistance to flow at room temperature of the specimen extended at 600° F to the beginning of the third stage was somewhat greater than that of the specimens similarly extended at higher temperatures (700° and 800° F). As is to be expected, the resistance to flow of all the specimens aged at elevated temperatures was lower than that of the specimen aged at room temperature, but this decrease in flow stress was accompanied by a corresponding increase in ductility. The significant feature brought out by the tension tests at room temperature is that no appreciable deterioration in these mechanical properties of initially cold-drawn ingot iron resulted from its extension into the beginning of the third stage of creep (about 1% extension at 600°, 700°, or 800° F.

No cracks were visible on the surface of any of these specimens as extended into the third stage of creep. Furthermore, no indication of cracking was observed in a metallographic examination at magnifications of 500 to 1,000 diameters in the necked section extending from the axis to the surface of another specimen tested at 500° F to nearly the end of the third stage; that is, this particular creep test was carried out to the point where the load required to maintain a constant creep rate dropped sharply, and complete fracture would have occurred in a few minutes had the test continued without changing the load.

Determinations made on the specimens fractured in creep also supports the view that the third stage of creep was initiated in each specimen without the occurrence of necking. However, regardless of the rate of extension, some necking occurred during the third stage of creep in each specimen tested to complete fracture.

Some of the structural features of the ingot iron before and after testing in creep are illustrated by the typical photomicrographs reproduced in figure 12. The average size of the ferrite grains in the initially cold-drawn bar corresponds to the lower range of American Society for Testing Materials grain number 5 (fig. 12, A). These grains were elongated only slightly in the direction of cold-working, and the inclusions were frequently alined in streaks parallel to the direction of hot- and cold-working Some of these inclusions were fractured during the hot- and cold-working, but apparently no further change occurred in either their form or distribution during creep. Although the ingot iron contained the usual numerous oxides, these inclusions had no appreciable effect on the type of fracture produced in creep.

The fracture of the specimen tests at 600° F with a strain rate of 1.6 percent per 1,000 hr (fig. 12, B) was essentially transcrystalline, whereas the fractures of specimens tested with higher strain rates (380 and 1,340 percent per 1,000 hr) were partially intercrystalline but predominantly transcrystalline (fig. 12, C). The fractures of all specimens at 700° and 800° F were predominantly intercrystalline (fig. 12, D, E, and F).

The general tendency for the ferrite grains to elongate in the vicinity of complete fracture and to separate at points other than at complete fracture is also shown by a comparison of these photomicrographs. The maximum distortion of the grains during creep was obtained in a specimen tested at 600° F with a relatively high strain rate (fig. 12, C), and cracking was observed only in the region of complete separation; this specimen had a pronounced neck and relatively high ductility. Appreciable elongation of the grains also occurred in another specimen tested at 600° F with a creep rate of 1.6 percent per 1,000 hrs (fig. 12, B), but there was some separation of the grains in regions away from the position of complete fracture. The general trend was for the flow to increase with a decrease in test temperature and to increase with an increase in strain rate. The tendency for the ferrite grain to separate in the regions away from the position of complete fracture was promoted by decreasing the strain rate and by increasing the temperature. No appreciable difference was detected in the structure of the specimens near the center and surface in the vicinity of the fractures. Where minor differences were observed, possibly somewhat greater amounts of flow occurred at the surface than in the center.

The effect of plastic deformation during creep at different temperatures on change in hardness

at room temperature is shown by the results given in figure 13. The change in hardness as determined at room temperature was affected by the degree of plastic deformation, strain rate, temperature of the creep test, and rate of loading. For example, in a test made at 700° F with a strain rate of 2.63 percent per 1,000 hr, no change in hardness was observed with increase in plastic deformation up to 20-percent reduction in area, whereas in another test at 700° F, with a strain rate of 46 percent per 1,000 hr, the hardness increased as the specimen was deformed to this same degree. With further plastic deformation the propensity of each of these two specimens to strain harden (and age) was less than in their response to recovery (anneal), and both showed relatively rapid decrease in hardness as the deformation increased. At temperatures of 500° and 600° F, the maximum increase in hardness with plastic deformation was greater than that obtained at the higher test temperatures, and the peak in the curve also occurred at greater amounts of plastic deformation. The general trends were for the amount of induced hardness to increase with an increase in strain rate and with a decrease in both test temperature and rate of loading and the recovery to increase with an increase both in temperature and plastic deformation; the exception to this trend was that in the tests at 700° and 800° F with a strain rate of about 45 percent per 1,000 hr, slightly greater induced hardness was observed in the latter than in the former specimen.

The amount of uniform deformation in creep (extension to the beginning of necking) varied with the strain rate in that at a constant temperature (600° and 700° F, specimens loaded alike) the amount increased continuously as the strain rate increased. No consistent relationship, however, was shown between test temperature and the extent of uniform extension (constant strain rate).

A significant feature is the extent of this plastic deformation in creep before necking occurred. As already pointed out, the plastic extension at the beginning of the third stage was less than 1 percent in all specimens tested at slow strain rates, except one at 500° F with a strain rate of 14.5 percent per 1,000 hr; the extension at the start of the third stage was also greater than 1 percent in two specimens tested at 600° F with relatively high strain rates for testing in creep. Thus, in general, the initially cold-drawn specimens of ingot iron continued to extend uniformly in creep for an appreciable time after the start of the third stage.

It should be emphasized that the curves in figure 13 show the *change* in hardness at room temperature of specimens extended in creep at elevated temperatures, and the relative positions of these curves do not indicate the order or the actual hardness values of the test specimens during creep.

The hardness tests were extended to include specimens tested in tension at room temperature and aged at room or at elevated temperatures. A summary of these results (fig. 14) shows that there was a continuous increase in hardness with plastic deformation up to about 50-percent reduction in area; thereafter the hardness either remained constant or decreased as the distance from the point of fracture diminished. Although the general shape of the family of curves is quite similar, the hardness induced by plastic deformation was increased appreciably by heating at 500° or 800° F. This increase in hardness is believed to be due to a state of more complete aging at elevated temperatures (overaged at 800° F in 48 hr) of the cold-worked specimen.

These hardness tests were made solely to supplement the data obtained in the creep tests. Obviously, no definite correlation could be expected between hardness measurements made at room temperature and creep behavior at elevated temperatures. However, the hardness measurements give some indication of the aging characteristics of this particular lot of initially cold-drawn ingot iron and its resistance to plastic deformation occurring during creep, especially after the beginning of necking. The results confirm the already known fact that the history of the specimen is continuously changing during creep, and they show that changes in hardness of ingot iron similar to its creep properties are affected by variations in amounts of plastic deformations, strain rates, and temperatures.

IV. Summary

Tension tests were made at different strain rates and temperatures on ingot iron initially cold-drawn approximately 13-percent reduction in area. Some of the creep tests at 600°, 700°, and 800° F were discontinued after the beginning of the third stage, and these specimens were subse-

quently tested in tension at room temperature. In another series of tests in which the specimens were carried to complete fracture at 500°, 600°, 700°, and 800° F, the strain rate during the third stage was maintained nearly constant and equal to that in the second stage by repeatedly adjusting the load during the third stage. Hardness measurements at room temperature and metallographic examination were made on specimens representative of the initial material and after testing in creep under the varying conditions used.

The relationship between true stress and the creep rate in the second stage was not linear when either the stress or the logarithm of the stress was plotted against the logarithm of the strain rate. The use of a linear relationship in either of these plots for extrapolating to very slow strain rates is not justified.

The resistance to creep in the second stage and the extension at complete fracture at 700° F were materially affected by variations in rate of loading in the first stage.

Although variations within the range of strain rates used in the creep tests at 700° and 800° F had no significant effect on plastic extension at the beginning of the third stage, evidence obtained in tests at 500° and 600° F supports the belief that this extension is markedly increased with sufficiently high strain rates. The strain rates required to produce relatively high plastic extension at the beginning of the third stage were affected by the test temperature in that the high ductility was obtained at slower rates as the test temperature was decreased.

The third stage of creep was initiated without necking of the specimens, and the results of tension tests made at room temperature on specimens previously extended into the third stage at different temperatures showed that no general deterioration or microcracking of the specimen occurred up to the time this stage was reached. Regardless of strain rate or temperature used, however, considerable necking occurred during the third stage of each specimen tested to complete fracture.

The general trend was for the ductility (plastic extension and reduction of area) at fracture to increase as the strain rate increased. The plastic extension at fracture decreased with an increase in test temperature, but in the creep test no consistent relation was obtained between temperature and reduction of area at fracture.

The resistance to both creep and fracture increased as the temperature was decreased. The stress at fracture also increased as the strain rate increased.

The fractures were predominantly transcrystalline in the tension tests with the different strain rates used at and below 600° F and intercrystalline at test temperatures of 700° and 800° F.

The authors are indebted to G. W. Geil for his assistance in planning the testing program and to Fannie A. Wilkinson for making many of the measurements during the course of the investigation.

V. References

[1] D. J. McAdam, Jr., G. W. Geil, and D. H. Woodard, Influence of strain rate and temperature on the mechanical properties of Monel metal and copper, Proc. Am. Soc. Test. Mat. **46,** 902 (1946).

[2] C. H. M. Jenkins and G. A. Mellor, Investigation of the behavior of metals under deformation at high temperatures. Part I—Structural changes in mild steel and commercial irons during creep, J. Iron & Steel Inst., **132,** 179 (1935).

[3] H. J. Tapsell and W. J. Clenshaw, Mechanical properties of Armco iron, 0.17 percent carbon steel, and 0.24 percent carbon steel, with special reference to creep, Great Britain Department of Scientific and Industrial Research Engineering Research Special Report No. 1 (1927–29).

[4] H. J. Tapsell. Note on the "creep" of Armco iron, Great Britain Department of Scientific and Industrial Research, Engineering Research, Special Report No. 6 (1927–29); H. J. Tapsell, Creep of metals, (Oxford Univ. Press, 1931).

[5] J. A. Bennett and D. J. McAdam, Jr. Creep rates of cold-drawn nickel-copper alloy (Monel metal), J. Research NBS, **28,** 417 (1942) RP1462.

[6] R. H. Greaves and J. A. Jones, The effect of temperature on the behavior of iron and steel in notched-bar impact tests, J. Iron & Steel Inst. **112,** 123 (1925).

[7] H. Carpenter and J. M. Robertson, Metals **1,** 174 (Oxford Univ. Press, 1939).

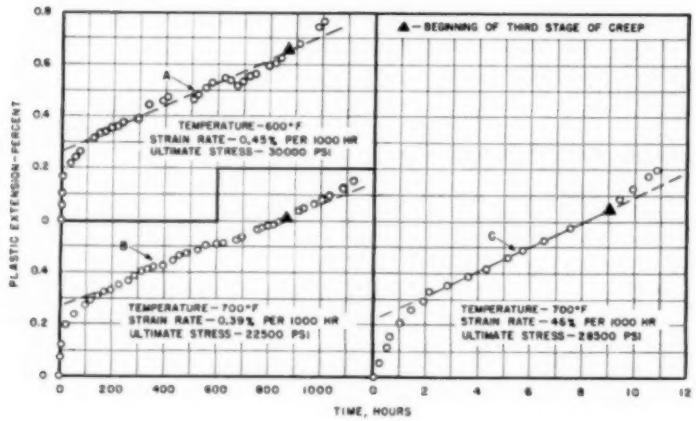
▲ — BEGINNING OF THIRD STAGE OF CREEP
PLASTIC EXTENSION - PERCENT
TEMPERATURE - 600°F
STRAIN RATE - 0.45% PER 1000 HR
ULTIMATE STRESS - 30000 PSI
TEMPERATURE - 700°F
STRAIN RATE - 0.39% PER 1000 HR
ULTIMATE STRESS - 22500 PSI
TEMPERATURE - 700°F
STRAIN RATE - 46% PER 1000 HR
ULTIMATE STRESS - 28300 PSI
TIME, HOURS

FIGURE 1. *Extension-time curves for specimens extended into the third stage of creep.*

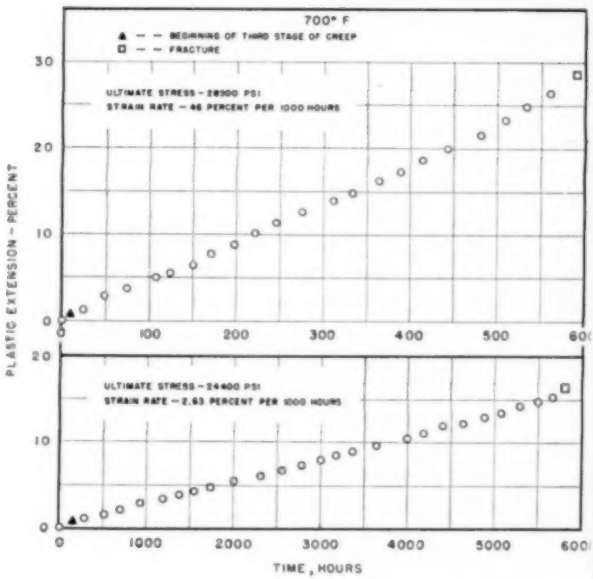
700° F
▲ — — BEGINNING OF THIRD STAGE OF CREEP
□ — — FRACTURE
ULTIMATE STRESS - 28300 PSI
STRAIN RATE - 46 PERCENT PER 1000 HOURS
ULTIMATE STRESS - 24400 PSI
STRAIN RATE - 2.63 PERCENT PER 1000 HOURS
PLASTIC EXTENSION - PERCENT
TIME, HOURS

FIGURE 2. *Extension-time curves for specimen tested in creep to complete fracture.*

The strain rate during the third stage was maintained nearly constant and equal to that of the second stage by repeatedly decreasing the load during the third stage.

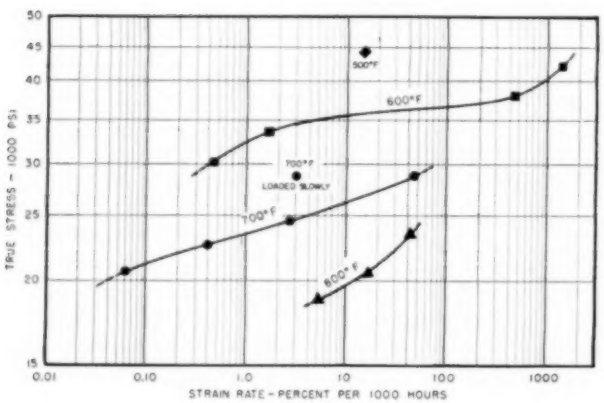

FIGURE 3. *Relation between true stress and strain rate at different temperatures.*

The true stress as plotted in this figure is the stress required to initiate the third stage of creep, and its numerical value is obtained by dividing the load by the area of the specimen at this point. All specimens were loaded at a rate of 30- to 50-percent extension in 1,000 hr in the first stage, except the one tested at 700° F (designated as loaded slowly), which was loaded at a rate of 3-percent extension in 1,000 hr. The strain rate is the average value obtained during the second stage.

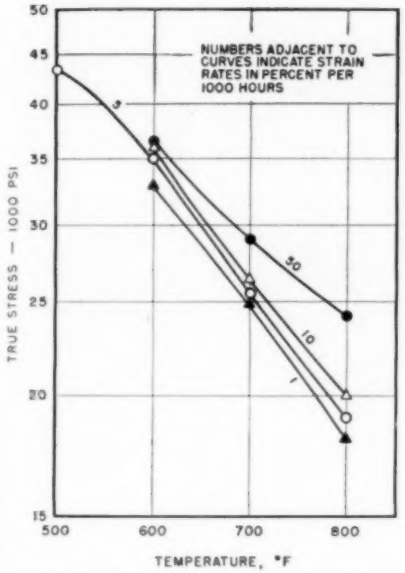

FIGURE 4. *Relation between temperature and the stress required to produce different strain rates.*

The values were derived from figure 3.

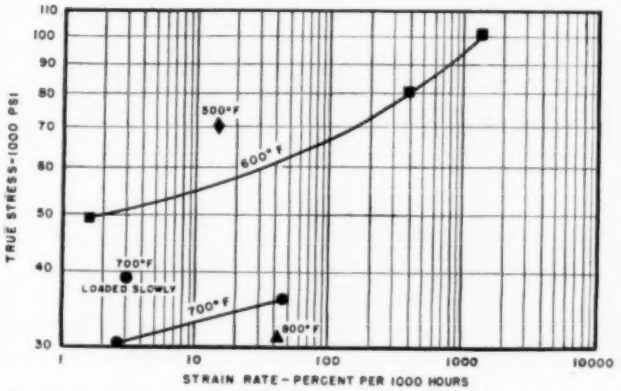

FIGURE 5. *Relation between strain rate and true stress at fracture.*

The true stress at fracture is obtained by dividing the load at the time of fracture by the area of the specimen at the point of fracture. The strain rate is the average rate obtained in the second stage of creep. The strain rate during the third stage was maintained nearly constant and equal to that of the second stage by repeatedly decreasing the load during the third stage.

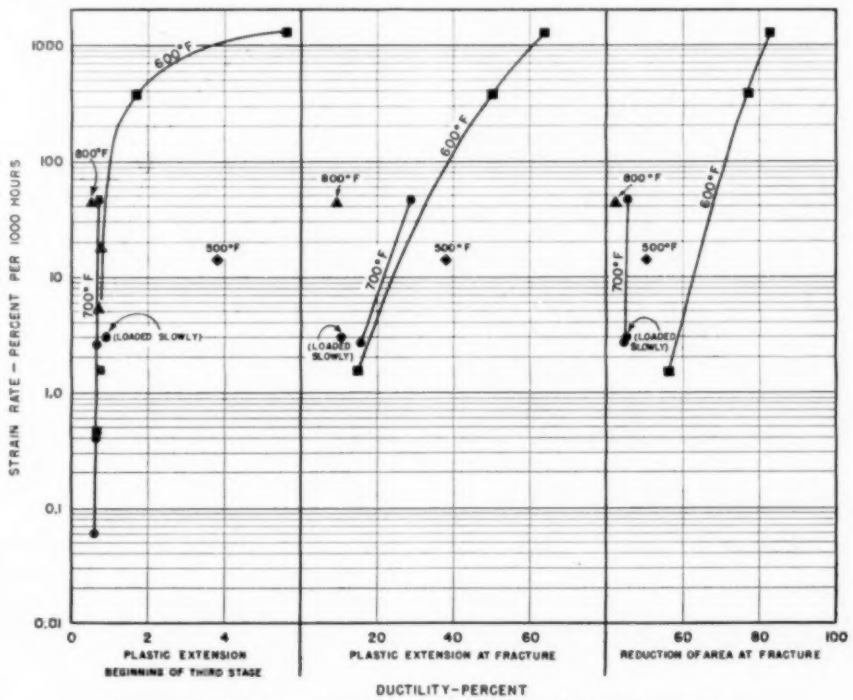

FIGURE 6. *Influence of strain rate on ductility at different temperatures.*

The strain rate is the average rate obtained during the second stage of creep. The strain rate during the third stage was maintained nearly constant and equal to that of the second stage by repeatedly decreasing the load during the third stage.

843576—49——3

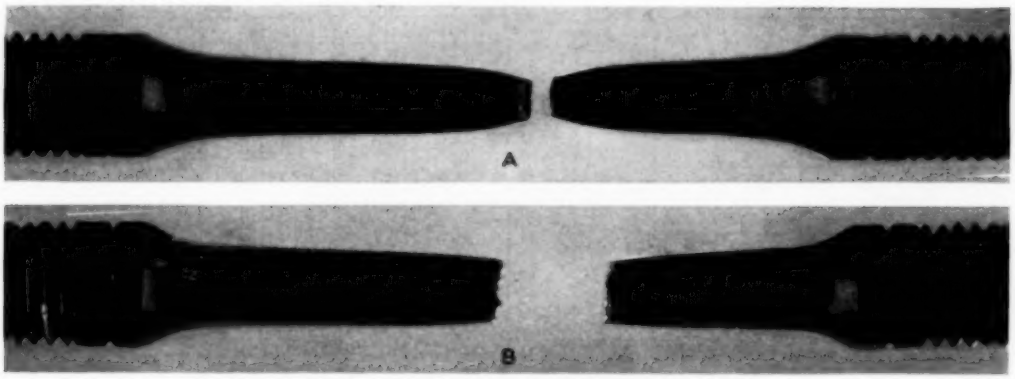

FIGURE 7. *Photographs of specimens after fracturing in creep.* $\times 1$.

A, Specimen tested at 600° F with a strain rate of 380 percent per 1,000 hr. Necking extended over a considerable portion of the gage length. $L/L_0 = 1.50$; $A_0/A = 4.30$. B, Specimen tested at 700° F with a strain rate of 46 percent per 1,000 hr. Necking was confined principally to the region near the fracture. $L/L_0 = 1.29$; $A_0/A = 1.84$. L_0 and A_0 are the initial gage length and area of cross section respectively; L and A are the length and area at fracture, respectively.

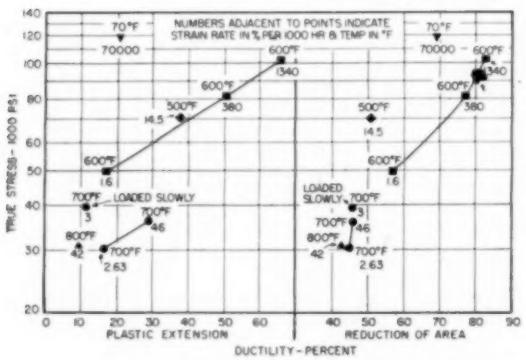

FIGURE 8. *Relation between stress at fracture and ductility at different temperatures and strain rates.*

The true stress at fracture is obtained by dividing the load at the time of fracture by the area of the specimen at the point of fracture. All specimens were loaded at a rate of 30- to 50-percent extension in 1,000 hr in the first stage of creep, except one tested at 700° F (designated as loaded slowly), which was loaded at a rate of 3-percent extension in 1,000 hr. The strain rate in the third stage was maintained nearly constant and equal to that of the second stage (values given in fig.) by repeatedly decreasing the load during the third stage.

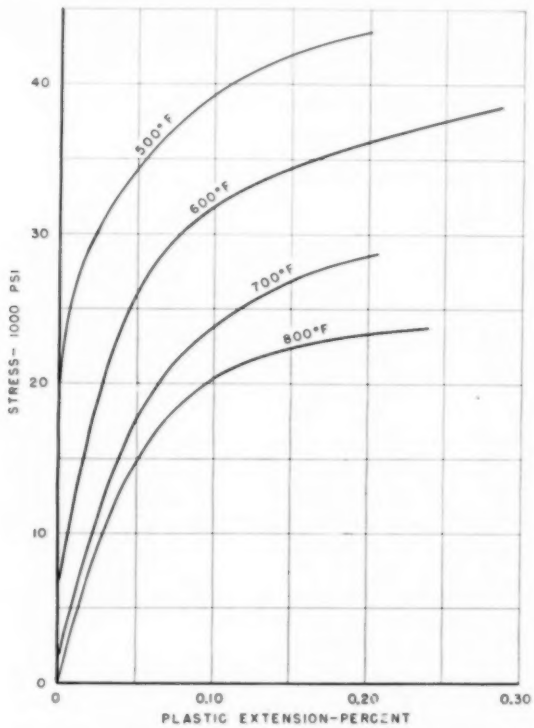

FIGURE 9. *Effect of nominal stress on plastic extension in the initial stage of creep at different temperatures.*

The specimens were prepared from the bar as cold-worked 13 percent and were loaded under conditions required to produce a rate of extension of 30 to 50 percent per 1,000 hr. The curves are drawn through the mean positions of numerous experimental points.

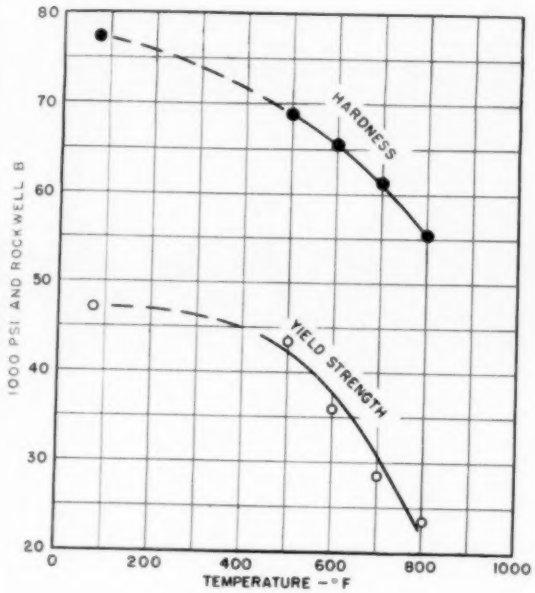

FIGURE 10. *Effect of temperature on yield strength and Rockwell B Hardness.*

Values for yield stress (0.2% offset) at elevated temperatures were derived from figure 9. The Rockwell hardness tests were made at room temperature on the initially cold-worked bar and on the undeformed portion (shoulder) of the specimen after testing in creep at different temperatures.

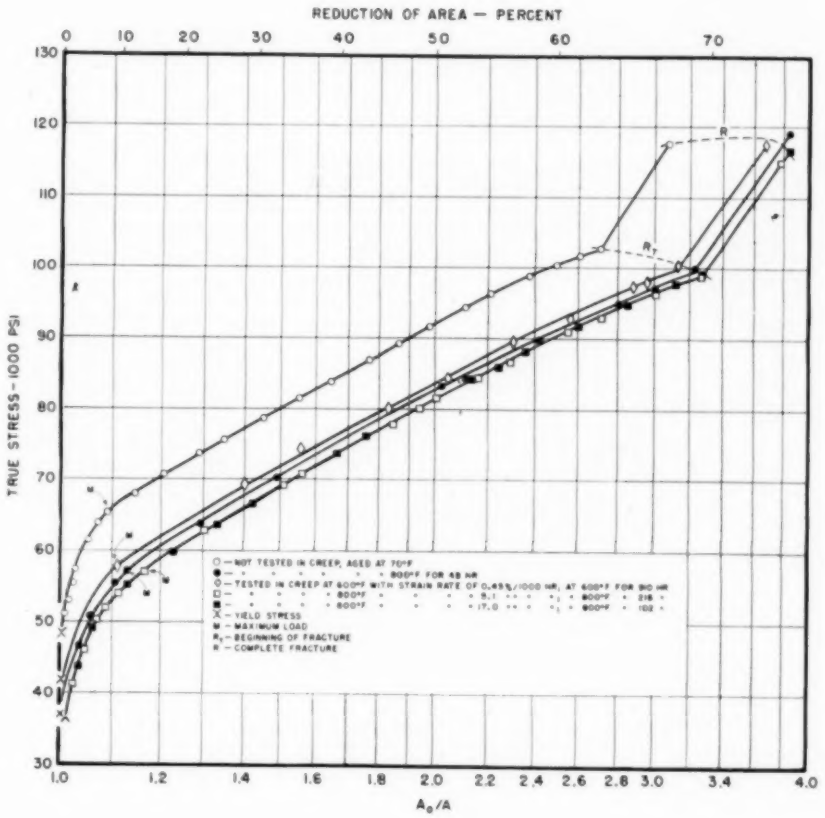

FIGURE 11. *Effect of extending in creep at different temperatures to the beginning of the third stage and of aging at 800° F on the tensile properties at room temperature of cold-drawn ingot iron.*

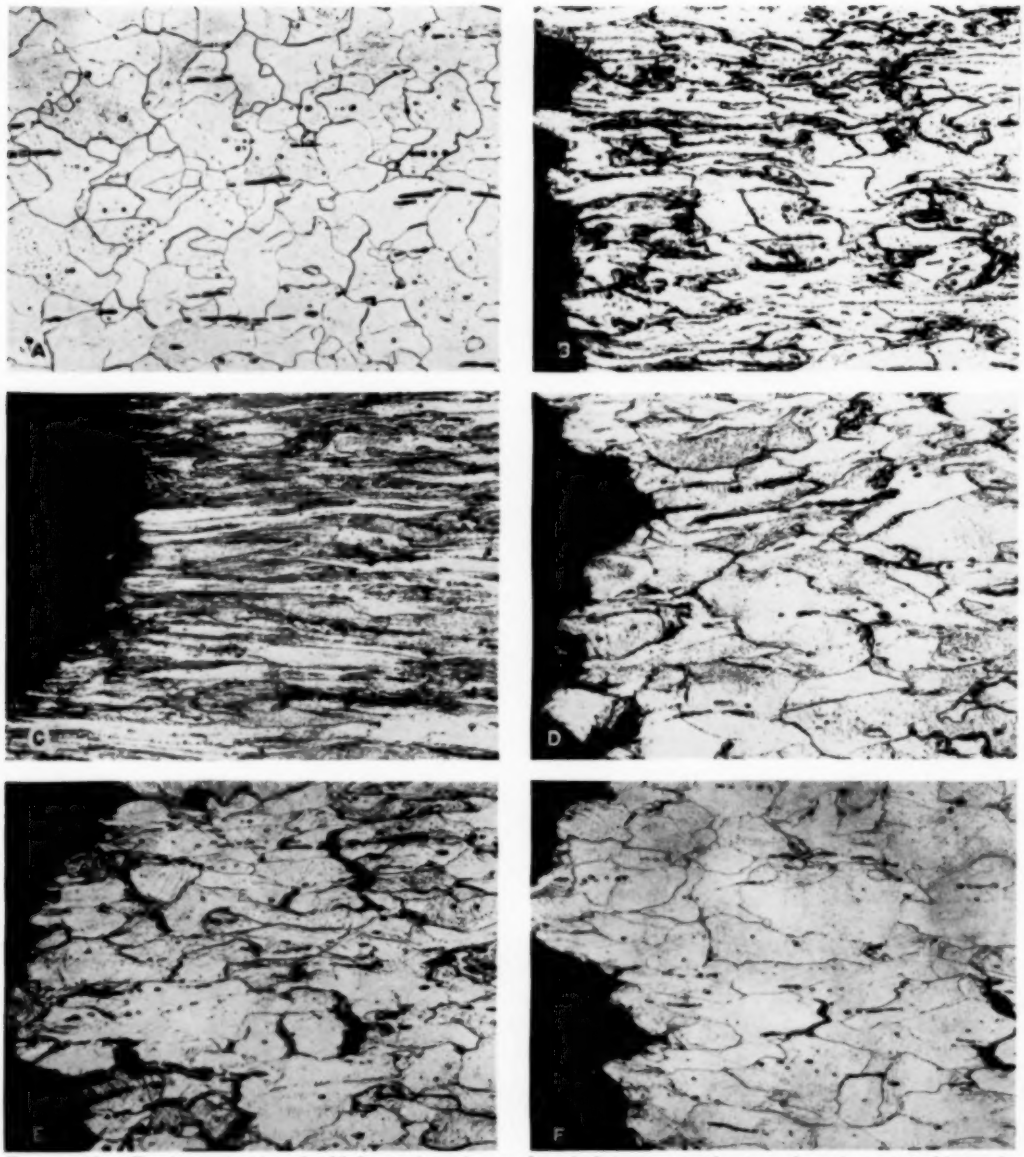

FIGURE 12. *Ferrite grain size of cold-drawn ingot iron and typical structures at fracture of specimens tested in tension at different temperatures and strain rates; longitudinal sections, etched in nital, × 100.*

Figure	Test		Elongation in 4 in.	Reduction in area	Remarks
	Temperature	Strain rate			
	° F	%/1,000 hr	%	%	
A	.....	.....	.....	.....	As cold-drawn; AVG ASTM grain No. lower 5.
B	600	1.60	16.5	56.6	.....
C	600	1340	[a] 65.1	82.5	.....
D	700	2.63	16.4	44.7	.....
E	700	3.00	11.2	45.4	Loaded slowly.
F	800	42	9.2	42.3	.....

[a] Elongation in 2 in., percent.

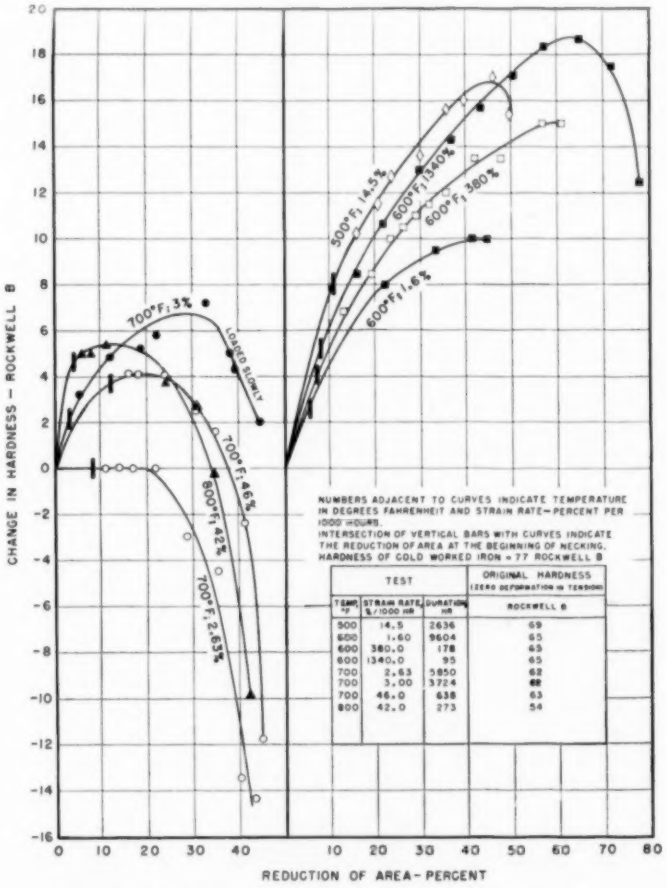
CHANGE IN HARDNESS – ROCKWELL B
REDUCTION OF AREA – PERCENT
700°F; 3%
LOADED SLOWLY
700°F; 46%
800°F; 42%
700°F; 2.63%
500°F; 14.5%
600°F; 1340%
600°F; 380%
600°F; 1.6%
NUMBERS ADJACENT TO CURVES INDICATE TEMPERATURE IN DEGREES FAHRENHEIT AND STRAIN RATE – PERCENT PER 1000 HOURS.
INTERSECTION OF VERTICAL BARS WITH CURVES INDICATE THE REDUCTION OF AREA AT THE BEGINNING OF NECKING.
HARDNESS OF COLD WORKED IRON = 77 ROCKWELL B

TEST			ORIGINAL HARDNESS (ZERO DEFORMATION IN TENSION)
TEMP. °F	STRAIN RATE, %/1000 HR	DURATION HR	ROCKWELL B
500	14.5	2636	69
600	1.60	9604	65
600	380.0	178	65
600	1340.0	95	65
700	2.63	5850	62
700	3.00	3724	62
700	46.0	638	63
800	42.0	273	54

FIGURE 13. *Effect of plastic deformation during creep at different temperatures and strain rates on change in hardness.*

The hardness tests were made at room temperature on specimens after fracturing in creep. The creep during the third stage was maintained nearly constant and equal to that in the second stage by repeatedly decreasing the load during the third stage.

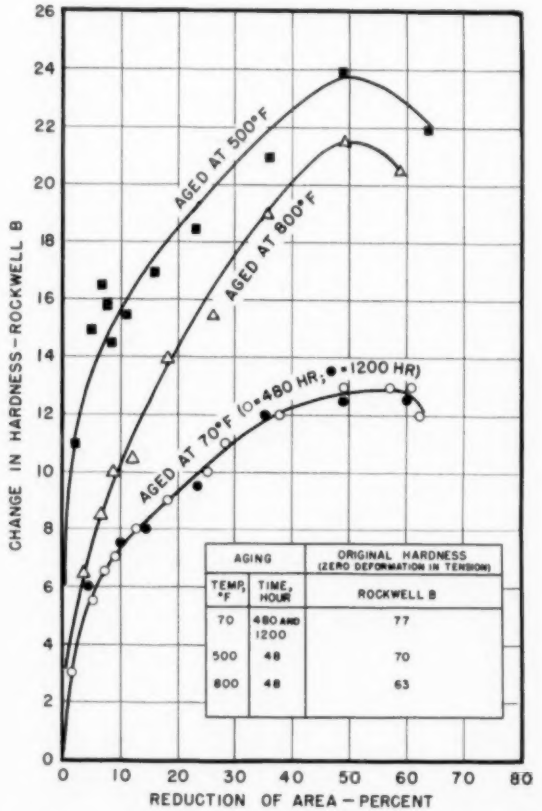

AGING		ORIGINAL HARDNESS (ZERO DEFORMATION IN TENSION)
TEMP, °F	TIME, HOUR	ROCKWELL B
70	480 AND 1200	77
500	48	70
800	48	63

FIGURE 14. *Effect of aging at different temperatures on change in hardness at room temperature of a specimen plastically deformed to fracture in tension at room temperature.*

The tensile specimen was prepared from the bar as cold-drawn 13-percent reduction in area. The values for reduction of area as plotted in the figure do not include this 13 percent.

WASHINGTON, March 18, 1949.

U. S. Department of Commerce
National Bureau of Standards

Research Paper RP2014
Volume 42, August 1949

Part of the Journal of Research of the National Bureau of Standards

Differences Between the International Temperature Scales of 1948 and 1927

By Robert J. Corruccini

Tables and a graph are presented showing differences that exist between temperatures expressed on the International Temperature Scale of 1927 and the recently adopted International Temperature Scale of 1948.

The experimental difficulties inherent in the measurement of temperature on the thermodynamic scale led to the adoption in 1927, by the Seventh General Conference on Weights and Measures, of a practical scale that was designated as the International Temperature Scale.[1] The first revision of this scale came with the adoption of the International Temperature Scale of 1948 [2] [2] by the Ninth General Conference on Weights and Measures. The revised scale was designed to conform as nearly as practicable to the thermodynamic centigrade (Celsius) scale as then known, while incorporating certain refinements, based on experience, to make the scale more uniform and reproducible than its predecessor.

In the following sections, tables, and a graph are presented showing differences that exist between temperatures expressed on the International Temperature Scales of 1948 and 1927.

Platinum resistance thermometer range (oxygen point to freezing point of antimony). The changes [3] adopted in this range have the effect of making the scale more definite and reproducible but cause little or no change in the numerical values of temperatures.

Standard thermocouple range (freezing point of antimony to the gold point). The change in the value for the silver point from 960.5° to 960.8° C changes the numerical values of temperatures measured with the standard thermocouple.[4] Because both the 1927 and 1948 scales provide for some variation of thermoelectric properties of standard thermocouples, the differences between the two scales in the thermocouple range cannot be stated explicitly. The differences have been calculated for the median standard thermocouple allowed by the International Temperature Scale of 1948, namely, $E_{Au}=10{,}300$ microvolts, $E_{Ag}=9{,}117$ microvolts, $E_{Sb}=5{,}530$ microvolts, as follows.

The temperature, t, is defined by the formula,

$$E=a+bt+ct^2, \tag{1}$$

where E is the electromotive force of a standard thermocouple of platinum and platinum-rhodium alloy when one junction is at 0° C and the other is at the temperature, t. The constants, a, b, and c, are to be calculated from measured values of E at the freezing point of antimony and at the silver and gold points. The fixed points will be referred to by subscripts 1, 2, and 3, respectively, in what follows. For a given set of values of E, it is desired to determine the effect upon calculated values of t of changing the value assigned to t_2. Differentiating eq 1 with respect to t_2 and setting $\partial E/\partial t_2$ equal to zero leads to the following equation:

$$\partial t/\partial t_2=\frac{-\partial a/\partial t_2-t\partial b/\partial t_2-t^2\partial c/\partial t_2}{b+2ct},$$

[1] G. K. Burgess, The International Temperature Scale, BS J. Research **1**, 635 (1928) RP22.

[2] H. F. Stimson, The International Temperature Scale of 1948, J. Research NBS **42**, 209 (1949) RP1962.

[3] These changes are: (a) The termination of the scale at the oxygen point (−182.970° C) instead of at −190° C, (b) the division of the scale at the freezing point of antimony (about 630.5° C) instead of at 660° C, (c) the requirement for higher purity of the platinum of the standard resistance thermometer. In addition, a resolution was adopted that the zero of the thermodynamic centigrade scale should be defined as the temperature 0.0100 degree below that of the triple point of pure water.

[4] In addition there are changes of the type mentioned in footnote 3 that cause little or no change in the numerical values of temperatures. These include requirements for higher purity of the platinum of the standard thermocouple and for smaller permissible limits for the electromotive force of the standard thermocouple at the gold point.

where

$$a=\frac{E_1(t_2t_3^2-t_3t_2^2)+E_2(t_3t_1^2-t_1t_3^2)+E_3(t_1t_2^2-t_2t_1^2)}{x}$$

$$b=\frac{E_1(t_2^2-t_3^2)+E_2(t_3^2-t_1^2)+E_3(t_1^2-t_2^2)}{x}$$

$$c=\frac{E_1(t_3-t_2)+E_2(t_1-t_3)+E_3(t_2-t_1)}{x}$$

$$x=t_2t_3^2-t_3t_2^2+t_3t_1^2-t_1t_3^2+t_1t_2^2-t_2t_1^2$$

$$\frac{\partial a}{\partial t_2}=\frac{E_1(t_3^2-2t_3t_2)-E_3(t_1^2-2t_1t_2)}{x}-\frac{a}{x}\frac{\partial x}{\partial t_2}$$

$$\frac{\partial b}{\partial t_2}=\frac{2t_2(E_1-E_3)}{x}-\frac{b}{x}\frac{\partial x}{\partial t_2}$$

$$\frac{\partial c}{\partial t_2}=\frac{E_3-E_1}{x}-\frac{c}{x}\frac{\partial x}{\partial t_2}$$

$$\frac{\partial x}{\partial t_2}=t_3^2+2t_1t_2-t_1^2-2t_3t_2.$$

Inserting the values

$$\begin{array}{llll} t_1= & 630.5 & E_1= & 5{,}530 \\ t_2= & 960.8 & E_2= & 9{,}117 \\ t_3= & 1{,}063 & E_3= & 10{,}300 \end{array}$$

gives

$$\frac{\partial t}{\partial t_2}=\frac{-226.466+0.5722281t-0.0003378967t^2}{8.227+0.003309t}.$$

Values of Δt obtained by multiplying values of $\partial t/\partial t_2$ by $\Delta t_{Ag}=0.3$ deg are given in table 1 and figure 1.

Calculation indicates that the maximum variation in Δt from the values in table 1, due to the variation in standard thermocouples permitted under the International Temperature Scale of 1948, is 0.002 deg. This is sufficient to change certain values of Δt by 0.01 deg upon rounding, which is not significant in comparison with the reproducibility of 0.1 deg C usually ascribed to standard thermocouples. The corresponding temperatures on the two scales between 630.5° and 1,063° C that appear in table 2 were calculated from table 1.

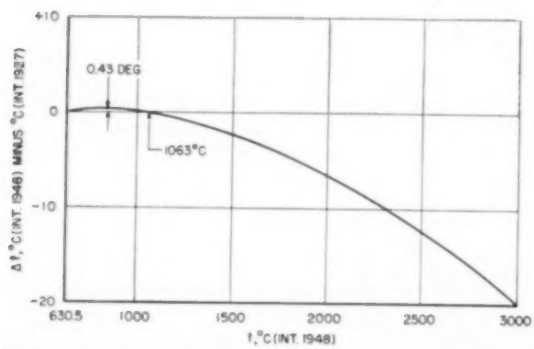

FIGURE 1. *Differences between the International Temperature Scales of 1948 and 1927.*

TABLE 1. *Differences between the International Temperature Scales of 1948 and 1927 in the standard thermocouple range*

t °C (Int. 1948)	Δt °C (Int. 1948) minus °C (Int. 1927)
630. 5	0. 00
650	+. 08
700	. 24
750	. 35
800	. 42
839. 5	. 43 (max)
850	. 43
900	. 40
950	. 32
960. 8	. 30
1000	. 20
1050	. 05
1063	. 00

Radiation law range (above the gold point). The adoption of a different value for the radiation constant c_2 changes all temperatures above the gold point, while the use of the Planck radiation formula instead of the Wien formula affects the very high temperatures. The Planck formula is consistent with the thermodynamic scale and consequently removes the upper limit that was imposed by Wien's law in the 1927 scale.

Above the gold point the temperature, t, in degrees Centigrade (Int. 1948) is defined by the formula,

$$\frac{J_t}{J_{Au}}=\frac{e^{\frac{c_2}{\lambda(t_{Au}+T_0)}}-1}{e^{\frac{c_2}{\lambda(t+T_0)}}-1}, \qquad (2)$$

in which J_t and J_{Au} are the radiant energies per unit wavelength interval at wavelength, λ, emitted per unit time by unit area of a black body at the

TABLE 2. *Corresponding temperatures on the International Temperature Scales of 1948 and 1927*

Degrees C (Int.)		Corresponding degrees F	
1948	1927	1948	1927
630. 50	630. 50	1166. 9	1166. 9
650	649. 92	1202	1201. 9
700	699. 76	1292	1291. 6
750	749. 65	1382	1381. 4
800	799. 58	1472	1471. 2
850	849. 57	1562	1561. 2
900	899. 60	1652	1651. 3
950	949. 68	1742	1741. 4
960. 80	960. 50	1761. 4	1760. 9
1000	999. 80	1832	1831. 6
1050	1049. 95	1922	1921. 9
1063. 00	1063. 00	1945. 4	1945. 4
1100	1100. 2	2012	2012
1200	1200. 6	2192	2193
1300	1301. 1	2372	2374
1400	1401. 7	2552	2555
1500	1502. 3	2732	2736
1600	1603. 0	2912	2917
1700	1703. 8	3092	3099
1800	1804. 6	3272	3280
1900	1905. 5	3452	3462
2000	2006. 4	3632	3644
2100	2107	3812	3825
2200	2208	3992	4007
2300	2310	4172	4189
2400	2411	4352	4372
2500	2512	4532	4554
2600	2613	4712	4736
2700	2715	4892	4919
2800	2816	5072	5102
2900	2918	5252	5285
3000	3020	5432	5468
3100	3122	5612	5651
3200	3223	5792	5834
3300	3325	5972	6018
3400	3428	6152	6202
3500	3530	6332	6386
3600	3632	6512	6570
3700	3735	6692	6754
3800	3837	6872	6939
3900	3940	7052	7124
4000	4043	7232	7309
4100	4146	7412	7495
4200	4249	7592	7681

temperature, t, and at the gold point, t_{Au}, respectively.

c_2=1.438 centimeter degrees.

T_0=temperature of the ice point in degrees Kelvin.

λ=wavelength of the visible spectrum.

e=base of Naperian logarithms.

On the International Temperature Scale of 1927 the temperature, t', was defined by the formula

$$\log_e \frac{J_t}{J_{Au}} = \frac{c_2}{\lambda}\left[\frac{1}{1{,}336} - \frac{1}{(t'+273)}\right], \qquad (3)$$

where c_2 is taken as 1.432 cm degrees and J_t and J_{Au} have the same meanings as in eq 2. The equation is valid if $\lambda(t'+273)$ is less than 0.3 cm degree. Equating the logarithm of the right-hand side of eq 2 to the right-hand side of eq 3, one obtains the following formula relating t in degrees Centigrade (Int. 1948) and t' in degrees Centigrade (Int. 1927), in which t_{Au} is taken as 1,063 °C, T_0 is taken as 273.16 following the prevailing American usage and λ must be expressed in centimeters.

$$\log_e \frac{e^{\frac{1.438}{1336.16\lambda}} - 1}{e^{\frac{1.438}{\lambda(t+273.16)}} - 1} = \frac{1.432}{\lambda}\left[\frac{1}{1{,}336} - \frac{1}{(t'+273)}\right].$$

Corresponding values of t and t' have been calculated from this formula for temperatures above the gold point and for $\lambda = 0.65 \times 10^{-4}$ cm (which is approximately the effective wavelength of most optical pyrometers) and are given in table 2, together with corresponding temperatures below the gold point obtained as mentioned on p. 134. In figure 1, the difference, degrees Centigrade (Int. 1948) minus degrees Centigrade (Int. 1927), is plotted as a function of degrees Centigrade (Int. 1948). Values below 1,063° C are from table 1.

In the range above the gold point, the differences between the two scales cannot be stated explicitly due to the range of permissible values of λ. To indicate the possible variation of the differences due to variation of λ, table 3 has been prepared giving corresponding values of t and t' at $\lambda = 0.65 \times 10^{-4}$ cm and $\lambda = 0.4738 \times 10^{-4}$ cm. The latter wavelength occupies a position at the blue end of the visibility function of the human eye, which corresponds to the position of $\lambda = 0.65 \times 10^{-4}$ cm at the red end. It will be noted that the variation in difference due to variation of λ is in all cases much less than the accuracy of measurement of temperature with existing instruments.

845576—49——4

Tables 2 and 3 have not been carried above the maximum temperatures to which the International Temperature Scale of 1927 extends, namely, 4,342° C for $\lambda=0.65\times10^{-4}$ cm and 6,059° C for $\lambda=0.4738\times10^{-4}$ cm.

TABLE 3. *Corresponding temperatures on the International Temperature Scales of 1948 and 1927 at two wave lengths*

t °C (Int. 1948)	t' °C (Int. 1927)	
	($\lambda=0.65\times10^{-4}$ cm)	($\lambda=0.4738\times10^{-4}$ cm)
1063	1063	1063
1500	1502. 31	1502. 31
2000	2006. 41	2006. 39
2500	2512. 14	2512. 02
3000	3019. 76	3019. 22
3500	3529. 79	3528. 07
4000	4042. 99	4038. 72
5000	.....	5066. 51

In determining temperatures with an optical pyrometer, the following approximate formula (based upon Wien's law),

$$\log_e \frac{J_t}{J_{As}} = \frac{1.438}{\lambda}\left[\frac{1}{1{,}336}-\frac{1}{(t_w+273)}\right], \qquad (4)$$

will usually yield values that are not significantly different from those yielded by eq 2. Corresponding values of t, degrees Centigrade (Int. 1948) and t_w are given in table 4.

TABLE 4.—*Corresponding temperatures on the International Temperature Scale of 1948 and from eq 4*

t °C (Int. 1948)	t_w °C
1063	1063. 0
1500	1499. 9
2000	1999. 7
2500	2499. 6
3000	2999. 8
3500	3500. 7
4000	4003. 2
4500	4508. 2
5000	5016. 8

Acknowledgment is due members of the Computation Laboratory of this Bureau and John I. Lauritzen, who have carried out most of the calculations involved in this work.

WASHINGTON, March 2, 1949.

U. S. Department of Commerce
National Bureau of Standards

Research Paper RP2015
Volume 42, August 1949

Part of the Journal of Research of the National Bureau of Standards

An Instrument for Measuring Longitudinal Spherical Aberration of Lenses

By Francis E. Washer

An instrument is described that permits the rapid determination of longitudinal spherical and longitudinal chromatic aberration of lenses. Specially constructed diaphragms isolate successive zones of a lens, and a movable reticle connected to a sensitive dial gage enables the operator to locate the successive focal planes for the different zones. Results of measurement are presented for several types of lenses. The instrument can also be used without modification to measure the small refractive powers of goggle lenses.

I. Introduction

In the course of a research project sponsored by the Army Air Forces, an instrument was developed to facilitate the inspection of lenses used in the construction of reflector sights. This instrument enabled the inspection method to be based upon a rapid determination of the axial longitudinal spherical aberration of the lens. This measurement was performed with the aid of a series of diaphragm plates that enabled the operator to select any zone of the lens at will and quickly determine the separation of its focal plane from that of any other zone by movement of a reticle whose movements were registered by a sensitive dial gage.

The instrument proved so simple and accurate that a second one has been constructed for use in measuring axial longitudinal spherical and longitudinal chromatic aberration of lenses. In addition, the instrument can be readily used in the measurement of small refractive powers in the region from -0.06 to $+0.06$ diopters. It is therefore extremely useful, in the determination of the refractive power of goggle lenses in the course of tests, to determine compliance with federal specifications.

II. Apparatus

The apparatus consists of a movable, illuminated reticle, a sensitive gage to record the movement of the reticle, a collimating lens, one movable and one fixed diaphragm, and a viewing device. The arrangement of these elements is shown diagrammatically in figure 1. To simplify the description, the optical system will be considered in three parts, each of which forms a definite member of the whole system. The axis, A, is common to the entire system; the axis is bent at the mirror, M, to conserve space and simplify operation by a single observer.

Objective lens L_1, mirror M, and viewing screen, S form the first part. The viewing screen, S, lies in the focal plane of lens L_1, so that light, parallel to the axis, A, incident on the front of L_1, passes through it, is reflected by M, and is brought to a focus at S. The screen, S, may be replaced by an ocular, so that the combination of L_1, M, and the ocular form a telescopic system focused for parallel light. Mirror M is a plane front-surface mirror mounted in a fixture equipped with adjusting screws, and its function is to bring the image formed by L_1 to the center of screen S. The choice of the focal length of lens L_1 is determined by several factors. These are easy viewing, ready observation of small lateral shifts of the image, and the minifying of error in L_1. A lens having a focal length of 1,143 mm is used at present in the instrument. Accordingly, an angular change of 1 mil in the light incident upon L_1 produces a lateral displacement of approximately 1.14 mm of the image formed by L_1 on screen S. The long focal length of L_1 insures negligible error of parallax from any residual longitudinal spherical aberration in L_1.

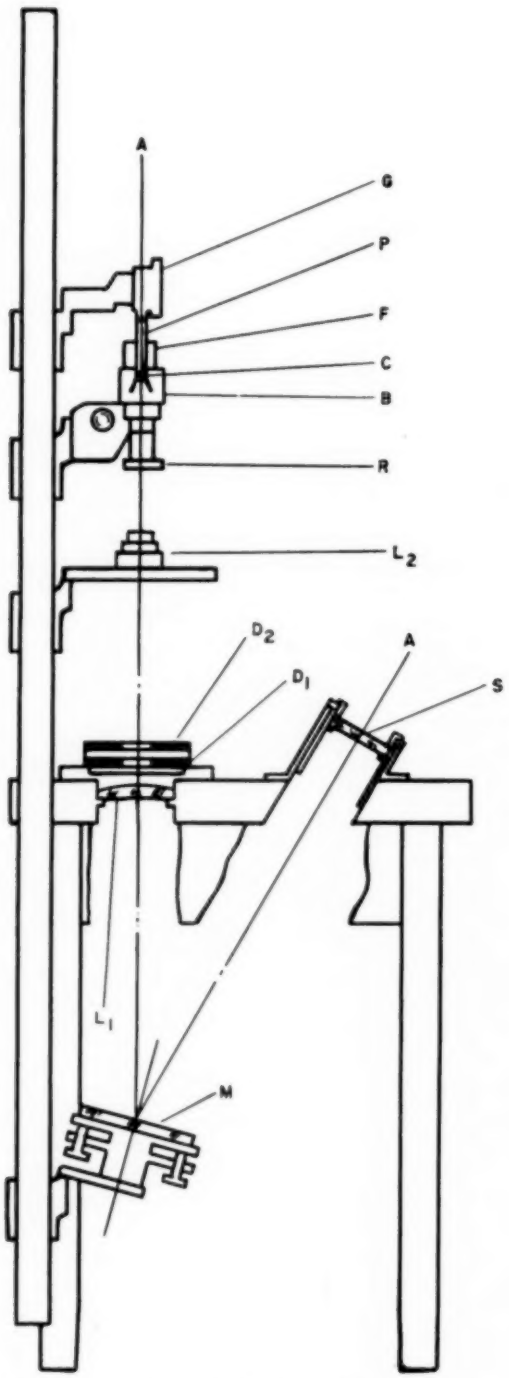

FIGURE 1. *Diagrammatic sketch of the instrument.*

Lens L_2, which frequently is a lens corrected for parallel incident light, and the diaphragms, D_1 and D_2, form the second part of the system. L_2 is the lens to be tested and is mounted over an opening in the supporting plate. The supporting plate is provided with adjustable brackets that facilitate easy insertion, proper positioning, and easy removal of the lens. Lens L_2 is so placed that its "infinite conjugate" is facing lens L_1. Diaphragm D_1 contains a rectangular slot whose length is equal to the effective aperture of L_1 and

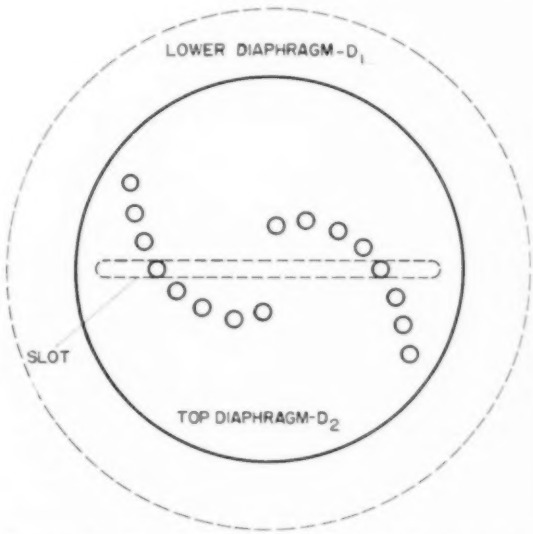

FIGURE 2. *Diagrammatic sketch showing the manner in which the successive pairs of holes in the upper diaphragm, D_2, are isolated by the slot in the lower diaphragm, D_1.*

whose width is approximately 5 mm. Its function is to isolate a narrow region along the diameter of L_2. Diaphragm D_2 is located above D_1 and contains circular holes of small diameter arranged in pairs about the center of the diaphragm. The arrangement of these pairs of holes is shown in figure 2. The two members of a pair are equidistant from the center and on the same diameter. The linear separation of the members of a pair proceeds in steps of 5 mm from 5 to 100 mm. Rotation of the diaphragm D_2 above D_1 therefore brings successive pairs of holes over the slot in D_1 and so isolates successive zones of lens L_2. In order to provide a sufficient number of holes, so spaced that only one pair is above the opening in D_1 at a time, it is necessary to have several interchangeable diaphragms that can be used at

D_2. Each of the diaphragm plates has from two to eight pairs of holes.

The reticle, R, lamp F, movable member B, and dial gage G form the third part of the system. Member B is movable in a vertical direction by means of a rack and pinion. The friction opposing the movement is sufficiently great to prevent appreciable drift between adjustments. Member B supports a lamp house containing lamp F and reticle R. Reticle R is a transparent cross and is mounted on a support that permits small displacements necessary for centering. Reticle R is illuminated by lamp F and is so situated that its center lies at or near the focal point of lens L_2. The upper portion of B is provided with a cap that transmits its vertical motion to the sensitive length-measuring gage, G, through plunger P. Thus, any raising or lowering of reticle R is done by moving B, and the magniture of the movement is indicated on gage G.

Figure 3 is a photograph of the actual instrument showing the manner in which the apparatus is arranged for easy use by a seated observer. The ocular assembly is removable and can be replaced by a ground-glass viewing screen. Telescope lens, L_1, mounted in the opening in the table top, can be focused by rotating the ocular mount or by sliding the mirror mount, M, up or down the supporting shaft. The other elements of the system are attached to the upright shaft by clamps that can be moved up and down by large amounts and so permit the use of a wide variety of collimating lenses with focal lengths ranging from 1 to 30 in. The lamp house includes a prism, movable condensers, and filter holders to provide controlled illumination of the reticle. The collimating lens support is provided with a series of attachments, so that lenses having diameters ranging from 10 to 100 mm may be firmly held.

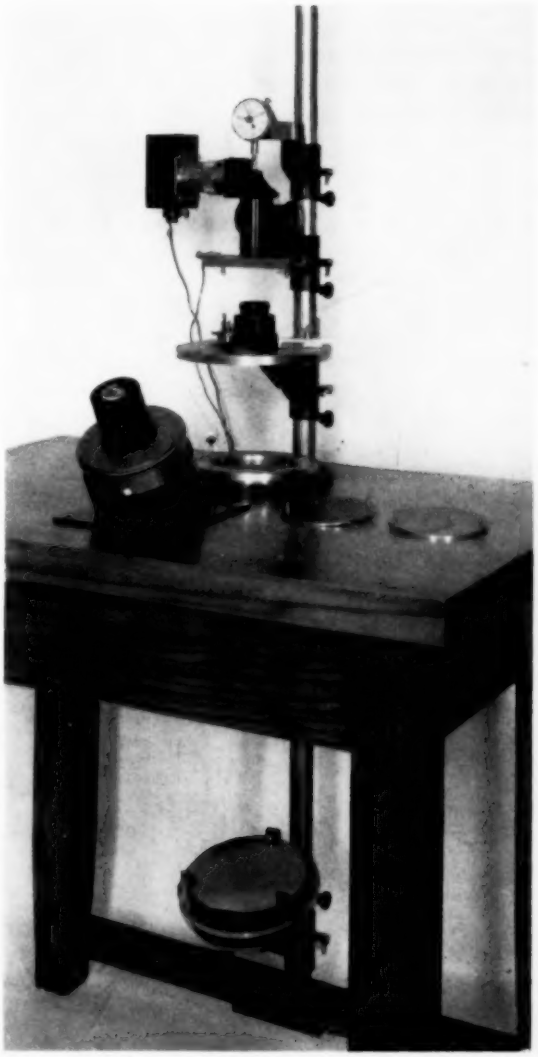

FIGURE 3. *Photograph showing the instrument and two of the auxiliary diaphragms.*

III. Theory of the Instrument

Longitudinal spherical aberration is the variation in focal length with differing annular zones of a lens. To measure the spherical aberration, it is customary to intercept parallel light before incidence on the lens by an appropriate diaphragm that limits the transmitting area of the lens to a selected annular zone; the position of the focal plane for this particular zone is then determined. The process is repeated for a series of diaphragms that successively isolate each annular zone until the entire surface has been covered. The position of the focal plane is determined for each of these zonal diaphragms with respect to the position determined for the first diaphragm. The resulting values of change in focus Δf are plotted against zone radius r and the typical longitudinal spherical-aberration-curve results.

The changes in focal length for successive zones of the lens under test in the foregoing method are

measured on a lens bench, using a moving microscope to observe the successive positions of best focus for the various zones. A collimator serves as the source of parallel light.

In the present instrument the light path is reversed. The collimator target is replaced by a viewing screen at the plane of focus for parallel light, or by an ocular so placed that the combination of viewing lens and ocular form a telescopic system. The moving microscope is replaced by a movable reticle whose displacements are registered on a sensitive dial gage. Light from the illuminated reticle passes through the lens under test and is properly imaged on the viewing screen only when the reticle is in the focal plane of the lens under test. When this condition is presented, parallel light is emerging from the lens under test. The isolation of successive zones of the lens under test is accomplished by the paired holes in diaphragm D_2.

In figure 4, a schematic drawing of the light paths through the instrument is shown. Light

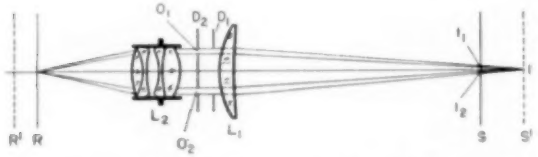

FIGURE 4. *Light paths through the instrument when reticle R is nearer to the collimating lens, L_2, than the focus of the zone determined by the diaphragm openings, O_1 and O_2.*

R must move to *R'* in order that a single image be seen on screen *S*.

from the reticle R, which is near the true focal plane of the lens, passes through lens L_2. The diaphragms, D_2 and D_1, intercept all light emerging from L_2, except for two small cylindrical beams that pass through the small openings, O_1 and O_2. These beams would normally be brought to a focus by lens L_1 at I in the plane, S'. However, the viewing screen, S, lying in the focal plane of L_1, intercepts the light so that the observer sees two images, I_1, and I_2, on screen S. Definite images are formed at S even though S is appreciably distant from the true image plane, S'. This is possible, as the beams of light passing through O_1 and O_2 are finite in size, and each beam is capable of forming an image of reticle R. The depth of focus is so great at small apertures that distinct images, I_1 and I_2, are seen at S, even though S does not coincide with the plane of best imagery.

Movement of reticle R along the axis of lens L_2 causes the images, I_1 and I_2, to separate from or to aproach each other, depending upon the direction of movement of R. In the present instance, if R moves to R', the two images, I_1 and I_2, coalesce to form a single image at S. If R moves beyond R', the images will again separate, but I_1 and I_2 will interchange their positions and I would lie between L_1 and S. When R and R' coincide, the reticle is at the focus of lens L_2 for the given zone, the beams of light passing through the openings O_1 and O_2 are parallel to each other and to the optic axis, and a single image appears on screen S. The reading on gage G is recorded, and a second pair of holes in D_2 is brought over the slot in D_1. The process of locating a position of R such that a single image appears at S is repeated, and the reading of gage G is recorded. The difference between the successive readings of the gage is the longitudinal spherical aberration, Δf, that exists between the two selected zones of the lens. This procedure can be extended for a sufficient number of zones to cover the entire lens and the complete longitudinal spherical-aberration data obtained.

IV. Results of Measurement

The longitudinal spherical and longitudinal chromatic aberration of a group of lenses having focal lengths varying from 3 to 13.5 inches have been measured with this instrument. The lenses are of various types and include telescope objectives, photographic objectives, and collimating or projection lenses. The results of measurements are shown graphically in figures 5 to 9. The zone radius is plotted as ordinate against the variation in focal length as abscissa.

In making these measurements, a set of diaphragm plates are used that permit isolation of successive zones at 2.5-mm intervals of zone radius, from the smallest for which fission of the image occurs to the maximum radius of the lens aperture. Wratten monochromatic filters Nos. 71A (Orange Red), 73 (Yellow Green), and 75 (Blue Green) provide a sufficient range of color separation to illustrate the nature of the longitudinal chromatic aberration.

In plotting the curves in figures 5 to 9, the values of Δf, corresponding to a given zone radius, are shown as circles for filter No. 75, as crosses for filter No. 73, and as solid circles for filter No. 71A.

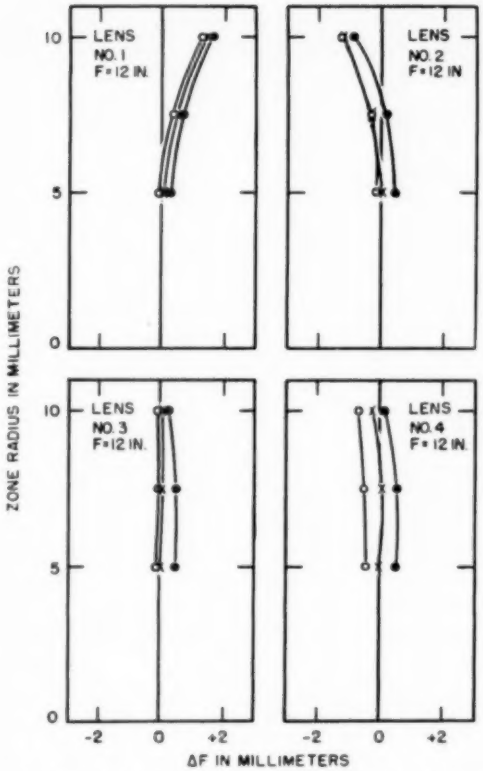

FIGURE 5. *Axial longitudinal spherical- and chromatic-aberration curves for a group of four telescope objectives.*

The open circles are determinations made with Wratten filter No. 75, the crosses with Wratten filter No. 73, and the solid circles with Wratten filter No. 71A. Lens No. 3 is a well-corrected lens having a flint front element, lens No. 1 is over-corrected spherically, lens No. 2 is not corrected for spherical aberration, and lens No. 4 is not corrected for axial chromatic aberration.

If a lens had no longitudinal spherical aberration, the resulting curve for a given filter would be a straight line parallel to the axis of ordinates. If a lens had zero longitudinal chromatic aberration, the points for the various colors of light for a given zone radius would coincide, and there would be no separation of the curves. However, these aberrations are always present to some extent in actual lenses, so that the maximum separation of points on a given curve measured along the axis of abscissae may be used to judge the excellence of the longitudinal spherical correction. The separation of the curves for the different colors is a measure of the amount of longitudinal chromatic aberration present in the lens.

The results shown in figure 5 are for a group of telescope lenses belonging to a laboratory demonstration set. Lens No. 1 is over-corrected spherically, which is evidenced by the curve, the focal length for the outer zone being approximately 1.5 mm larger than that for the innermost zone shown. Lens No. 2 is not spherically corrected and in consequence has an appreciably shorter focal length for the outer zone. Lens No. 3 is a well-corrected lens having a flint front element; it is clear from the flatness of the curves that the longitudinal spherical aberration is negligibly small, although there is appreciable longitudinal chromatic aberration as is shown by the separation of the curves. Lens No. 4 is not chromatically corrected, and all three of the longitudinal spherical aberration curves are well separated.

Figures 6, 7, and 8 illustrate the results obtained on photographic objectives of various focal lengths and types. Lens No. 6 in figure 6 is a telephoto lens having a large amount of spherical aberration. Lens No. 5 is a photographic objective having a moderate amount of spherical aberration. Lenses

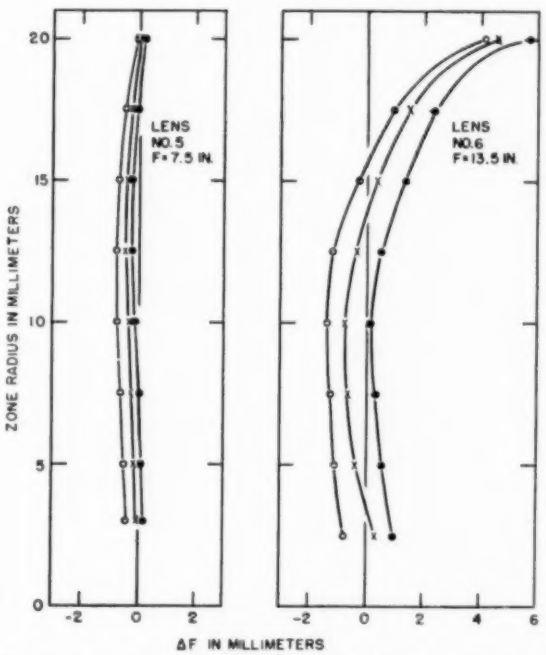

FIGURE 6. *Axial longitudinal spherical- and chromatic-aberration curves for two photographic objectives.*

The open circles are determinations made with Wratten filter No. 75, the crosses with Wratten filter No. 73, and the solid circles with Wratten filter No. 71A. Lens No. 6 is a telephoto lens having a large amount of spherical aberration, and lens No. 5 is a photographic objective having a moderate amount of spherical aberration.

Nos. 7 and 8 in figure 7 are of the same type but of different focal lengths; the amount of spherical aberration is great enough to produce noticeable change in focus when this type of lens is stopped down. Lenses Nos. 9 and 10 in figure 8 have so little spherical aberration that it is necessary to magnify the scale of abscissae to show it. However, the testing instrument is sufficiently sensitive that even these small amounts are readily measurable.

The spherical aberration of lens No. 11 is shown in the left-hand portion of figure 9. Lens No. 11 is a short-focus collimating lens and has a considerable amount of axial astigmatism. This is shown in the right half of figure 9. The measurements for curve 2 are taken along a diameter of the lens at right angles to the diameter used for curve 1. There are marked differences in the focal length through the range of zone radii. These two curves illustrate the capacity of the instrument to detect and measure astigmatic effects in lenses.

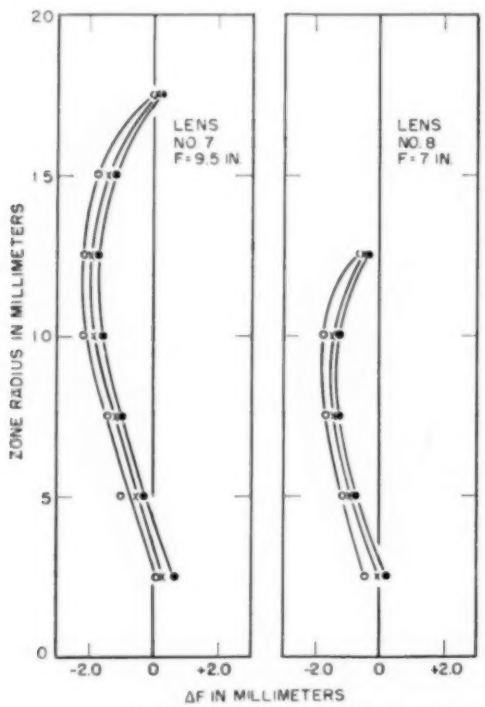

FIGURE 7. *Axial longitudinal spherical and axial chromatic aberration curves for two photographic objectives of the same type but having different focal lengths.*

The open circles are determinations made with Wratten filter No. 75, the crosses with Wratten filter No. 73, and the solid circles with Wratten filter No. 71A.

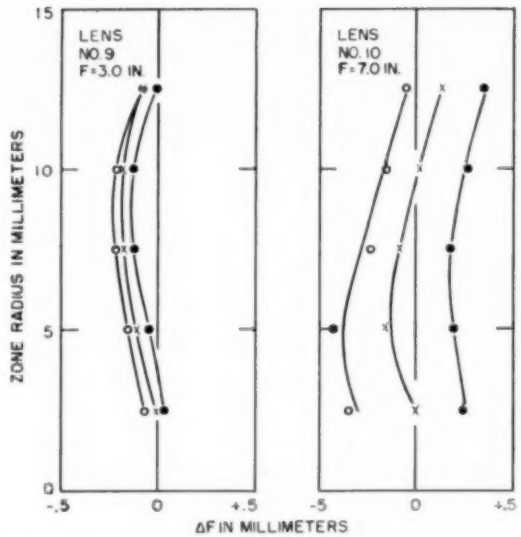

FIGURE 8. *Axial longitudinal spherical and axial chromatic aberration curves for two photographic objectives that have very small amounts of spherical aberration.*

The open circles are determinations made with Wratten filter No. 75, the crosses with Wratten filter No. 73, and the solid circles with Wratten filter No. 71A.

The accuracy with which the values of Δf can be measured with this instrument depends upon the f-number of the lens for the selected zone and the quality of the imagery. For good-quality imagery the probable error in millimeters of a single observation seldom exceeds ± 0.004 times the f-number. Accordingly, the accuracy varies from ± 0.02 mm for a zone with aperture ratio f/5 to ± 0.10 mm for a zone with aperture ratio f/25. The values of Δf can therefore be measured with good precision over most of the effective area of the lens, and as the depth of focus is so great at the large f-numbers, the accuracy of the method is adequate for most purposes even at the large f-numbers.

V. Additional Uses of the Instrument

The present instrument is the second to be constructed. The first instrument was built for the Army Air Forces and was primarily intended for use in measuring the parallax arising from longitudinal spherical aberration present in collimating lenses of the type used in reflector sights. During the course of investigation of the properties

of the primary instrument, it was found that the instrument was ideally suited for the rapid measurement of small refractive powers of goggle lenses in addition to its principal task of measuring longitudinal spherical aberration in connection with the computation of parallax. This section therefore discusses the manner in which the instrument is used to measure small refractive powers and the manner in which it is used to measure parallax of collimating lenses.

1. Measurement of Small Refracting Powers

One of the constantly recurring tasks at this Bureau is the measurement of the spherical refracting power of eye-protective lenses having, nominally, zero refractive power to determine compliance with the optical requirements contained in federal specifications. The tolerances

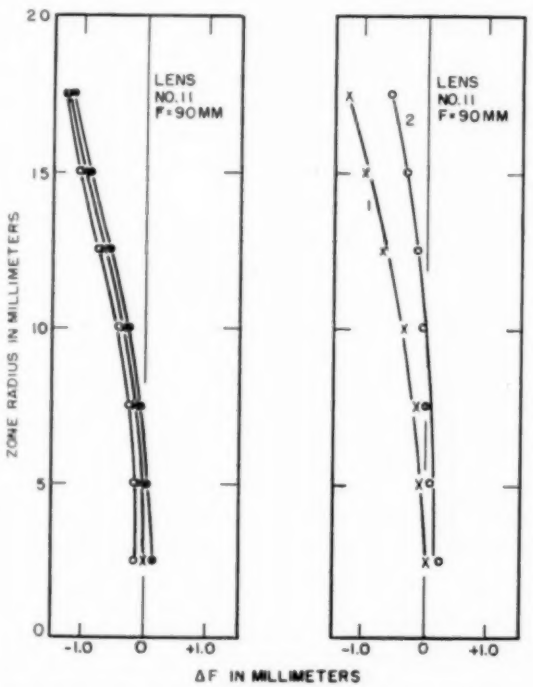

FIGURE 9. *Axial longitudinal spherical and axial chromatic aberration curves for a short-focus collimating lens is shown in the left-hand figure.*

The open circles are determinations made with Wratten filter No. 75, the crosses with Wratten filter No. 73, and the solid circles with Wratten filter No. 71A. The right-hand figure shows the effect of astigmatism, curve No. 1 shows the longitudinal spherical aberration along a selected diameter determined with Wratten No. 73 filter, and curve No. 2 shows the results obtained along a diameter at right angles to that used in determining curve No. 1.

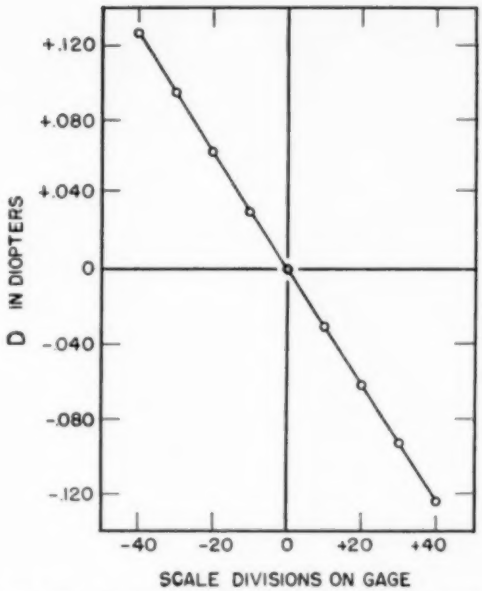

FIGURE 10. *Calibration curve for the instrument when being used to measure small refractive powers.*

on spherical power, which range from 0.00 to +0.06 diopter, are too small to permit accurate determination of compliance on the usual type of lens-testing instrument. The small range of 0.06 diopter amounts to only one-half scale division on most commercial-type instruments.

This new instrument may be readily used for the rapid measurement of small refractive powers. For this condition of use, lens L_2 is considered a part of the instrument, and its function is the providing of parallel light in the space between L_1 and L_2. The instrument is focused for a given pair of diaphragm openings by moving reticle R so that a single image is formed by lens L_2. The light entering the openings, O_1 and O_2, is accordingly parallel. The dial gage is set to read zero for this condition. If a goggle lens is placed over diaphragm openings O_1 and O_2 in the parallel light beams, no effect on the image formed by L_1 is noticed if the goggle lens has zero refracting power. However, if the lens does possess appreciable power, the image splits and reticle R must be moved to cause the two images to coalesce. The change in reading on the gage can then be interpreted in terms of the dioptric power of the goggle lens under test. For example, if the collimating lens, L_2, has a focal length of 90 mm, and

the goggle lens has a spherical refracting power of +0.06 diopter, the reticle must move −0.483 mm to neutralize the spherical power of the goggle lens. As the dial gage is calibrated in thousandths of an inch, this movement of 0.483 mm is equivalent to 19 scale divisions on the gage. Figure 10 shows the relation between gage readings and dioptric power of the goggle lens when collimating lens L_2 has a focal length, f, of 90 mm. The points on the curve are located from the relation

$$D=\frac{-1{,}000\ \Delta f}{f^2+f\cdot\Delta f},$$

where Δf is the change in position of reticle R, and D is the dioptric power of the goggle lens. With this arrangement, it is possible to measure the dioptric power of the goggle lens to the nearest 0.003 diopter. To determine compliance with the usual tolerances of 0 to +0.06 diopter, it is only necessary to see that the pointer of the gage always lies in the range 0 to −19 scale divisions.

2. Measurement of Parallax of Collimating Lenses

When the instrument is used to measure the parallax arising from longitudinal spherical aberration in short, focal-length, collimating lenses, such as are commonly used in reflector sights, the problem is mainly the rapid measurement of the maximum and minimum parallax of a lens for compliance with set tolerances, a typical tolerance being ±1 mil. Parallax, as here considered, is simply angular spherical aberration resulting from longitudinal spherical aberration, Δf, in millimeters and is related to it by the formula,

$$\epsilon=\frac{1019h\Delta f}{f^2}\text{ mils},$$

where ϵ is the parallax in mils, h is the radius of the selected zone, in millimeters and f the equivalent focal length of the lens in millimeters.

By proper selection of an intermediate zone and setting the dial gage to read zero when a single image is formed by L_1 for this zone, the value of Δf in the above equation becomes zero for this zone. Positive and negative values of ϵ can then be obtained for the other zones with respect to this selected zone. By establishing the condition of zero parallax for the proper intermediate zone, it is possible to obtain maximum positive and maximum negative values of ϵ approximately equal in magnitude for two other values of the zone radius. The three values of zone radius that satisfy the above conditions will vary from one type of lens to another. However, for a given type of lens the three values of zone radius remain remarkably constant, providing the focal lengths of the various lenses of the given type are approximately equal. The three values of zone radius for a given type of lens are determined initially from a study of the longitudinal spherical-aberration curves of a representative group of lenses of the given type. The curves vary so little from lens to lens that no difficulty is experienced in arriving at an appropriate set of values of zone radius that will be valid for setting the zones of zero, maximum-positive and maximum-negative parallax.

For one type of collimating lens of focal length of 90 mm and effective aperture of 40 mm, the zone of zero parallax has a radius of 17 mm, the zone of maximum-positive parallax has a radius of 10 mm, and the zone of maximum-negative parallax has a radius of 20 mm. If ϵ has a value of ±1 mil, then Δf is equal to +0.81 mm for $h=10$ mm and −0.40 for $h=20$ mm. Accordingly if a lens of this type is placed on the parallax comparator and focused to yield zero parallax for $h=17$, the zero of the gage may be set under the movable pointer and the two tolerance hands set at +0.81 and −0.40 mm, respectively. Then, the zones of maximum-positive and negative parallax may be quickly brought into position and the instrument focused for each in turn. If the movable hand does not take a position for either of these settings outside the range on the dial of the gage marked by the tolerance hands, the parallax does not exceed ±1 mil, and the lens is within tolerance. Lenses of this type can be checked for compliance with parallax tolerances at the rate of 30 per hour without placing any strain on the operator.

Washington, March 31, 1949.

U. S. Department of Commerce
National Bureau of Standards

Research Paper RP2016
Volume 42, August 1949

Part of the Journal of Research of the National Bureau of Standards

Volume Dilatometry[1]

By Norman Bekkedahl

The volume dilatometer, although inexpensive and simple in construction and principle, is found to be a valuable research tool, not only for obtaining data on volume coefficients of thermal expansion, but also for studying phase changes in solids and liquids. The preparation and operation of the volume dilatometer are described in detail. An illustrative calculation is given using data obtained from volume-temperature measurements on a sample of butyl rubber from about −30° to +90° C, using mercury as a confining liquid in the dilatometer.

I. Introduction

Dilatometers have been employed in various forms for the measurement of expansivity of both solids and liquids. Linear dilatometers of various types have frequently been used to advantage in determining the expansivity of metals and other solid materials. They cannot, of course, be used for measuring the expansivity of liquids, nor can they be relied upon to give correct results for nonrigid solid materials. In the latter instance, however, the volume dilatometer can be used successfully.

In addition to the simple determination of thermal expansivity of solids and liquids, this instrument has been used to great advantage in the study of phase changes. In experiments performed on unvulcanized natural rubber at this Bureau, it was found necessary, because of time lags in transitions, to study the phase changes of rubber by means of the dilatometer [5][2] before satisfactory calorimetric measurements of specific heats could be made. The volume dilatometer offered a convenient means for studying rates of crystallization of vulcanized rubber [6], unvulcanized rubber [5, 24, 39], of glycerine [35], and also of sugar from a saturated solution [19]. Change of volume of rubber compounds has been studied while they are in the process of being stretched [18, 22]. In the dilatometric work of Holt and McPherson [18] on the crystallization of rubber upon stretching, this method proved simpler and produced more useful information than was obtained by the more elaborate X-ray techniques [1, 23]. Mondain-Monval [26] determined the various transition temperatures for sulfur and for selenium. Several investigators used dilatometers to study volume changes during polymerization [14, 30, 33] and other reactions [15]. The quantity of bound water in solids has been determined accurately by similar procedures [2, 8].

Second-order transitions have been studied by this simple method. Raw rubber, using alcohol as a confining liquid in the dilatometer, was found to undergo this type of transformation at about −70° C [5], whereas vulcanized rubber showed a corresponding change at higher temperatures, depending on the degree of vulcanization [5, 37, 38]. Various investigators have obtained considerable information on the characteristics of the second-order transition by studying volume-temperature relationships for polystyrene and other plastic materials [3, 7, 13, 21, 27, 32]. Some of these authors, and also others [3, 20, 27, 32, 36], have studied the nonequilibrium features of this type of transition. Boyer and Spencer [7] found the volume technique valuable in investigating the nature of polymeric mixtures and the homogeneity of copolymers. Jenckel and Ueberreiter [20, 21] likewise studied various substances, determining the effects of different molecular weights of polymers and also the effects of addition compounds on the temperature of this transition.

[1] This work was financed, in part, by funds transferred from the Office of Naval Research.

[2] Figures in brackets indicate the literature references at the end of this paper.

In previous papers on volume dilatometers [5, 6, 10, 12, 13, 15, 16, 19, 21, 28, 33, 36, 38, 39], the emphasis has always been on the results obtained, and the descriptions of methods of operation have usually been very brief or missing completely. Standard texts on measurements in physical chemistry do not include descriptions of the construction and operation of volume dilatometers. This paper has, therefore, been written in considerable detail. The construction, operation, and method of calculating the results are described in full. The practices are similar to, but include marked improvements over, those previously used in this laboratory for investigations on rubber [5, 6, 39]. Illustrative data are given, together with detailed calculations, yielding, for the first time, information on the expansivity of a butyl rubber pure-gum vulcanizate.

II. Sample

A number of samples of different types of rubber in different compounding formulas have been measured for expansivities by means of volume dilatometers. However, only one of these samples was chosen for use in this article to illustrate the procedures of volume dilatometry and the methods of calculating the results from the data. This sample was a vulcanized gum stock of butyl rubber, compounded according to the formula

GR–I synthetic rubber (butyl)	100 parts
Zinc oxide	1. 0 part
Sulfur	1. 5 parts
Butyl zimate	1. 0 part
Total	103. 5 parts

The compound was cured in the form of sheets of 2-mm thickness for 60 minutes at 153° C.

III. Preparation of Dilatometer

The dilatometer is made solely from glass tubing and a glass capillary. The tubing from which the bulb of the dilatometer is made can be of any size convenient to fit the size and shape of the sample. The size of the capillary depends on the range of volume expected to be covered in a given set of measurements, which in turn depends on the size of the sample, its expansivity, and the range of temperature to be covered. The greater the uniformity of bore throughout the length of the tube, the simpler are the calculations and more reliable are the results.

1. Calibrating the Capillary

The capillary used to make the dilatometer described here was approximately 500 mm in length and about 2 mm in inside diameter. The thickness of the wall of the capillary was about 3 mm. It was made from Pyrex glass by the Corning Glass Company and was described as "specially selected as to uniformity." It was graduated along its entire length in millimeters.

The capillary is calibrated by weighing mercury, at a known temperature, that had occupied known portions of the tube. In order to determine this volume with considerable accuracy, the zero (lower) end of the capillary is sealed to one arm of a capillary stopcock, the other arm of which is drawn to a smaller opening, thus forming a burette. In order to prevent air from being trapped in the stopcock, the mercury is introduced into the capillary by "sucking" it up through the stopcock and into the capillary by means of a vacuum pump.

After the level of the mercury in the completely filled capillary is recorded, a portion of the mercury, say from about 50 to 75 mm in length, is run out into a container and weighed. The volume of the capillary between these two levels is determined from the weight of the mercury and tables of its density [34]. This same operation is then repeated, beginning at each new level of the mercury in the capillary, until some level near the bottom of the capillary is reached. Care should be taken, however, not to work too close to the seal because of a possible abnormal size of the capillary in this region. From the volume of mercury occupying the space between the highest and the lowest levels, the average change of volume per unit length, in milliliters per millimeter, is calculated. For the capillary used in these experiments the value was determined to be 0.003720 ml/mm.

Using the lowest recorded level of the capillary as a reference point, or as zero volume, the nominal volumes of the capillary at the other levels of calibration are calculated, assuming complete uniformity of internal diameter throughout the length of the capillary. At the various levels of calibration, these nominal or uncorrected volumes are compared with the actual volumes as obtained

by calibration. The differences between these two sets of values give the corrections of the capillary at these readings. If the true volume is greater than that obtained by assuming uniformity of bore, then the correction is positive; and if it is less, then the correction is negative.

From these data a graph is prepared in which the correction for nonuniformity of the capillary is plotted as a function of the reading of the capillary graduations. Corrections are zero, of course, at the highest and lowest levels of calibration of the capillary. From this curve is determined the correction to be applied to the linearly calculated volumes for any given level of capillary. For the capillary used in the present investigation the correction curve is shown in figure 1. For

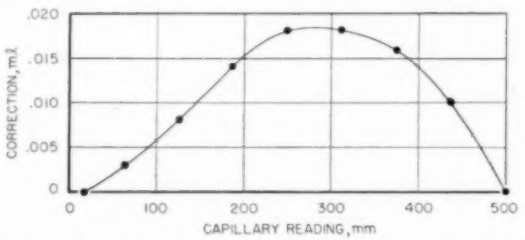

FIGURE 1. *Corrections to be applied to the volume of the capillary at various heights to account for irregularity in cross section.*

reasons that will be seen later in this paper, it is advisable to estimate the readings of the capillary to the nearest 0.5 mm and the weight of the mercury to the nearest 10 mg. From these calculations the volumes can be obtained to the nearest 0.002 ml.

2. Adding the Sample

The stopcock is removed from the capillary, and the zero end of the capillary is then sealed to one end of the 20-mm tube (see fig. 2, A and B). Into the large, open end of the glass tube is inserted the weighed sample. In this experiment, the sample of rubber was introduced in the form of strips cut from vulcanized sheets. These strips were cut in various widths, so as to fill up the cross-sectional area of the tube. The weight of the rubber sample was 27.321 g.

After the sample, there is inserted a hollow bulb made from the same type of glass as the dilatometer. The arrangement up to this point, which can be seen in figure 2, C, is sealed off just

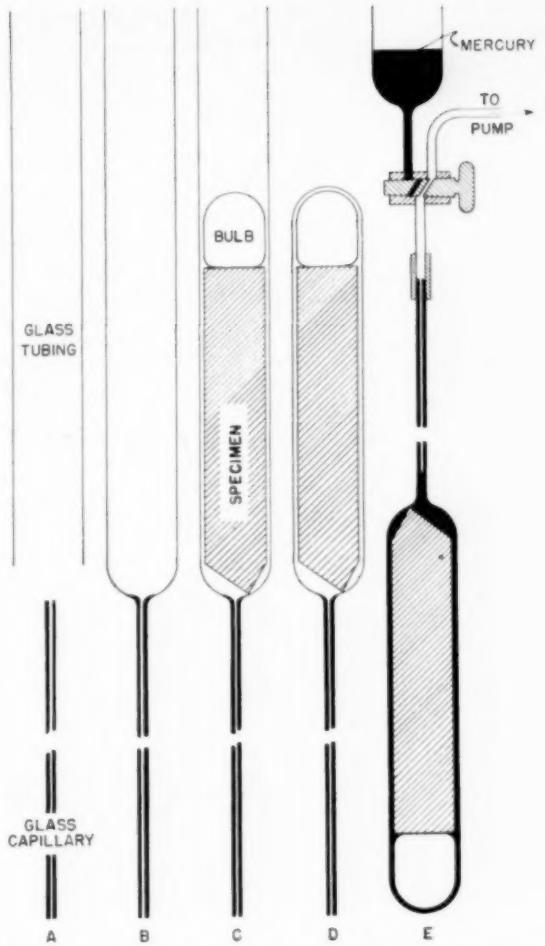

FIGURE 2. *Steps in the construction and filling of a volume dilatometer.*

above the hollow bulb, forming the completed dilatometer illustrated in figure 2, D. The sole object of the small, hollow bulb is to allow the sealing of the dilatometer without unduly heating the specimen and without increasing the net volume of the dilatometer. Sealing the dilatometer at the same distance from the specimen without the presence of the bulb may avoid overheating the sample, but it leaves more space to be occupied by the confining liquid, thus decreasing the precision of measurement. As the hollow bulb is made of the same material as the rest of the dilatometer, no correction need be made for its volume or its expansivity. The insertion of the bulb is therefore equivalent to reducing the net

volume of the dilatometer. Depending on the shape of the specimen, the volume of a sample in a dilatometer constructed in this manner may occupy as much as 75 percent or more of the total volume of the dilatometer. The dilatometer in this form is then weighed. For the experiment described here the weight of the dilatometer including the sample was 122.22 g.

In an effort to eliminate the process of heat-sealing the glass bulb, one of the experimental dilatometers was prepared a little differently. Its bulb was made up of two parts, the bottom and the top halves joined to each other by means of a ground joint held together by springs. Although this bulb gave no real trouble, it required considerable care to keep it tightly closed, and less confidence was felt in the ground-glass joints through which there was always the possibility of a leak.

Still another variation from the above-described dilatometers has been found necessary when the sample under investigation is soft enough to flow and is less dense than the confining liquid. In one experiment a soft polymeric material, under upward pressure from the mercury, was forced into the capillary on a rising temperature but would not return to the bulb on cooling. For use with substances of this type the capillary can be given a U-bend near the bottom, thus inverting the bulb.

3. Choosing the Confining Liquid

A confining liquid to be used in the dilatometer, in order to be entirely suitable for the purpose, must satisfy certain requirements. It must exist in the liquid state over the entire range of temperature in which measurements are desired. It must have a vapor pressure sufficiently low that none of the liquid is lost by evaporation during the course of experiment. Its viscosity must not become unduly high at the lower temperatures. It must have little or no swelling action on the specimen. Its expansivity must be known accurately over the entire range of temperature for which it is to be used. In the present investigation mercury was used as the confining liquid because it satisfied all these requirements. Mercury is to be strongly recommended for use in all investigations not requiring measurements below $-39°$ C.

In earlier work on rubber in this laboratory other confining liquids have been used [5]. Water is satisfactory near room temperature, but the relatively small range of temperature between its freezing and boiling points greatly limits its usefulness. There are a number of organic liquids that are suitable for use at low temperatures. Acetone and the alcohols have been used. However, these liquids produce some swelling of natural rubber over long periods of time. This swelling was not observed to produce any change in expansivity, but in one instance swelling by acetone probably displaced the second-order transition of unvulcanized natural rubber to a lower temperature [5]. It is recommended that methyl alcohol be used in work at temperatures below $-39°$ C. Some of the new liquid silicones may also prove to be useful in this range of temperature.

4. Adding the Confining Liquid

The dilatometer is placed in its normal upright position (see fig. 2, E) for the insertion of the confining liquid. Into the capillary is inserted a fine wire, about 0.4 mm in diameter, of such length that it reaches into the bulb of the dilatometer and rests against the specimen. The composition of the wire must be such that it is inert to both the sample and the confining liquid. The wire is then cut off at a point about 5 cm above the top of the capillary. The object of this wire is only to allow any entrapped air to pass more freely through the confining liquid in the capillary, and it is removed before measurements are made. A three-way stopcock is connected, by means of a short length of heavy-walled rubber tubing, to the top of the capillary, allowing the top of the wire to enter into the tube of the stopcock. A diagram of these connections can be seen in figure 2, E; but in order not to make the drawing too involved the wire is not shown. Through the three-way stopcock the dilatometer can be connected either to a mercury reservoir or to an efficient mechanical-type vacuum pump.

The dilatometer is first connected to the vacuum pump in order to remove the air from the confining spaces of the dilatometer and also from the sample. This operation sometimes requires but a few minutes, and other times it takes several days, depending on the quantity of gas dissolved in the speci-

men. Gases must be removed quantitatively, because their expansivities are usually much different from that of the sample, and their volume changes are also greatly dependent on variations in pressure exerted upon them. After the dissolved or entrapped air is thought to be removed, the stopcock is turned in order to allow the confining liquid to enter the dilatometer, including part of the capillary.

Any small amount of gas entrapped in the dilatometer can be determined quantitatively. The level of the liquid in the capillary is measured when the dilatometer is at atmospheric pressure. Then, at the same temperature, a vacuum is applied to the capillary tube. The presence of entrapped air in the dilatometer causes the level to rise to a steady state in the capillary. The amount of rise, however, depends not only on the quantity of gas entrapped and the pressure change, but also on the compressibility of the materials in the dilatometer and of the dilatometer itself. The increased level of the liquid is noted.

For the dilatometer and its contents described in this investigation the increase in height of the mercury upon application of the vacuum was 1 mm, which is equivalent to a volume of 0.0037 ml. From the volume compressibility of soft vulcanized rubber, about 50×10^{-6} per bar [31], the volume of the rubber in the dilatometer increases by about 0.0015 ml for a decrease in pressure of one atmosphere. Similarly the volume of the mercury increases by about 0.0001 ml. A decrease of pressure inside the dilatometer also tends to decrease the volume of the dilatometer by an amount that has not been calculated. All three of these factors, therefore, cause the level of the mercury to rise in the capillary when the dilatometer is subjected to a reduced pressure. This means that the increase in volume arising from these factors must be subtracted from the total observed increase in volume in order to calculate the volume of any gas inside the sample. The value thus obtained is 0.0021 ml or less.

The reading for the mercury level in the capillary at room temperature was 368 mm above the zero. If it is assumed that the gas bubble was near the middle of the specimen, about 90 mm below the reference zero, a hydrostatic pressure of 458 mm of mercury was exerted on this bubble of gas while vacuum conditions existed above the mercury. Under normal atmospheric conditions the pressure on the gas bubble was therefore about 1,218 mm of mercury. From the gas laws,

$$V_a=\frac{458}{1{,}218}\cdot V_v,$$

in which V_a is the volume of the gas bubble with atmospheric pressure on the mercury and V_v the volume with vacuum. The difference in these volumes was measured in the capillary as

$$V_v-V_a=0.0021 \text{ ml}.$$

Solving the two equations for the volume V_a, one arrives at a value of 0.0013 ml of gas in the dilatometer. Experience has shown that this small quantity of gas is negligible. After volume-temperature measurements for the dilatometer are completed, the resulting data may be used to calculate the error caused by this quantity of gas.

After adjustment of the level of the liquid in the capillary, the dilatometer is again weighed in order to determine the quantity of confining liquid. If some of the confining liquid must be removed from the capillary, it can easily be done by inverting the dilatometer and playing the wire inside the capillary. The weight of the dilatometer, including the sample and the liquid used in the present investigation, was 386.93 g, of which 264.71 g were therefore mercury.

If a confining liquid is used that is too volatile to be added conveniently by the above procedure employing a vacuum, the liquid can be added by subjecting the dilatometer bulb alternately to high and low temperatures. In this case, a funnel containing the confining liquid is fastened to the top of the capillary.

IV. Experimental Procedure

The assembly of apparatus used for making these measurements is quite simple. A cylindrical flask of about 6-liter capacity contains the baths of alcohol and of water that are used, depending on the temperature range of the experiment. For temperatures below 0° C it is recommended that a vacuum-jacketed cylinder be used as the container for the bath. This type of bath container is not actually necessary for proper operation but provides easier control of temperature. Measurements may be conducted on several dilatometers in the bath during the same run. An efficient stirrer is required to maintain uniform tempera-

ture throughout the bath. Heat may be furnished the bath by means of an electrical immersion heater controlled by a variable-ratio autotransformer. The temperature of the bath can be measured by calibrated thermometers capable of reading to the nearest 0.1° C.

A determination of the density of the sample must be made in order to obtain the volume of the specimen in the dilatometer. The preparation of the rubber sample for the density measurements and the method of determining the density were the same as those described in detail in another article [40]. This method of hydrostatic weighings is an excellent method for measurement of density [4] if a liquid is available whose density is accurately known, and if the liquid has no solvent action on the sample to be measured. Utilizing an analytical balance having a sensitivity of 0.1 mg, density values can be obtained that are reproducible to about 0.0002 g/cm^3 or better.

For each set of measurements of volume-temperature in the dilatometer there must be recorded the room temperature, the reading of the dilatometer-stem at the surface of the bath, and also the reading of the thermometer-stem at the bath level. These data are necessary for the subsequent stem corrections for both the dilatometer and the thermometer.

With the stirrer operating and a constant and uniform temperature attained, readings are first made of the liquid levels of the dilatometer capillary and of the thermometer. Dry ice is then added to the alcohol bath in order to cool to the proper temperature. With mercury as a confining liquid, the lower temperature of measurement is limited to about −39° C because of the freezing of mercury. After the bath and dilatometer have remained at the lower temperatures sufficient time to be sure of temperature equilibrium, measurements are made of capillary and thermometer readings. The temperature is then allowed to rise slowly, usually less than 0.5° C per minute. A faster rate of heating may cause a lag of temperature between the sample and the bath. The safe rate of heating can easily be checked by adding powdered dry ice in a quantity just sufficient to hold the temperature constant. If the capillary reading at this constant temperature checks with the equivalent one made on a rising temperature the rate of heating can be considered safe. If the test indicates a lag of temperature in the dilatometer the heating rate should be reduced. The maximum allowable rate is, of course, dependent on the heat conductivity of the confining liquid and the sample, and also on the size and shape of the specimen in the dilatometer. The rate of heating can be regulated very easily by either the controlled addition of dry ice or by the controlled application of current in the heater.

When the temperature is reached where the liquid of the dilatometer approaches the top of the capillary, the heating is discontinued and the temperature allowed to attain that of the room, at which time the temperature and volume readings are again noted. A rought graph is plotted between the temperature and the capillary readings. The two values obtained at room temperature, before and after the run, should both lie on the smooth curve obtained from data of the run unless there has been introduced some disturbing influence, such as the transformation to a different phase of the material or the formation of gas in the dilatometer.

Where data are desired at temperatures higher than those attained in the previous experiment, confining liquid must be removed from the dilatometer in order to bring the level nearer the bottom of the capillary. The dilatometer and contents need not be reweighed after this operation, as the volume of the dilatometer has already been established from previous data. Experimental data above room temperature are then taken in the same manner as in the previous run.

1. Calculations

Table 1 includes all the data taken from the present experiment that are necessary for calculation of results, with the exception of the calibrations of the capillary tube, which are shown in figure 1. The experimental data in the table begin with the weight of the sample, on line 1, and continue through line 11, the capillary readings as measured. All figures in the table below this latter line are calculated from the previously listed data.

In the bottom line of the table are recorded the corrected temperatures. These figures include the previously determined corrections for the inaccuracies of the thermometer and also the corrections for emergent stem. The latter corrections are made according to the usual procedure [11], taking

TABLE 1. *Experimental data and calculated values for the volumes and densities of a sample of butyl gum rubber in a dilatometer*

1	Weight of sample	27.321 g.								
2	Weight of sample and dilatometer	122.22 g								
3	Weight of sample, dilatometer, and mercury (first series)	386.93 g.								
4	Temperature of room during dilatometric measurements	27° C.								
5	Capillary stem reading at level of bath	100 mm.								
6	Thermometer stem reading at level of bath	50° C.								
7	Capillary size, assuming uniform	0.003720 ml/mm.								
8	Density of sample at 25° C [1]	0.9333 g/cm.³								
9	Capillary calibration	Figure 1.								
		First series				Second series				
10	Thermometer readings (measured) °C.	.....	−23.7	−4.8	10.2	.....	41.3	53.9	67.2	81.0
11	Capillary readings (measured) mm.	(368.0)	111.0	212.5	290.5	(80.5)	163.0	227.0	297.0	370.0
12	Capillary readings (stem-corrected) mm.	368.0	111.0	212.0	290.0	80.5	163.0	227.5	298.0	372.5
13	Capillary volumes (uncorrected for irregularity) ml.	1.369	0.413	0.789	1.079	0.299	0.606	0.846	1.109	1.386
14	Corrections for irregularity (fig. 1) ml.	+0.016	+.006	+.016	+0.018	+.004	+.012	+.017	+0.018	+0.016
15	Capillary volumes (corrected for irregularity) ml.	1.385	.419	.805	1.097	.303	.618	.863	1.127	1.402
16	Total volume of contents (uncorrected) ml.	48.834	47.868	48.254	48.546	47.752	48.067	48.312	48.576	48.851
17	Total volume of contents (corrected for glass expansion) ml.	48.834	47.845	48.240	48.539	47.752	48.075	48.326	48.586	48.878
18	Volumes of mercury ml.	19.560	19.385	19.457	19.508	18.478	18.533	18.575	18.620	18.667
19	Volumes of sample ml.	29.274	28.460	28.783	29.031	29.274	29.542	29.751	29.976	30.211
20	Densities of sample g/cm.³	[1] 0.9333	0.9600	0.9492	0.9411	[1] 0.9333	0.9248	0.9183	0.9114	0.9043
21	Specific volumes of sample cm.³/g.	1.0715	1.0417	1.0535	1.0626	1.0715	1.0813	1.0889	1.0972	1.1058
22	Temperatures (corrected) °C.	(25.0)	−24.2	−5.0	10.3	(25.0)	41.3	53.9	67.3	81.3

[1] Hydrostatic weighings.

into account the coefficients of expansion of both the glass and the liquid inside the thermometer.

The corrections for the emergent stem of the dilatometer are made in a manner similar to that used for the emergent stem of the thermometer. The difference between the expansivity of mercury used in the present dilatometer [34] and that of Pyrex glass [9, 17, 29] is 0.00017 per degree C. In table 1, line 12, are given the capillary readings after correction for emergent stem. The formula by which they are corrected is

$$\text{correction} = K\ (t - t_r)\ (R - R_b),$$

in which K is the coefficient previously described (0.00017, if mercury is used in Pyrex glass), t is the temperature of the bath in degrees centigrade, t_r is the temperature of the liquid in the emergent stem, which is practically the same as that of the room, R is the reading of the level in the capillary in millimeters, and R_b is the capillary stem-reading at the level of the bath. These corrections are made to the experimental readings to the nearest 0.5 mm.

From the stem-corrected dilatometer capillary readings (table 1, line 12) and the average size of the capillary in milliliter per millimeter (line 7), the capillary volumes, uncorrected for irregularity (line 13), are calculated for all of the temperatures of measurement recorded in the table. To these figures are added the corrections for nonuniformity of bore of the capillary (line 14), giving the corrected volume of mercury in the capillary (line 15). For the capillary used in these experiments the corrections (see fig. 1) are all positive, which indicates a continuous decrease in the diameter of the tube in going up the capillary. Any abnormal size of the capillary near the zero reading or below the calibrated portion of the capillary will cause no error in the calculations, as the difference caused by this abnormality is taken care of in the calculations for the size of the bulb of the dilatometer.

A curve plotted from the original data, capillary readings versus temperature, showed that the mercury in the dilatometer stood at 368.0 mm at 25° C. Since the values for temperature and dilatometer readings in the first column of figures were obtained from the graph and not directly from measurements, they are placed in parentheses. A similar situation exists in the fifth column of figures, the level of the mercury being different because some of the confining liquid had been removed, and the total volume was therefore changed. There is, of course, no stem correction to be made at room temperature. From the zero reading of the capillary, which is used as a

reference point, the volume occupied by the mercury of the stem, assuming a uniform bore throughout, is 368.0×0.003720, or 1.369 ml. From the calibration curve for the capillary, which was made previous to the preparation of the dilatometer and shown in figure 1, the correction at this height for nonuniformity of bore is found to be +0.016 ml. Therefore, the true volume of mercury in the capillary at 25° C is 1.385 ml.

The volume of the dilatometer contents is determined from the weights and densities of the specimen and the confining liquid. For the present experiment the density of the sample of vulcanized butyl gum rubber was measured by means of hydrostatic weighings in distilled water and found to be 0.9333 g/cm³ at 25° C. The 27.321-g specimen therefore occupies a volume of 29.274 cm³ at 25° C. At this same temperature the density of mercury is 13.5340 g/ml, and therefore the 264.71 g of confining liquid used in the first series of experiments occupies a volume of 19.560 ml at 25° C. This gives a total volume of 48.834 ml for the contents of the dilatometer at 25° C.

The weight of mercury of 264.71 g was that used only for the first series of experiments, performed below room temperature, and therefore could not be used in calculating the results tabulated in the second series, which were made above room temperature. The experiment described in the second series was made after some mercury had been removed in readjusting the level of the confining liquid in the capillary. At 25° C, the mercury level after readjustment stood at 80.5 mm in the dilatometer capillary. This height corresponds to a volume in the capillary of 0.299+0.004, or 0.303-ml corrected volume. The capillary volume at 25° C in the first series was calculated to be 1.385 ml. Therefore, the amount of mercury removed was 1.082 ml, or 14.644 g. This left a weight of mercury of 250.07 g in the dilatometer for the second series of experiments.

The volume of the contents of the dilatometer (mercury plus sample) in the first series of measurements was calculated to be 48.834 ml at 25° C. Subtracting the volume of the mercury in the capillary at this temperature, 1.385 ml, leaves a volume of 47.449 ml for the bulb at 25° C. In order to determine the total volume of the contents at other temperatures, the bulb volume of 47.449 ml is added to the corrected capillary volumes. This total volume (table 1, line 16) must, of course, be corrected further for the expansion or contraction of the glass of the dilatometer itself. The corrected volumes at other temperatures, V_t, may be calculated from the equation

$$V_t = V_{25} \quad [1+0.000010 \quad (t-25)],$$

in which V_{25} is the total volume of the dilatometer contents at 25° C, t is the temperature in degrees centigrade, and 0.000010 is the volume coefficient of expansion of laboratory Pyrex glassware [9, 17, 29]. These corrected volumes are recorded in line 17 of the table.

The volumes of the mercury at the different temperatures (table 1, line 18) are calculated from the densities of mercury given in International Critical Tables [34]. It was found that, for the range of temperatures covered in these experiments, the volumes of mercury could be calculated to a precision of nearly one part in 100,000 by means of the equation,

$$V = M \ (0.073554 + 0.0000134 \ t),$$

in which V is the volume of the mercury in the dilatometer in milliliters, M is its weight in grams, 0.073554 is its specific volume in milliliters per gram at 0° C, 0.0000134 is the temperature coefficient for its specific volume, and t is the temperature in degrees centigrade.

The volumes of mercury (table 1, line 18) are subtracted from the corrected total volumes (line 17) in order to obtain the volumes of the sample at the various temperatures (line 19). The calculations for the densities (line 20) and the specific volumes (line 21) are then made from the calculated volumes and the weight of the sample in the dilatometer.

Table 1 illustrates the method of calculating the specific volumes and densities of the specimen at different temperatures. It contains only a representative portion of all the capillary and temperature data recorded in the experiments. The results calculated in the table, together with the results calculated from all the other data not recorded here, are reproduced in figure 3, which shows a graph in which the densities and the specific volumes of the sample of rubber are plotted as a function of the temperature. The

slope of these curves gives the changes in density and specific volume with respect to temperature,

$$\frac{d\rho}{dT} \text{ and } \frac{dV}{dT}$$

A differentiation with respect to temperature of the equation, $\rho = m/V$, where m is the mass of the sample, gives

$$\frac{d\rho}{dT} = \frac{d}{dT}\left(\frac{m}{V}\right) = -\frac{m}{V^2}\left(\frac{dV}{dT}\right).$$

From this, one may obtain the equation

$$\frac{1}{\rho}\left(\frac{d\rho}{dT}\right) = -\frac{1}{V}\left(\frac{dV}{dT}\right).$$

It will be noted that all of the values of specific volume are represented in the graph by a straight line. The points representing the densities, however, fall on a curve that is slightly concave upward. Since $\rho = m/V$, it is evident that ρ and V cannot simultaneously vary linearly with T at any given temperature. If one of these varies linearly, the other must vary hyperbolically. Instead of drawing a curve to try to fit all of the values of density, a straight line was drawn that represents its tangent at a temperature of 25° C. The object of this curve is to calculate the density coefficient at room temperature. From a large-scale drawing of the same graph, both the specific volume and the density curves show the coefficients

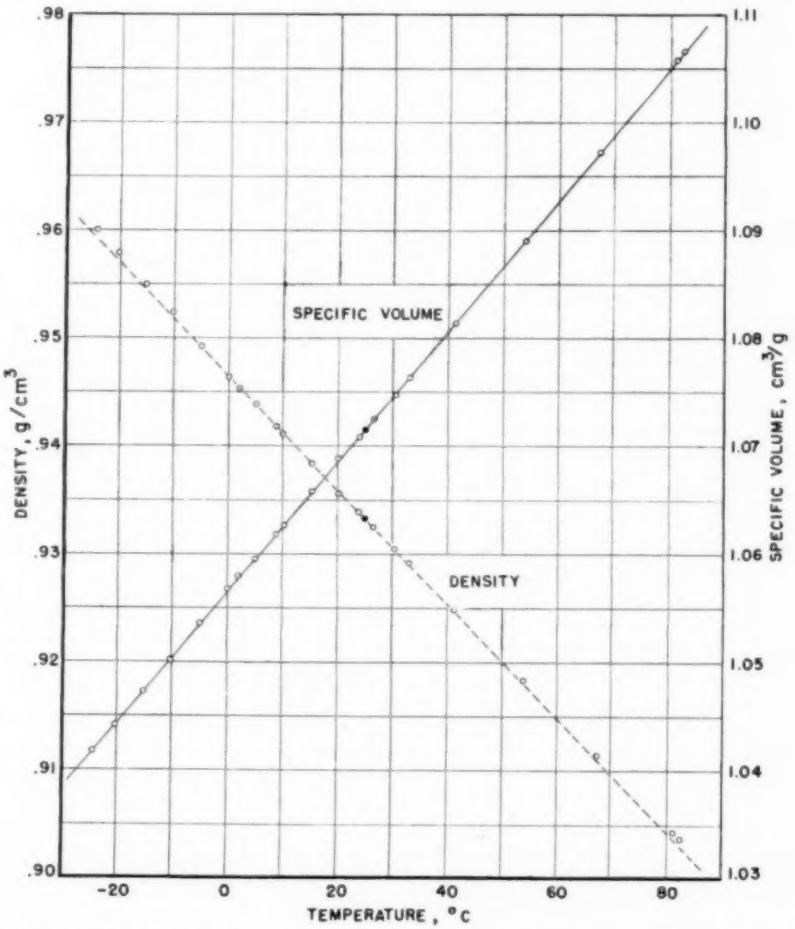

FIGURE 3. *Specific volume in cm³/g and the density in g/cm³ of a butyl gum rubber at different temperatures.*
These values are obtained from volume measurements in a dilatometer and are based on a density measurement at 25° C by means of hydrostatic weighings.

$(1/V)$ (dV/dT) and $-(1/\rho)$ $(d\rho/dT)$ to be 0.000567/deg C at 25° C. This value is about 15 percent lower than that found for pure-gum vulcanizates of natural rubber [6].

2. Precision of Measurements

The values of the densities of a sample determined in a dilatometer at different temperatures can be of no greater precision or accuracy than the density value used as reference. For samples such as that used in these experiments and the method used to measure the density, the reproducibility of values of this constant is about ±0.0002, or about two parts in 10,000. Therefore all other measurements should, if possible, be carried out to insure this continued precision. In order to do this, the weight of the specimen should be measured to the nearest 1 mg. The mercury, and thus the dilatometer too, should be weighed to the nearest 10 mg. The readings of the capillary of the dilatometer should be estimated to the closest 0.5 mm, which is equivalent to about 0.002 ml. The accuracy of the temperature should be within 0.1 deg, as an error of 0.1 deg is equivalent to about 0.002-ml volume change for the contents of the dilatometer. The corrections for the capillary must, of course, fall within these same limits.

It seems, therefore, that the limiting factors in the precision of the method are the ability to make precise measurements of temperature and of height of mercury in the capillary. The precision of these measurements could, of course, be stepped up to some degree, but this would serve no useful purpose unless the density values were more reliable. From the position of the individual specific volume values with relation to the curve in figure 3, it would appear that the expansivity values are good to within 1 percent. This is equivalent to an error of ±0.0003 in the density or specific-volume values at the extreme ends of the curves.

In order to obtain precise results in expansivities the samples must be free from gases. The error caused by the presence of small amounts of gas can, however, be calculated. For example, it has been demonstrated that in the experiments described in this article there was about 0.0013 ml of gas in the dilatometer at room temperature. At the lowest temperature at which measurements were made, −23.7° C, the capillary reading was 111 mm above the zero. If, as before, the bubble is assumed to be in the center of the sample, 90 mm below the zero reference, the pressure on the bubble of gas would be 961 mm of Hg. At 25° C it was found to be 1,218 mm. The 0.0013 ml of gas in the dilatometer at 25° C had therefore been changed at −23.7° C to

$$0.0013 \times \frac{273-23.7}{273+25} \times \frac{1,218}{961} = 0.0014 \text{ ml.}$$

The difference in volume of the gas between 25° C and −23.7° C is therefore only 0.0001 ml, which is beyond the limits of experimental measurement. The effect of this quantity of gas can therefore be disregarded. The same holds true for those experiments performed above room temperature for the same dilatometer and contents.

The precision of this type of a dilatometer can, of course, be increased to beyond that described here. In order to do this one must be able to measure more accurately the temperature and the volume. The temperature-measuring instrument must be able to read smaller intervals of temperature and to have greater accuracy. The rate of heating must be made slower and more uniform, or it may be advisable to make measurements at constant temperatures and increase the temperature stepwise. The volume could be read more precisely if a capillary of smaller diameter were used. This, however, introduces more trouble in adding the confining liquid and regulating the level in the capillary before measurements are started. Madorsky [25] inserted wire of known and uniform diameter into the larger capillaries of his dilatometers, thus making them more sensitive. The range of temperature that a dilatometer can cover in a single experiment is, however, greatly decreased when using smaller capillaries. Gibson and Loeffler [16] and Burlew [10] used dilatometers of a different design and were able to weigh the mercury equivalent to the change in volume, thus increasing their precision. Their dilatometers were simplified by the fact that they were made for liquids only.

V. Summary and Conclusions

A somewhat detailed description has been given of the construction, calibration, and operation of a simple volume dilatometer, and also of the method of calculating specific volumes, densities,

and expansivities of solids or liquids from data obtained by measurements employing this type of dilatometer. The instrument is a relatively simple and inexpensive piece of equipment to construct. It can give volume expansivity measurements to a precision of about 1 percent. Its use provides an excellent method for the study of transitions. Illustrative data are given showing that the expansivity $(1/V)\ (dV/dT)$ of a puregum vulcanizate of butyl rubber at 25° C is 567×10^{-6} per deg C, about 15 percent lower than that for natural rubber.

VI. References

[1] M. F. Acken, W. E. Singer, and W. P. Davey, X-ray study of rubber structure, Ind. Eng. Chem. **24,** 54 (1932). Reprinted in Rubber Chem. Tech. **5,** 30 (1932).

[2] A. B. C. Anderson and N. E. Edlefsen, Volume-freezing point relations observed with new dilatometer technique, Soil Sci. **54,** 221 (1942).

[3] T. Alfrey, G. Goldfinger, and H. Mark, The apparent second-order transition point of polystyrene, J. Applied Phys., **14,** 700 (1943).

[4] N. Bauer, Determination of density, chapter III in Weissberger's "Physical methods of organic chemistry", **1,** 69. (Interscience Publishers, Inc., New York, N. Y. 1945).

[5] N. Bekkedahl, Forms of rubber as indicated by temperature-volume relationship, J. Research, NBS **13,** 411 (1934) RP717. Reprinted in Rubber Chem. Tech. **8,** 5 (1935).

[6] N. Bekkedahl and L. A. Wood, Crystallization of vulcanized rubber, Ind. Eng. Chem. **33,** 381 (1941). Reprinted in Rubber Chem. Tech. **14,** 347 (1941).

[7] R. F. Boyer and R. S. Spencer, Thermal expansion and second-order transition effects in high polymers. I. Experimental results, J. Applied Phys. **15,** 398 (1944). Reprinted in Rubber Chem. Tech. **17,** 802 (1944).

[8] T. F. Buehrer and M. S. Rose, Bound water in normal and puddled soils, Univ. of Arizona Agricultural Experiment Station Technical Bulletin No. 100, June 20, 1943.

[9] R. M. Buffington and W. M. Latimer, The measurement of coefficients of expansion at low temperatures, J. Am. Chem. Soc. **48,** 2305 (1926).

[10] J. S. Burlew, Coefficient of thermal expansion of benzene and of toluene measured with a new type of weight dilatometer, J. Am. Chem. Soc. **62,** 690 (1940).

[11] J. Busse, Liquid-in-glass thermometers, chapter in "Temperature; its measurement and control in science and industry", p. 228. (Reinhold Publishing Co., New York, N. Y. 1941.)

[12] H. F. Church and B. E. Waye, Method for determining the cubical coefficient of thermal expansion of solids and liquids, J. Rubber Research **17,** 124 (1948).

[13] R. F. Clash, Jr., and L. M. Rynkiewicz, Thermal expansion properties of plastic materials, Ind. Eng. Chem. **36,** 279 (1944).

[14] M. L. Corrin, Kinetic treatment of emulsion polymerization, J. Polymer. Sci. **2,** 257 (1947).

[15] A. Furst, An improved dilatometer, J. Chem. Education **18,** 335 (1941).

[16] R. E. Gibson and O. H. Loeffler, Pressure-volume-temperature relations in solutions, J. Am. Chem. Soc. **61,** 2515 (1939).

[17] P. Hidnert, Comparative tests of chemical glassware. Values reported by Wichers, Finn, and Clabaugh. J. Research, NBS **26,** 537 (1941) RP1394.

[18] W. L. Holt and A. T. McPherson, Change of volume of rubber on stretching; effect of time, elongation, and temperature, J. Research, NBS **17,** 657 (1936) RP936. Reprinted in Rubber Chem. Tech. **10,** 412 (1937).

[19] B. Ingelman, The dilatometer method for studying the rate of crystallization of saturated solutions of sugar, "The Svedberg" (Mem. Vol.) **1944,** 155 (Almquist and Wiksells Boktryckeri A. B., Uppsala, Sweden, 1944).

[20] E. Jenckel, The cooling processes in glasses and artificial resins, Z. Elektrochem. **43,** 796 (1937).

[21] E. Jenckel and K. Ueberreiter, Polystyrene glasses of different chain lengths, Z. physik. Chem. **A182,** 361 (1938).

[22] H. C. Jones and H. A. Yiengst, Dilatometer studies of pigment-rubber systems, Ind. Eng. Chem. **32,** 1354 (1940); reprinted in Rubber Chem. Tech. **14,** 113 (1941).

[23] J. D. Long, W. E. Singer, and W. P. Davey, Fibering of rubber. Time lag and its relation to structure. Ind. Eng. Chem. **26,** 543 (1934). Reprinted in Rubber Chem. Tech. **7,** 505 (1934).

[24] V. E. Lucas, P. H. Johnson, L. B. Wakefield, and B. L. Johnson, Dilatometric measurement of molecular regularity in polymers, Ind. Eng. Chem. **41,** 1629 (1949).

[25] I. Madorsky, National Bureau of Standards, unpublished work.

[26] P. Mondain-Monval, Studies in allotropy and crystallization of vitreous substances, Ann. chim. [11] **3,** 5 (1935).

[27] W. Patnode and W. J. Scheiber, The density, thermal expansion, vapor pressure, and refractive index of styrene, and the density and thermal expansion of polystyrene, J. Am. Chem. Soc. **61,** 3449 (1939).

[28] M. O. Samsoen, Study of the vitreous state and the expansion of glasses, Ann. phys. **9,** 35 (1928).

[29] J. B. Saunders and A. Q. Tool, Effect of heat treatment on the expansivity of a pyrex glass, BSJ Research **11,** 799 (1933) RP626.

[30] G. V. Schulz and G. Harborth, A dilatometric method for observing the progress of polymerization, Angew. Chem. **A59,** 90 (1947).

[31] A. H. Scott, Specific volume, compressibility, and volume thermal expansivity of rubber-sulfur compounds. J. Research, NBS, **14,** 99 (1935) RP760. Reprinted in Rubber Chem. Tech. **8,** 401 (1935).
[32] R. S. Spencer and R. F. Boyer, Thermal expansion and second-order transition effects in high polymers. III Time effects. J. Applied Phys. **17,** 398 (1946).
[33] H. W. Starkweather and G. B. Taylor, The kinetics of polymerization of vinyl acetate, J. Am. Chem. Soc. **52,** 4708 (1930).
[34] V. Stott and P. H. Bigg, Density of liquid mercury, International Critical Tables **2,** 457 (McGraw-Hill Book Co., New York, N. Y., 1926).
[35] G. Tammann and E. Jenckel, The crystallization velocity and the number of nuclei in glycerine and their dependence on temperature, Z. anorg. allgem. Chem. **193,** 76 (1930).
[36] G. Tammann and A. Kohlhaas, The limits of the softening interval of glasses and the abnormal change of specific heat and volume in the softening region, Z. anorg. allgem. Chem. **182,** 49 (1929).
[37] K. Ueberreiter, The freezing of normal liquids and liquids with "fixed" structures such as rubber and synthetic resins, Z. physik. Chem. **B45,** 361 (1940).
[38] K. Ueberreiter and K. Klein, The dilatometer in plastics research, Chemische Technik **15,** 5 (1942).
[39] L. A. Wood and N. Bekkedahl, Crystallization of unvulcanized rubber at different temperatures, J. Applied Phys. **17,** 362 (1946); J. Research NBS **36,** 489 (1946) RP1718. Reprinted in Rubber Chem. Tech. **19,** 1145 (1946).
[40] L. A. Wood, N. Bekkedahl, and F. L. Roth, Measurement of densities of synthetic rubbers, Ind. Eng. Chem. **34,** 1291 (1942); J. Research NBS **29,** 391 (1942) RP1507. Reprinted in Rubber Chem. Tech. **16,** 244 (1943).

WASHINGTON, March 15, 1949.

U. S. Department of Commerce
National Bureau of Standards

Research Paper RP2017
Volume 43, August 1949

Part of the Journal of Research of the National Bureau of Standards

Relation Between Entrance and Exit Pupils of Telescopic Systems

By Irvine C. Gardner

The definitions of the entrance and exit pupils, as commonly given, are formulated in terms of paraxial imagery only. For telescopic systems the definitions have been extended to apply to extra-axial points and to include the effects of pupil aberrations. If a telescopic system is free from distortion and an incident plane wave emerges as a plane wave free from aberrations, it is shown that exact relations between conjugate chords in the entrance and exit pupils can be derived by application of principles of the wave theory. These results are applied to give the variation in theoretical resolving power over the field of a telescopic system. Equivalent relations are derived by equating the flux of energy in the incident beam to that in the emergent beam. A relation between the illuminations of the object and image planes is derived.

Several publications[1] have appeared recently in which it has been shown that there are departures from the cosine-fourth-power law governing the brightness of an image formed by an optical system that have their origin in the aberrations that exist between the entrance and exit pupils considered as conjugate areas. By conservation of energy considerations, general relations between conjugate areas in the pupils can be derived. In this discussion it is shown that for an idealized telescopic system in which the entering and emergent wave fronts are rigorously plane, it is possible, by applying the wave theory of light, to derive relations between conjugate chords in the entrance and exit pupils that indicate the presence of aberrations. The values of these aberrations are shown to be consistent with the relations between conjugate areas derivable by energy considerations to which reference has been made.

For the derivation based on the wave theory of light, let it be assumed that figure 1 represents a telescopic system that produces an image of an infinitely distant object free from all aberrations except distortion. Incident and emergent wave fronts, therefore, are assumed to be rigorously plane. An incident beam of parallel rays making an angle, β, with the axis is shown entering the system from the left. The line AB of length l is the trace, in the meridional plane, of the segment of the wave front that is transmitted. Similarly, $A'B'$, of length l', is the trace of the emergent wave front corresponding to a beam of parallel rays making an angle β', with the axis. The value of the radial magnification, M_β, is defined by the equation

$$M_\beta = \frac{d(\tan \beta')}{d(\tan \beta)} = \frac{\cos^2 \beta d\beta'}{\cos^2 \beta' d\beta}. \tag{1}$$

If the telescopic system is free from distortion, the magnification is independent of β, and eq 1 becomes

$$M = \tan \beta' / \tan \beta. \tag{2}$$

The dotted line, AC, is the trace of a second incident wave front that makes a small angle, $d\beta$, with AB. If $d\lambda$ represents the length CB,

$$d\beta = d\lambda / l, \tag{3}$$

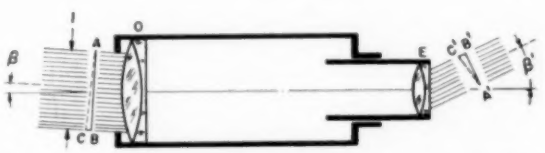

FIGURE 1. *Diagrammatic sketch of telescopic system showing conjugate beams in the object and image spaces.*

[1] G. Slusareff, J. Phys. USSR 4, 537 (1941); M. Reiss, J. Opt. Soc. Am. 35, 283 (1945); I. C. Gardner, J. Research NBS 39, 213 (1947) RP1824.

an expression that is approximate for small values of $d\lambda$ and $d\beta$, and exact for the limit as $d\beta$ approaches zero. Similarly $A'C''$ represents the wave front AC after transmission through the telescopic system and

$$d\beta' = d\lambda'/l'. \tag{4}$$

Since wave fronts AB and AC are conjugate to wave fronts $A'B'$ and $A'C''$ respectively, it follows that the optical paths $A \ldots A'$, $B \ldots B'$, and $C \ldots C'$ are equal. Therefore, if the indices of refraction are the same in the object and image spaces, BC and $B'C''$ are equal and $d\lambda/d\lambda' = 1$. Combining eq 1, 3, and 4,

$$\frac{l'}{l} = \frac{1}{M_s} \frac{\cos^2 \beta}{\cos^2 \beta'}, \tag{5}$$

which is a general relation between the diameters of right cross sections of any pair of conjugate incident and emergent beams measured in the meridional plane.

At this point it is convenient to formulate exact definitions for the entrance and exit pupils of a telescopic system applicable to object and image points not on the axis and in which the effects of aberration are not ignored. Let it be assumed that the entrance and exit pupils for paraxial rays are determined in the usual manner. These pupils determine two planes, which will be designated the pupil planes, normal to the axis of the system and conjugate in terms of first-order imagery. For an infinitely distant object at any angular distance, β, from the axis there are conjugate cylindrical beams in the object and image spaces, which have the maximum cross sections that are transmitted without obstruction by the diaphragms of the optical system. The oblique cross section of the incident beam in the entrance pupil plane is the entrance pupil corresponding to the angle β, and similarly the cross section of the emergent beam in the exit pupil plane is the exit pupil corresponding to the same object point. In general, because of the aberrations existing in the two pupil planes, the pupil areas and perimeters will vary with the angle of obliquity of the incident beams. An exception will occur in a pupil plane that contains a physical diaphragm.

Now, in accordance with these definitions, if p and p' are the diameters of the entrance and exit pupils measured in the meridional plane, $p = l/\cos \beta$ and $p' = l'/\cos \beta'$, respectively. Consequently, from eq 5

$$\frac{p'}{p} = \frac{1}{M_s} \frac{\cos^3 \beta}{\cos^3 \beta'}. \tag{6}$$

Equation 6 indicates that the entrance and exit pupils, though conjugate so far as first-order image theory is concerned, are not sharply defined but that the ratio of the meridional diameters is a function of the angles of incidence and emergence of the beams under consideration. Furthermore, since the incident and emergent wave fronts are rigorously plane, the second member of eq 6 is not only the ratio of the meridional diameters, but is also the ratio of any pair of conjugate chords, in the entrance and exit pupils respectively, parallel to a meridional plane.

Now assume that m is the diameter of the entrance pupil measured in a direction at right angles to the meridional plane. Furthermore, assume that a wave front of the incident beam shown in figure 1 is rotated about an axis parallel to the meridional diameter (a rotation analogous to that illustrated in fig. 1 but with the axis of rotation turned through 90° in the plane of the wave front) through the small angle $d\psi$, thereby advancing one end of the diameter through the length dy from the original plane of the wave front.
then

$$d\psi = dy/m, \tag{7}$$

a relation rigorously true in the limit. As a consequence of this rotation, the azimuth of an incident ray normal to the wave front, measured as a rotation about the axis of the telescopic system, is changed by the amount $d\phi$, where

$$d\phi = dy/m \sin \beta. \tag{8}$$

For an analogous rotation in the image space, if m' is the diameter of the exit pupil, measured in a direction at right angles to the meridional plane,

$$d\phi' = dy'/m' \sin \beta'. \tag{9}$$

In a symmetrical telescopic system $d\phi$ always equals $d\phi'$.

Furthermore, as before $dy = dy'$ if the indices of refraction of the media of the object and image spaces are the same. Combining eq 8 and 9

$$\frac{m'}{m} = \frac{\sin \beta}{\sin \beta'}, \tag{10}$$

and a general relation between the diameters, measured in a direction normal to the meridian plane, of a pair of conjugate beams in the object and image space, respectively, has been obtained. Furthermore, by an extension similar to that previously made, the ratio of the second member of eq 10 applies not only to the two diameters but to any pair of conjugate chords, one lying in the object space and one in the image space, respectively, and normal to the meridional plane.

From eq 6 and 10 it follows that

$$\frac{S'}{S}=\frac{1}{M_\beta}\frac{\sin\beta\cos^3\beta}{\sin\beta'\cos^3\beta'}=\frac{1}{M_\beta}\frac{\tan\beta\cos^4\beta}{\tan\beta'\cos^4\beta'}, \quad (11)$$

where S and S' are the areas of the entrance and exit pupils corresponding to conjugate incident and emergent beams of rays making angles β and β', respectively, with the axis.

If the telescopic system is free from distortion and is of magnification M, eq 11 becomes

$$\frac{S'}{S}=\frac{1}{M^2}\frac{\cos^4\beta}{\cos^4\beta'}. \quad (12)$$

Equations 6 and 10 have interesting application to the variation of resolving power and brightness of image with angular distance from the center of the field. If a telescopic system is used for visual purposes and is so designed that the exit pupil is larger than the entrance pupil of the observer's eye, it follows that the angular limit of resolution in the image space is the same in any plane containing the axis of the eye. In the object space the corresponding angular limits of resolution in the meridional plane and in a plane at right angles to it are $\cos^2\beta/(M\cos^2\beta')$ and $\cos\beta/(M\cos\beta')$ times the corresponding values (which are equal) in the image space. These ratios correspond to constant values, independent of β, of the ratios $[d(\tan\beta)]/[d(\tan\beta')]$ and $d\phi/d\phi'$ over the entire field.

On the other hand, if the telescopic system is so designed that the clear aperture of the objective is the limiting diaphragm of the system and the exit pupil is smaller than the eye of the observer, then the limits of angular resolution in the object space are proportional to $1/(p\cos\beta)$ and $1/m$, respectively, in the meridional plane and in a plane at right angles to it which contains the chief ray. The corresponding limits of resolution in the image space are proportional to $(M\cos^3\beta')/\cos^3\beta$ and $(M\cos\beta')/\cos\beta$, respectively. In most telescopic systems the angular field of view is so small that this variation of resolving power is not of great practical value but it is of interest as precisely defining the idealized performance of a perfect telescopic system.

It should perhaps be mentioned that a similar application of the principles of wave theory to a photographic objective is not as straightforward as the application that has just been made. If either the object or image is at a finite distance, the ratio of the tangents is not sufficient to define distortion because there is an additional contribution arising from the spherical aberration of the pupil points.

Equation 11 may also be derived by energy consideration in a manner similar to that described by Slussareff, Reiss, and others (see footnote 1). In this direction, referring to figure 2, assume that

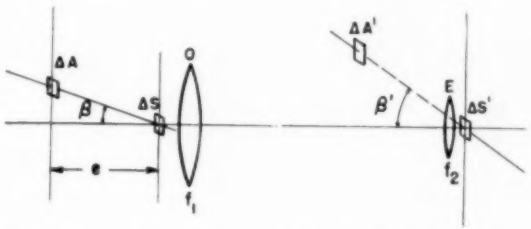

FIGURE 2. *Diagrammatic sketch of telescopic system showing elements of area used in energy summation.*

f_1 and f_2 are the objective and eyepiece parts of a telescopic system and that ΔA and $\Delta A'$ are two conjugate elements of area in the object and image planes, respectively, of the complete system. Similarly, ΔS and $\Delta S'$ are two conjugate elements of area in the entrance and exit pupils respectively, and B and B' are the brightnesses in the directions β and β' respectively, of the object and image elements. The length, e, is represented as finite to simplify the formulation of eq 13, which is valid for all values of e. If ΔF is the flux transmitted from ΔA to ΔS,

$$\Delta F=\frac{B\,\Delta A\,\Delta S}{e^2}\cos^4\beta'. \quad (13)$$

Similarly, for the flux transmitted from $\Delta S'$ to $\Delta A'$ in the image space

$$\Delta F'=\frac{B'\,\Delta A'\,\Delta S'}{e'^2}\cos^4\beta'. \quad (14)$$

Since only the geometrical relations of the system are under consideration, it can be assumed that there are no reflection or absorption losses, in which case $\Delta F = \Delta F'$ and $B = B'$. Therefore

$$\frac{\Delta S'}{\Delta S} = \frac{\Delta A\, e'^2 \cos^4 \beta}{\Delta A'\, e^2 \cos^4 \beta'} \tag{15}$$

It is evident that

$$\frac{\Delta A}{\Delta A'} = \frac{e^2 \tan \beta \cos^2 \beta' d\phi d\beta}{e'^2 \tan \beta' \cos^2 \beta d\phi' d\beta'}, \tag{16}$$

$$\frac{d\phi}{d\phi'} = 1, \tag{17}$$

and from eq 1

$$\frac{d\beta}{d\beta'} = \frac{1}{M_\beta} \frac{\cos^2 \beta}{\cos^2 \beta'}. \tag{18}$$

Substituting in eq 15 and writing $\Delta S'/\Delta S = S'/S$ (permissible because β and β' are constant over S and S', respectively) eq 11 is obtained.

It follows, therefore, that the application of the wave theory and the application of energy considerations lead to identical results so far as the relative areas of the entrance and exit pupils are concerned, but the first application gives the more detailed information in that it analyzes the areal magnification into two linear magnifications in directions mutually perpendicular.

If E denotes the luminous flux emitted per unit area by ΔA and received by ΔS, and E' denotes the illumination (luminous flux per unit area) received by the conjugate elementary area $\Delta A'$ from the surface $\Delta S'$, from eq 13 and 14

$$\frac{E'}{E} = \frac{\Delta S' e^2 \cos^4 \beta'}{\Delta S e'^2 \cos^4 \beta}. \tag{19}$$

It can be shown that

$$\lim_{e \doteq \infty} \frac{e^2}{e'^2} = \frac{f_2^4}{f_1^4} = M^4, \tag{20}$$

the subscript having been dropped from M because the telescopic system will be assumed free from distortion. From eq 2, 11, 19, and 20

$$\frac{E'}{E} = M^2. \tag{21}$$

The ratio of illumination of image to illumination of object is independent of β, and the image is uniformly illuminated. At first eq 21 appears confusing because the illumination of the image is greater than the flux per unit area proceeding from the object, and the image is apparently larger than the object. However, it will be recalled that the linear magnification for a telescopic system is the same for all pairs of conjugate planes, including the infinite pair, and is equal to the reciprocal of the angular magnification. Also, eq 20 indicates that the two infinite planes are not equally distant but that the distance to the object plane, divided by the distance to the image plane, gives a quotient equal to the square of the magnification. As an illustration, if a ten-power telescope is assumed, linear dimensions in the image plane are one-tenth the conjugate lengths in the object plane, but the image plane is only one-hundredth as far away. Hence the angular magnification is 10, and these values accord with eq at 21. In other words, a telescope that apparently enlarges a distant object actually produces an image that is smaller than the object, but the image is so much nearer the observer that a pair of points in the image subtend a larger angle than the conjugate pair of points in the object.

Washington, April 6, 1949.

U. S. Department of Commerce
National Bureau of Standards

Research Paper RP2018
Volume 43, August 1949

Part of the Journal of Research of the National Bureau of Standards

Mechanisms for the Formation of Acetylglycosides and Orthoesters from Acetylglycosyl Halides

By Horace S. Isbell and Harriet L. Frush

To obtain information concerning the stereomeric factors that affect the course of replacement reactions, a study has been made of the replacement of the halogen of certain acetylglycosyl bromides by methanol in the presence of silver carbonate (the Koenigs-Knorr reaction). The investigation shows that the solvent and the temperature greatly influence the course of the reaction when the configuration is *trans* but have little influence when the configuration is *cis*. The experimental data support the concept that under definite stereomeric conditions a solvated orthoester intermediate takes part in the reaction at low temperatures. At higher temperatures part of the reaction appears to take place through a free orthoester ion. By selection of suitable experimental conditions, it was possible to direct the orthoester reaction in large measure to either the methyl orthoacetate or the methyl acetylglycoside with apparent retention of configuration.

I. Introduction

One of the most useful reactions for the synthesis of glycosidic compounds consists of the interaction of a substance containing a free hydroxyl group with an acetylglycosyl halide in the presence of silver carbonate or other substance capable of removing the halide ion. The reaction, commonly known as the Koenigs-Knorr reaction [1],[1] leads to the formation of a number of products.

When the halogen and the neighboring acetyl group of the acetylglycosyl halide are *trans*, the reaction with methanol in the presence of silver carbonate produces an orthoacetate I and the anomeric acetylglycosides II and III. It was pointed out in previous publications from this laboratory [2, 3, 4] that the orthoester is formed from *trans* acetylglycosyl halides by an intramolecular, opposite-face attack upon the glycosidic carbon by the nucleophilic oxygen of the neighboring acetyl group, with the addition of methanol at the carboxylate carbon and the elimination of a proton from the resultant orthoester intermediate (eq 1). The acetylglycoside of like configuration to the parent halide is formed by a secondary reaction of the orthoester intermediate with methanol at the glycosidic carbon (eq 2). The acetylglycoside of unlike configuration is formed by an intermolecular, opposite-face attack by the methanol from the environment upon the glycosidic carbon with the elimination of a proton (eq 3). The last reaction is in competition with reactions involving the orthoester intermediate.

When the halogen and the neighboring acetyl group of the acetylglycosyl halide are *cis*, intramolecular reaction is impossible, and no orthoester is formed. Replacement takes places by the mechanism of eq 3, to yield the acetylglycoside of configuration opposite to that of the parent halide.

[1] Figures in brackets indicate the literature references at the end of this paper.

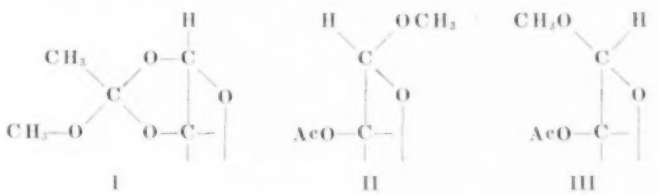

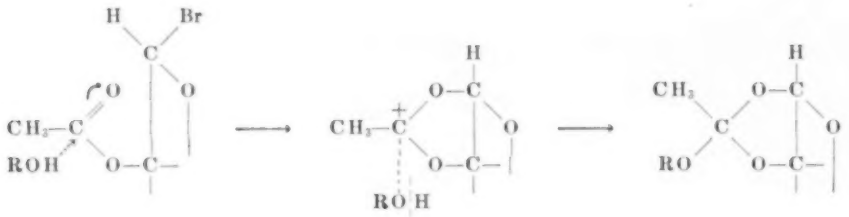

(1)

(R = H, CH_3, $CH_3C{=}O$, etc.)

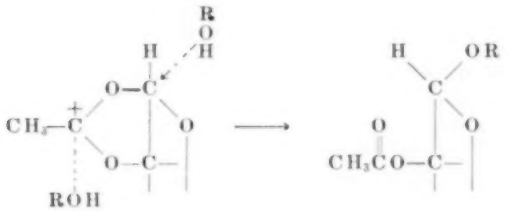

(2)

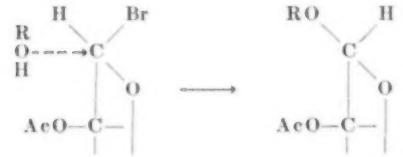

(3)

Shortly after the publication [2] presenting these mechanisms for the replacement reactions of the acetylglycosyl halides, Winstein and Buckles [5] advanced similar mechanisms to account for certain reactions outside the carbohydrate field. In reactions of the orthoester type, they emphasized the independent existence of the orthoester intermediate in the form of the ion IV. Although their mechanism does not differ markedly from that already presented, the question as to whether or not the orthoester intermediate exists in solution as a free ion or a solvated ion is of importance. In a recent publication Winstein, Hanson, and Grunwald [6] claim that results of a study of the acetolysis of *trans*-2-acetoxycyclohexyl-*p*-toluenesulfonate rule out the mechanism for orthoester formation symbolized by *V*, and remark that this mechanism was envisioned by one of us for orthoester formation from acetohalogen sugars. We believe that the evidence of Winstein and coworkers does not rule out the orthoester mechanism cited. In order to test the concept of a solvated orthoester intermediate, a quantitative study has been made of the Koenigs-Knorr reaction, and especially of the effect of solvents and temperature upon the composition of the reaction products. The results given in this paper show that at low temperatures the reaction products vary as required by the solvated orthoester intermediate rather than by the free orthoester ion.

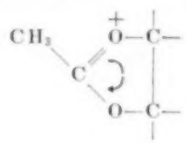

IV

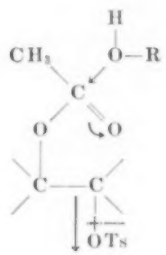

V

II. Role of the Solvent in the Koenigs-Knorr Reaction

Presumably, the role of the solvent in the reactions under consideration is somewhat similar to its role in some of the more common ionization reactions. The ionization of an acid in water, for instance, involves coordination of the acidic hydrogen with water, to form an oxonium ion, accompanied by separation of the anion. Similarly, the ionization of an acetylglycosyl halide may involve coordination of the solvent at a reactive center,

the effect of which is to facilitate release of the halogen anion.

In a *trans* acetylglycosyl halide, coordination of a nucleophilic solvent can occur either at the glycosidic carbon (eq 3) or at the carboxylate carbon of the neighboring acetyl group (eq 1). Presumably, coordination of the solvent with the carboxylate carbon releases electrons to the acetyl oxygen and thus increases its nucleophilic properties, and its capacity to combine with the glycosidic carbon, with release of the halogen. When the coordinating substance possesses an ionizable hydrogen, the solvated orthoester ion can yield a neutral substance by elimination of the proton. If the coordinating solvent Y (in place of ROH) does not have an ionizable hydrogen, the orthoester intermediate cannot yield a neutral substance by elimination of a proton; hence it exists in solution until decomposed by thermal agitation or by a secondary reaction, as for instance with methanol (eq 4). The secondary reaction yields the glycoside that has the same configuration as the original acetylglycosyl halide, and the proportion of this glycoside should therefore be increased by the presence of the coordinating solvent, Y.

In a *cis* acetylglycosyl halide, stereomeric conditions make reaction between the glycosidic carbon and the neighboring acetyl group impossible. Hence, the mechanism of eq 4 is not applicable, and the presence of the coordinating solvent, Y, should have no direct effect on the composition of the product.

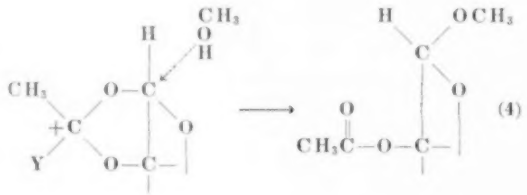

(4)

In the event that several nucleophilic substances are available for coordination with a *trans* acetylglycosyl halide, one can envision a competitive system in which several solvated orthoester intermediates are present. For instance, in a mixture of ether, methanol, and water, solvated orthoester intermediates can be formed from each constituent. The orthoester intermediates derived from methanol and water yield neutral compounds by elimination of a proton, as in eq 1.[2] The ether-containing intermediate, however, unable to become stabilized by elimination of a proton, will exist in solution until decomposed by thermal agitation, or by reaction with either methanol or water at the glycosidic carbon, in the manner depicted in eq 4. Thus the addition of the solvent Y should favor the formation of either the glycoside or the acetyl sugar having the same configuration as the parent acetylgylcosyl halide. On the other hand, if the reaction takes place through the free orthoester ion of Winstein and coworkers, the probability of the formation of either the orthoester or the acetylglycoside having the same configuration as the parent halide should be substantially independent of the presence of a solvent such as ether, which supposedly serves only as a diluent.

The foregoing considerations apply only to *trans* acetylglycosyl halides. We have already noted that if the acetylglycosyl halide has a *cis* configuration for the substituents of carbons 1 and 2, the orthoester mechanism is not applicable, and one would expect no appreciable effect of the solvent upon the character of the product formed.

III. Effect of the Byproduct, Water, on the Koenigs-Knorr Reaction

In addition to the alpha and beta acetylglycosides and the orthoester, which are formed in the Koenigs-Knorr reaction, two other products must be taken into consideration. These are the alpha and beta free acetylsugars, which are formed from water inevitably present as a byproduct. Theoretically, 1 mole of water is produced from 2 moles of methanol (eq 5), and 1 mole of water produces 2 moles of the free acetylsugar (eq 6). If all of the water were to react with the acetylglycosyl halide, the product would contain equal proportions of the free acetylsugar and the methoxy compounds.[3] The extent of the water reaction depends in part on the manner in which the replacement is conducted. When the alcohol

[2] Decomposition of the orthoacid formed from water would yield the free acetylsugar, $CH_2OAc.CH.(CH.OAc)_2.CH.OH$.

[3] In the preparation of orthoesters, other workers have found it advantageous to conduct the reaction in the presence of a drying agent, ordinarily Drierite [7]. In spite of the use of the drying agent, reaction with water could not be entirely eliminated in the present study.

is added slowly to the acetylglycosyl halide in another solvent, considerable opportunity is provided for the byproduct, water, to enter into the reaction, because it is in competition with a relatively small quantity of methanol. For this reason, more of the free acetylsugar should be formed when a large part of the methanol is replaced by ether or benzene. The present investigation has shown that this is indeed the case.

$$2RBr+Ag_2CO_3+2CH_3OH \rightarrow 2ROCH_3+2AgBr+H_2O+CO_2. \quad (5)$$

$$2RBr+Ag_2CO_3+H_2O \rightarrow 2ROH+2AgBr+CO_2. \quad (6)$$

The mechanisms that have been advanced on page 162 for the reactions of methanol with *cis* and *trans* acetylglycosyl halides apply equally well to the reactions with water. An intermolecular opposite-face attack on the glycosidic carbon of either *cis* or *trans* acetylglycosyl halides yields the acetylsugar of opposite configuration to that of the parent halide, as shown in eq 3. Thus, an alpha acetylglycosyl halide yields the beta modification of the free acetylsugar. The *trans* acetylglycosyl halide reacts also by the intramolecular orthoester mechanism of eq 1, but the orthoacid is unstable and rearranges to give the free acetylsugar (eq 7).[4] Therefore this mechanism yields the same product as that produced by the intermolecular, opposite-face reaction, namely, the beta acetylsugar. That is, the alpha halide yields the beta acetylsugar by two mechanisms. In the presence of a solvent such as ether, which cannot release a proton, decomposition of the solvated intermediate can yield the alpha acetylsugar by the mechanism of eq 4.

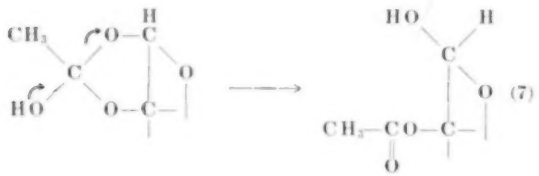

(7)

Since the free acetylsugars are interconvertible by the mutarotation reaction, the quantitative determination of the alpha and beta modifications is difficult. In this work, the sum of the two modifications has been determined by a titration method; and it has been ascertained polarimetrically that the beta modification, as anticipated, predominates in the reaction product.

[4] The rearrangement of the orthoacid to the hydroxy compound is essentially the same as that outlined in [5].

IV. Discussion of Experimental Results

1. Effect of the Solvent in the Koenigs-Knorr Reaction and Evidence for a Solvated Orthoester Intermediate

The results given in table 1 show that the composition of the products from tetraacetylmannosyl bromide (a *trans* acetylglycosyl halide) depends on the character of the solvent and on the experimental conditions. When the solvent is methanol, the product of the intramolecular reaction at 20° C is largely the methyl orthoacetate; no alpha acetylglycoside is formed. The production of the orthoester without the alpha acetylglycoside shows that the orthoester intermediate decomposes only by the reaction of eq 1, and there is no evidence for reaction at the glycosidic carbon as would be expected if the mechanism involved the free ion. The absence of a measurable quantity of the alpha acetylglycoside indicates that the orthoester intermediate loses a proton rapidly, before reaction can occur at the glycosidic carbon by eq 2. The results also show a small amount of the beta acetylglycoside, presumably formed by the competing intermolecular reaction of eq 3. When the methanol is largely replaced by either ether or benzene, the proportion of the orthoester decreases, and a substantial quantity of the alpha acetylglycoside appears. If the reaction took place through the free orthoester ion, one would not expect this striking change. Thus, it appears that a solvated orthoester intermediate enters into the reaction, as indicated in eq 4. The results in table 1 show that the effect of benzene in causing formation of the alpha acetylglycoside is less than that of ether, but nevertheless considerable. The marked effect of ether upon the composition of the reaction product is in accord with its well-known tendency to coordinate. Its basic properties arise from the unshared electrons of the oxygen. Although benzene is less basic than ether, its ability to coordinate likewise accounts for the changes observed. The marked increase in the proportion of the free acetylsugar when the amount of methanol is low and the reaction is conducted in either ether or benzene shows the effect of the competition of the byproduct, water, for the reactive centers, as mentioned on page 163.

TABLE 1. *Composition of products from reaction of acetylglycosyl bromides with methanol in the presence of silver carbonate at 20° C*

Experiment number	Solvent	Addition of methanol	Molecular composition of product				Optical rotation of product [a]	
			Acetylsugar	Acetylorthoester	Beta acetylglycoside	Alpha acetylglycoside	$[\alpha]_D^{20}$ at 60 min (MeOH)	$[\alpha]_D^{20}$ at equilibrium ($CHCl_3$)
Product from tetraacetyl-α-D-mannosyl bromide								
			Percent	*Percent*	*Percent*	*Percent*		
I	20 ml of methanol	Used as solvent.	6.9	78.5	14.6	0	−32.2°	−27.7°
II	20 ml of ether +0.5 ml methanol	Included in solvent.	25.9	41.0	11.4	21.7	−23.3	−0.7
III	15 ml of ether	0.5 ml of methanol in 5 ml of ether added dropwise over 2 min.	32.1	18.5	18.7	30.7	−16.8	+7.5
IV	15 ml of ether	0.5 ml of methanol in 5 ml of ether added dropwise over 18 min.	35.4	7.5	23.1	34.0	−7.3	+10.6
V	20 ml of benzene +0.5 ml of methanol	Included in solvent.	16.0	64.5	8.1	11.4	−32.7	−12.3
VI	15 ml. of benzene	0.5 ml of methanol in 5 ml of benzene added dropwise over 20 min.	28.7	36.1	12.9	22.3	−16.0	+0.7
Product from tetraacetyl-α-D-glucosyl bromide								
IX	20 ml of methanol	Used as solvent.	5.7	.....	93.8	0.5	−17.1	−12.5
X	20 ml of ether +0.5 ml of methanol.	Included in solvent.	28.1	.....	71.9	0	−5.7	+8.3
XI	20 ml of benzene +0.5 ml of methanol	Included in solvent.	25.2	.....	74.8	0	−9.9	+5.5

[a] Specific rotation, based on the weight of the acetylsugars, the acetylglycosides, and the orthoester formed from 2 g of the acetylglycosyl bromide.

In contrast to the results obtained with tetraacetyl-α-D-mannosyl bromide, the reaction products from tetraacetyl-α-D-glucosyl bromide (a *cis* halide) show considerably less variation with change of solvent. The effect of competition of the methanol and water for the glycosidic carbon is evidenced in the increase of the free acetylsugar when the amount of the methanol is small. The absence of the methyl orthoacetate and the alpha acetylglycoside in the reaction products clearly supports the prior concept that *cis* acetylglycosyl halides are incapable of reaction by the orthoester mechanism. That is, the reaction takes place almost entirely by an opposite-face attack on the glycosidic carbon by nucleophilic substances in the environment (eq 3). Since the alpha acetylglycoside is not found in the product, there is no evidence for the coordination of ether or benzene with the glycosidic carbon, since such coordination would yield the alpha acetylglycoside by a second opposite-face attack.

In all cases, the reaction products from tetraacetyl-α-D-mannosyl bromide and tetraacetyl-α-D-glucosyl bromide mutarotate in the dextro direction. In other words, the beta modification of the free acetylsugars predominates in the products, as required by the reaction mechanisms previously discussed.

2. Effect of Temperature on the Koenigs-Knorr Reaction

In the preceding section it was emphasized that the intramolecular reaction of tetraacetylmannosyl bromide with methanol at 20° C takes place through a solvated orthoester intermediate with the exclusive formation of the methyl orthoacetate. Inasmuch as this result is at variance with the conclusion of Winstein and coworkers, based on a study of the acetolysis of *trans*-2-acetoxycyclohexyl *p*-toluenesulfonate at 75° and 100° C, it seemed desirable to investigate the effect of temperature on the course of the Koenigs-Knorr reaction.[5] The data of table 2 show that the composition of the product from tetraacetyl-

[5] It was observed previously that the formation of orthoesters is favored by low temperatures [8].

TABLE 2. *Effect of temperature on composition of products from reaction of acetylglycosyl bromides with methanol in the presence of silver carbonate*

Experiment number	Temperature	Molecular composition of product				Optical rotation of product	
		Acetylsugar	Acetylortho-acetate	Beta acetyl-glycoside	Alpha acetyl-glycoside	$[\alpha]_D^{20}$ at 60 min (MeOH)	$[\alpha]_D^{20}$ at equilibrium ($CHCl_3$)
Product from tetraacetyl-α-D-mannosyl bromide							
	°C	*Percent*	*Percent*	*Percent*	*Percent*		
VII	−15	6.2	78.1	15.7	0	−35.7°	−29.0°
I	20	6.9	78.5	14.6	0	−32.2	−27.7
VIII	50	13.5	53.4	25.1	8.0	−22.2	−19.8
Product from tetraacetyl-α-D-glucosyl bromide							
XII	−15	5.0	.....	94.3	0.7	−16.5	−12.9
IX	20	5.7	.....	93.8	.5	−17.1	−12.5
XIII	50	6.7	.....	90.8	2.5	−12.6	−8.6

glucosyl bromide did not change significantly in the range from −15° to 20° C; the reaction product, aside from the acetylsugar,[6] was almost exclusively the beta acetylglucoside. Since an intramolecular reaction is stereomerically impossible for tetraacetyl-α-D-glucosyl bromide, the amount of the beta acetylglucoside may be taken as a measure of the intermolecular reaction with methanol. At 50° C, 2.5 percent of the alpha acetylglucoside was formed; the increase over that at 20° C may be due to racemization through a carbonium ion (the S_N1 mechanism of Gleave, Hughes, and Ingold [9]).

In contrast to the results obtained with tetraacetylglucosyl bromide, the results with tetraacetylmannosyl bromide show a striking effect of temperature on the course of the reaction at 50° C,[7] although the composition of the product was substantially the same at −15° and 20° C. Since no alpha acetylmannoside was found at low temperatures, the amount of the orthoester can be taken as a measure of the intramolecular reaction at 20° C or below. Presumably the amount of the beta acetylmannoside, by analogy to the glucose series, is a measure of the intermolecular reaction. When the temperature was raised to 50° C, the yield of orthoester dropped from 78 to 53 percent, and the yields of the alpha and beta acetylmannosides increased; the former from 0 to 8 percent, the latter from 16 to 25 percent. The increase in the beta acetylmannoside is evidence that at the higher temperature the intermolecular reaction is favored at the expense of the intramolecular. This may be due to the fact that less favorable conditions exist at 50° than at 20° C for the intramolecular reaction to take place, because of alteration in the positions of the reactive groups within the molecule. Certain conformations of the pyranose ring place the halogen and the acetyl group in stereomerically favorable positions for intramolecular reaction by the opposite-face mechanism; others do not. At the higher temperature, increased kinetic disturbance of the sugar molecule may alter ring conformation and thus affect the probability of reaction by the orthoester mechanism.

The increase in the alpha acetylmannoside at high temperatures is proportionately greater than the increase in the alpha acetylglucoside. Hence an intermolecular reaction, with an S_N1 mechanism such as that postulated for the formation of the alpha acetylglucoside, does not adequately account for the facts. It seems more probable that the marked increase in the yield of the alpha acetylmannoside at the higher temperature is caused by a modification of the intramolecular course. One would expect the solvated orthoester intermediate, which in the mannose series yields the methyl orthoester almost exclusively at low temperatures, to dissociate at higher temperatures with the formation of the free orthoester ion of Winstein and coworkers. The free ion, by reaction with methanol, would produce the orthoester and the

[6] The formation of the acetylsugar as a byproduct was discussed on page 163, and will not be considered here.

[7] To show that the differences in the amounts of orthoester and alpha acetylmannoside found at 20° and 50° C were real and not due to a secondary decomposition of the orthoester after its formation, a sample of triacetylmannose 1,2-(methyl orthoacetate) was heated at 50° C with methanol under the conditions used in the replacement reactions. No change was found.

alpha acetylglycoside in proportions different from those characteristic of the solvated intermediate in which methanol is already in position to yield the orthoester.[8] In this connection it should be pointed out again that the experiments that Winstein and coworkers claim to rule out the solvated orthoester mechanism were conducted at relatively high temperatures. The results given in this paper indicate that at low temperatures the intramolecular reaction takes place exclusively through the solvated orthoester intermediate, but at high temperatures part of the reaction takes place through the free ion.

V. Experimental Procedure

1. Discussion of the Analytical Method

The method for the analysis of the reaction products is based on the premise that the only substances present are the alpha and beta methyl tetraacetylglycosides, the methyl orthoacetate, and the free acetylsugar. It has been found possible to determine the amount of the acetylsugar by modification of the conventional method for the iodimetric determination of aldoses. The acetylsugar initially formed in the reaction is gradually converted to the alpha-beta equilibrium mixture; in the presence of a catalyst this equilibrium may be established quickly. From the known optical rotation of the pure acetylsugar in equilibrium, and the known amount of this substance in the mixture, it is possible to calculate the contribution of the acetylsugar to the equilibrium rotation of the reaction product. To determine the amount of the orthoester, advantage is taken of the observation [10] that methyl orthoacetates react rapidly with hydrogen chloride in chloroform and that the reaction is accompanied by a large change in optical rotation. Normal methyl acetylglycosides and the free acetylsugars are substantially inert to this reagent. Thus the difference between the rotation at equilibrium and the rotation after the addition of hydrogen chloride is a measure of the amount of orthoester present. The contribution of the orthoester to the equilibrium rotation can be calculated from the amount of orthoester in the reaction mixture and the known optical rotation of the pure substance. The residual optical rotation, after allowance is made for the contributions of the acetylsugar and the orthoester, is due to the mixture of the alpha and beta methyl acetylglycosides. After the determination of the acetylsugar and orthoester, the total yield of the acetylglycosides can be obtained by difference, and the proportions of the two acetylglycosides can be calculated from the residual rotation and the known optical rotations of the two substances.

By the procedure outlined in the preceding paragraph the yields of the acetylsugar, the methyl orthoacetate, and the alpha and beta methyl acetylglycosides from tetraacetyl-α-D-mannosyl bromide were determined. Application of the same method to the product from tetraacetyl-α-D-glucosyl bromide showed the absence of the methyl orthoacetate and gave the yields of the acetylsugar, and the alpha and beta methyl acetylglucosides.

The procedure was standardized by measurements made with the pure constituents as controls. The method for determining the orthoester, although convenient, is not very satisfactory because of the difficulty in maintaining a chloroform solution of hydrogen chloride of uniform strength. Because of variation in this reagent, it was necessary to standardize the procedure for each set of determinations by use of pure triacetylmannose 1,2-(methyl orthoacetate). Since the quantity of the methyl acetylglycosides was obtained by difference, the values recorded for these substances are subject to the combined errors in the values for the methyl orthoacetate and the free acetylsugar. In the experiments in which the percentage of the methyl acetylglycoside is shown as zero, the optical rotation for the methyl acetylglycoside fraction was calculated to be at least as great in the levo direction as that required for the beta acetylglycoside.

2. Experimental Details

(a) Materials

The ether and benzene used as solvents were of analytical grade, dried by sodium, and freshly distilled. The chloroform was USP grade. The methanol was dried by refluxing with barium oxide and distilling immediately before use.

The hydrogen chloride-chloroform reagent was prepared by passing dry hydrogen chloride into USP chloroform to the point of saturation at 20° C. The reagent was protected from atmospheric moisture and dispensed from a buret.

[8] Both the solvated and the free orthoester ion can yield the orthoester and the alpha acetylglycoside. It is noteworthy that both products were separated by application of the Koenigs-Knorr reaction to heptaacetyl-4-glucosido-mannosyl bromide at 0° C [10].

The silver carbonate was prepared by the addition of aqueous sodium bicarbonate to an aqueous silver nitrate solution. It was collected on a filter and thoroughly washed, first with water, and finally with acetone. It was then dried at room temperature in the absence of light in a vacuum desiccator containing phosphoric anhydride.

The Drierite was finely powdered and was redried at 230° C immediately before use. The following substances were prepared by the methods given in the corresponding literature references: tetraacetyl-α-D-mannosyl bromide [11], tetraacetylmannose [12], methyl tetraacetyl-α-D-mannoside [13], methyl tetraacetyl-β-D-mannoside [14], triacetylmannose 1,2-(methyl orthoacetate) [13], tetraacetyl-α-D-glucosyl bromide, page 500 of [15], tetraacetylglucose [16], methyl tetraacetyl-α-D-glucoside [1], methyl tetraacetyl-β-D-glucoside [1] and page 516 of [15].

(b) Method of Conducting the Replacement Reactions

The replacement reactions were conducted in 100-ml glass-stoppered flasks, carefully dried before use, and maintained at the temperature of the experiment by use of a suitable constant-temperature bath. Silver carbonate (2 g), Drierite (2 g), and the solvent were placed in the reaction flask and brought to temperature. The acetylglycosyl halide in a glass boat (2 g) was dropped into the flask, and the mixture was shaken for 15, 30, or 60 min [9] according to whether the temperature was 50°, 20° or −15° C, respectively. In some of the experiments, the methanol was introduced into the flask as the solvent or as a constituent of the solvent prior to the addition of the halide. In other experiments, 15 ml of a solvent was added at the beginning; after introduction of the silver carbonate, Drierite, and acetylglycosyl halide, 5 ml of the solvent containing 0.5 ml of methanol was added dropwise from a buret with exclusion of moisture by use of a rubber dam. After the reaction was completed, the mixture was filtered, the residue was washed with methanol, and the filtrate and washings were made to a volume of 50 ml with methanol. Portions of this solution were used for the measurements that follow.

(c) Analysis of the Reaction Product

(1) *Determination of the free acetylsugar.*—Twenty milliliters of the solution containing the reaction product was evaporated to dryness in a current of dry air, and the last trace of alcohol was removed by the addition of 5 ml of benzene and re-evaporation. The residue was taken up in 5 ml of peroxide-free dioxane, and the free acetylsugar was determined by oxidation with iodine by the method of Kline and Acree [17]. Control experiments showed that neither the methyl acetylglycosides nor triacetylmannose 1,2-(methyl orthoacetate) reacts with iodine, whereas tetraacetylmannose and tetraacetylglucose react stoichiometrically when an excess of 5 to 10 ml of 0.1-*N* iodine solution is used. The amount of free acetylsugar in the entire reaction product was calculated, and expressed in tables 1 and 2 as percentage of the acetylsugar theoretically equivalent to the acetylglycosyl halide employed.

(2) *Optical rotation of the reaction mixture at equilibrium.*—Preliminary experiments showed that the equilibrium of the free acetylsugars can be established readily by the addition of sodium acetate, without alteration of the rotation of the methyl acetylglycosides or of triacetylmannose 1,2-(methyl orthoacetate). Hence, sodium acetate was employed as catalyst to establish equilibrium. Ten milliliters of the solution containing the reaction product was evaporated to dryness in a 25-ml volumetric flask containing 0.05 g of crystalline sodium acetate. Sufficient USP chloroform was added to make a volume of 25 ml at 20° C. After 18 hr at room temperature, the chloroform solution was filtered, and the optical rotation was read in a 4-dm tube. The readings are recorded in table 3, and the corresponding specific rotations are given in tables 1 and 2.

(3) *Optical rotation of the reaction mixture at 60 minutes.*—Since the solution exhibits mutarotation because of the presence of the free acetylsugar, measurements of optical activity were made on the methanol solution of the reaction product at convenient times and were extrapolated to obtain the values at 60 min from the beginning of the reaction. These values were converted to specific rotations based on the weight of the reaction products.[10]

[9] The reaction times were so selected that the filtered reaction products were halogen-free.

[10] Since the acetylglycosyl bromide (of molecular weight 411.21) is converted to the free acetylsugar (of molecular weight 348.30) and to the methyl acetylglycosides and methyl acetylorthoester (of molecular weight 362.33), the weight of reaction product from 2 g of acetylglycosyl bromide is

$$2\left[\frac{348.30}{411.21}A+\frac{362.33}{411.21}(1-A)\right],$$

where A is the fraction of the acetylglycosyl bromide converted to the free acetylsugar, as determined by titration.

TABLE 3.—*Experimental data on products derived from acetylglycosyl bromides at 20° C*

Experiment number	Free acetylsugar in product [a]	Optical rotation		Change in optical rotation		Orthoester
		After NaOAc treatment [b]	After HCl-$CHCl_3$ treatment [b]	Product	Orthoester control	
Product from tetraacetyl-α-D-mannosyl bromide						
	(molecular) Percent	*° S*	*° S*	*° S*	*° S*	*(molecular) Percent*
I	6.9	−4.50	+9.39	+13.83	+17.61	78.5
II	25.9	−0.11	+6.45	6.35	15.47	41.0
III	32.1	+1.20	+4.32	2.86	15.47	18.5
IV	35.4	+1.71	+3.16	1.16	15.47	7.5
V	16.0	−1.99	+8.12	9.98	15.47	64.5
VI	28.7	+0.12	+5.95	5.59	15.47	36.1
VII	6.2	−4.72	+9.09	13.76	17.61	78.1
VIII	13.5	−3.21	+6.30	9.40	17.61	53.4
Product from tetraacetyl-α-D-glucosyl bromide						
IX	5.7	−2.03	−1.82	+0.21		
X	28.1	+1.33	+1.60	+.27		
XI	25.2	+0.89	+1.09	+.20		
XII	5.0	−2.09	−2.01	−.08		
XIII	6.7	−1.39	−1.16	+.23		

[a] Determined as described on page 168.
[b] 0.000973 moles in a volume of 25 ml, read in a 4-dm tube.

In order to evaluate the contributions of the several constituents of the product to the equilibrium rotation, the measurements given in table 4 were made with the pure substances under conditions like those used in the study of the reaction products. To obtain the equilibrium rotation, a 0.000973-mole sample of the substance in a 25-ml volumetric flask was dissolved in 10 ml of methanol; 0.05 g of sodium acetate was added, and the mixture was evaporated to dryness. The material was then dissolved in chloroform, the volume was adjusted to 25 ml, and the optical rotation was measured in the manner described for obtaining the equilibrium rotation of the reaction product. The observed rotations of +3.20° S and +12.49° S for tetraacetylmannose and tetraacetylglucose, respectively, and of −4.32° S for triacetylmannose 1,2-(methyl orthoacetate) were used to calculate the contributions of these three substances to the equilibrium rotations of the reaction products. The values of +7.95° S and −7.84° S were used to calculate the proportions of the alpha and beta methyl tetraacetylmannosides from the residual rotations, as described on page 167. The values of +21.20° S and −3.03° S were used for similar calculations for the alpha and beta methyl tetraacetylglucosides. The specific rotations for the glycoside fractions of the products from experiments I and VII in the mannose series were calculated to be −56.3° and −60.7°, respectively. These are higher values in the levo direction than the specific rotation, −48.2° of the methyl tetraacetyl-β-D-mannopyranoside. However, repetition of the experiments gave results in substantial agreement with those reported. Since the rotations of the glycoside fractions are based on only 15 percent of the product and are obtained by difference, they are greatly affected by all errors of measurement.

Better agreement was found in the glucose series in which experiments IX, X, XI, and XII gave specific rotations of −17.9°, −18.6°, −18.5°, and −17.5°, respectively, for the glycosidic fractions in comparison with −18.6° for the specific rotation of methyl tetraacetyl-β-D-glucopyranoside.

(4) *Determination of the orthoester.*—Ten milliliters of the methanol solution of the reaction product was evaporated in a current of dry air in order to remove the alcohol. The residue was dissolved in the hydrogen chloride-chloroform reagent, and the volume was adjusted to 25 ml. The optical rotation was read in a 4-dm tube, 30 min after the addition of the reagent, and

recorded in table 3. It was mentioned earlier that the method was standardized for each measurement in the mannose series by a control experiment with pure triacetylmannose 1,2-(methyl orthoacetate). The change in optical rotation for the control applicable to each experiment is also given in table 3.

The effect of the addition of the HCl reagent on the optical rotations of tetraacetylmannose, tetraacetylglucose, and the alpha and beta methyl tetraacetylglycosides of mannose and glucose was measured in separate experiments, and the results are recorded in table 4. The addition of the HCl reagent did not cause an appreciable change in the rotations of the glycosides and of tetraacetylglucose. A small change was observed in the rotation of tetraacetylmannose; in the calculation of the amount of orthoester, allowance was made for the corresponding change in the rotation of the acetylmannose present in the product. In each case the correction amounted to $0.8°S \times \%$ of free acetylsugar/100. The changes in optical rotation for the product recorded in table 3 were corrected for this factor. The percentage of the orthoester in the product was obtained from the ratio of the corrected change and the change found for the pure substance.

TABLE 4. *Experimental data obtained with pure compounds*

Reference substance	Optical rotations[a]	
	After NaOAc treatment	After HCl-$CHCl_3$ treatment
	°S	°S
Tetraacetyl-D-mannose	+3.20	+4.02
Tetraacetyl-D-glucose	+12.49	+12.31
Methyl tetraacetyl-α-D-mannopyranoside	+7.95	+8.01
Methyl tetraacetyl-β-D-mannopyranoside	−7.84	−7.80
Methyl tetraacetyl-α-D-glucopyranoside	+21.20	+21.21
Methyl tetraacetyl-β-D-glucopyranoside	−3.03	−3.02
Triacetylmannose 1,2-(methyl orthoacetate)	−4.32	[b]+11.16
Triacetylmannose 1,2-(methyl orthoacetate)	−4.32	[b]+13.30

[a] A 0.000973-mole sample in a volume of 25 ml, read in a 4-dm tube at 20° C.

[b] The values were obtained with different preparations of the HCl-$CHCl_3$ reagent.

VI. Summary

A study has been made of the effect of solvent and temperature on the course of certain organic replacement reactions. It was formerly postulated [2, 3, 4] that the reaction of *trans* acetylglycosyl halides with compounds containing a free hydroxyl group (ROH) takes place both by an opposite-face intermolecular course and by an opposite-face intramolecular course involving a solvated orthoester intermediate. The former yields the glycoside with inversion, the latter an orthoester ion, which then stabilizes by one of two mechanisms to yield either the orthoester or the glycoside with apparent retention of configuration. In this paper it has been shown that if the orthoester ion is solvated, the course of the intramolecular reaction should be drastically affected by a solvent that is able to coordinate in the formation of the orthoester ion, but unable to eliminate a proton. On the other hand, if the orthoester intermediate exists as a free ion, such a solvent should act only as an inert diluent in the reaction. A quantitative study has been made of the reaction with methanol of tetraacetyl-α-D-glucosyl bromide (a *cis* halide), and tetraacetyl-α-D-mannosyl bromide (a *trans* halide) in the presence of silver carbonate (the Koenigs-Knorr reaction). At −15°, 20°, and 50° C, tetraacetyl-α-D-glucosyl bromide yielded almost exclusively methyl tetraacetyl-β-D-glucoside. At 20° C and below, tetraacetyl-α-D-mannosyl bromide yielded 78 percent of triacetylmannose 1,2-(methyl orthoacetate) and 15 percent of methyl tetraacetyl-β-D-mannoside. No methyl tetraacetyl-α-D-mannoside was formed, a result that indicates that conversion of the orthoester intermediate to the orthoester is the preferred course when methanol alone is present. In the presence of ether and small quantities of methanol, tetraacetyl-α-D-mannosyl bromide yielded 7.5 percent of the orthoester, 23 percent of the beta acetylglycoside and 34 percent of the alpha acetylglycoside. The effect of benzene on the proportion of the products was similar to that of ether but less pronounced, in accord with its smaller tendency to co-ordinate. These striking changes support the mechanism involving a solvated orthoester intermediate rather than a free ion.

When the temperature of the reaction was raised to 50° C, the amount of the orthoester dropped from 78 to 53 percent, and 8 percent of the alpha acetylmannoside was formed. This shift in the proportions of the products of the intramolecular reaction seems to indicate that the solvated orthoester ion is somewhat thermally unstable, and that part of the reaction at the higher

temperature takes place through the free orthoester intermediate. This would react to yield the orthoester and the alpha acetylglycoside in different proportions from the solvated ion. The reaction of tetraacetyl-α-D-glucosyl bromide was only slightly affected by a change of solvent or of temperature. This is compatible with the stereomeric inability of the alpha glucose configuration to form an orthoester intermediate.

The authors express their appreciation to Nancy B. Holt for her assistance in conducting the analytical work reported in this paper.

VII. References

[1] W. Koenigs and E. Knorr, Ber. deut. chem. Ges. **34,** 957 (1901).
[2] H. S. Isbell, Ann. Rev. Biochem. **9,** 65 (1940).
[3] H. L. Frush and H. S. Isbell, J. Research NBS **27,** 413 (1941) RP1429.
[4] H. L. Frush and H. S. Isbell, J. Research NBS **34,** 111 (1945) RP1663.
[5] S. Winstein and R. E. Buckles, J. Am. Chem. Soc. **64,** 2780, 2787 (1942).
[6] S. Winstein, C. Hanson, and E. Grunwald, J. Am. Chem. Soc. **70,** 812 (1948).
[7] D. D. Reynolds and W. L. Evans, J. Am. Chem. Soc. **60,** 2559 (1938).
[8] W. W. Pigman and H. S. Isbell, J. Research NBS **19,** 199 (1937) RP1021.
[9] J. L. Gleave, E. D. Hughes, and C. K. Ingold, J. Chem. Soc. **1935,** 236; E. D. Hughes, J. Chem. Soc. **1946,** 968.
[10] H. S. Isbell, BS J. Research **7,** 1115 (1931) RP392.
[11] F. Micheel and H. Micheel, Ber. deut. chem. Ges. **63,** 386 (1930); D. H. Brauns, BS J. Research **7,** 573 (1931) RP358.
[12] P. A. Levene and R. S. Tipson, J. Biol. Chem. **90,** 89 (1931).
[13] J. K. Dale, J. Am. Chem. Soc. **46,** 1046 (1924).
[14] H. S. Isbell and H. L. Frush, J. Research NBS **24,** 125 (1940) RP1274.
[15] F. J. Bates and associates, Polarimetry, saccharimetry and the sugars, NBS Circular C440 (1942).
[16] E. Fischer and K. Hess, Ber. deut. chem. Ges. **45,** 912 (1912).
[17] G. M. Kline and S. F. Acree, BS J. Research **5,** 1081 (1930) RP247.

WASHINGTON, May 12, 1949.

U. S. Department of Commerce
National Bureau of Standards

Research Paper RP2019
Volume 43, August 1949

Part of the Journal of Research of the National Bureau of Standards

Studies on the Flame Photometer for the Determination of Na_2O and K_2O in Portland Cement

By William R. Eubank and Robert H. Bogue

A study has been made on the Perkin-Elmer model 52–A flame photometer to establish its suitability for the determination of Na_2O and K_2O in portland cements and cement raw materials, such as argillaceous limestones and clays. An essential factor in the successful application of the method is the use of suitable standard solutions for each type of material analyzed. Such solutions were developed and excellent results obtained. This paper gives the photometric results due to numerous variables and presents a recommended procedure. On cements, the averages of the differences between the direct-intensity photometric and the gravimetric values obtained were 0.012 percent for Na_2O and 0.024 percent for K_2O. Slightly closer agreement was obtained with the internal-standard method, but uncertainties due to the possible presence of Li_2O give greater reliability to the direct-intensity method. The advantages of flame photometry, both in time and accuracy, are such as to warrant its recommendation for the purpose examined.

I. Introduction

Flame photometry is an analytical procedure by which a solution to be analyzed is atomized into a flame, and light, characteristic of the element to be determined, is isolated and its intensity measured. In the method of flame photometry, the principles of analytical spectroscopy are applied under conditions that allow rapid determinations to be made with relatively simple apparatus and with personnel having only moderate training.

This method of analysis was advanced several years ago in Europe by Lundegårdh [9],[1] Heyes [7], Schmitt [13], and others. However, it was not until recently that the method of flame photometry was simplified by Barnes and coworkers [2] and a commercial apparatus (Perkin-Elmer Corp., Model 18–A, direct intensity) placed on the market. In a study with this instrument, Parks, Johnson, and Lykken [10] noted a number of sources of error due both to characteristics of the apparatus and to the presence of interfering elements. Berry, Chappell, and Barnes [4] further improved the flame photometer by employing a dual optical system that allowed both the direct-intensity method, and the internal-standard principle, often used in spectrographic determinations, to be used. By the latter method, the emitted light-intensity ratios of the element sought and of another element introduced in known concentration are measured, rather than the absolute light intensities of the element sought, as is the case with the direct-intensity method. The disturbing effects caused by gas and air-pressure fluctuations, the presence of foreign ions and molecules, and viscosity differences are minimized by the internal-standard procedure. A commercial instrument (Perkin-Elmer Corp., Model 52–A) permitting the use of either method has recently been marketed. Pritchard [12] has compared the two models and voiced the need for further investigation to define a procedure adequate for the determination of Na_2O and K_2O in portland cements.

A study of both methods has been made in this laboratory with the Model 52–A instrument. The purpose of the present paper is to evaluate the results obtained in this study as applied to the determination of soda and potash in portland cement and to present a recommended procedure. The results indicate that the use of the flame photometer for this purpose provides analytical data comparable with those obtained by the best

[1] Figures in brackets indicate the literature references at the end of this paper.

gravimetric methods and has the additional advantage of much greater speed. It is believed that these findings will be generally useful and of benefit, especially to analysts in cement-producing and testing laboratories where the determination of the alkalies constitutes a major problem.

II. Development of the Method

1. Standard Solutions

In applying the flame photometer, it is necessary to provide standard solutions with known alkali concentration and with characteristics such that excitation conditions obtained in the flame are similar to those for the solutions to be analyzed. Such solutions constitute the basis of reference in each determination. It is a matter of common knowledge that the spectral emission of an element may be affected by the presence of other elements in the solution, as also by acidity, viscosity, etc. [4,10]. Thus a spectrographic interference with the measured intensity of the lines of sodium and potassium may be caused by calcium, which has a strong line (5857.46 A) close to the double sodium line (5895.92-5889.95 A) and a weaker line (7610.0 A) close to the potassium lines (7698.98 and 7664.91 A). The hydrochloric acid that is used to bring the cement into solution may likewise be a source of interference. Other weak lines of calcium, iron, and magnesium appear near the principal lines of the alkalies in an arc spectrum but, at the much lower temperature of the air-propane flame (as recommended for the flame photometer), no interference seems likely to occur.

It would appear that the ideal standard solution, from the point of view of balancing the interference from various elements, would be one composed of the same elements and in about the same concentrations as are found in the cement solutions to be analyzed. Such standard solutions could be approximated by the addition of definite amounts of NaCl and KCl to a solution of a cement of known (by gravimetric analysis) but low alkali content. Solutions were accordingly made [2] from a laboratory-prepared portland cement,[3] which contained (by gravimetric analysis) no potash and only a trace of soda. A tabulation of the gravimetric and photometric values for Na_2O and K_2O in a series of portland cements, using these solutions in conjunction with the internal-standard method, is shown in columns 2 and 5 of table 1.[4] Agreement between the values obtained by the two methods is seen (col. 8) to be excellent, the average of the differences on the basis of the original cements being 0.02 percent for Na_2O and 0.03 percent for K_2O.

It was recognized, however, that there are serious objections attached to the use of a cement for making up the standard solutions.

In the first place, cements containing less than 0.1 percent of both Na_2O and K_2O are not commonly available, and any error in the values of those oxides, assigned by gravimetric determina-

TABLE 1. *Comparison of gravimetric and flame-photometric values for Na_2O and K_2O on a series of portland cements, using the internal-standard procedure with standard solutions of different composition*

1	2	3	4	5	6	7	8
Cement No.	Gravimetric	Flame photometric with standard aqueous solutions of NaCl and KCl			Difference		
PCA 5-types series 308	Berkroller	No additions	CaO +HCl	Low-alkali cement +HCl	Column 3−2	Column 4−2	Column 5−2
	Percent of Na_2O						
15394	0.42	0.46	0.45	0.42	+0.04	+0.03	0
15396	.24	.27	.25	.20	+ .03	+ .01	− .04
15482	.29	.32	.32	.27	+ .03	+ .03	− .02
15559	.28	.32	.33	.26	+ .04	+ .05	− .02
15399	.39	.43	.40	.36	+ .04	+ .01	− .03
15591	.21	.19	.17	.15	− .02	− .04	− .06
15614	.10	.12	.13	.10	+ .02	+ .03	0
*43	1.04	[b]1.15	[b]1.10	1.05	+ .11	+ .06	+ .01
Averages	.....	.....	.....	.....	±0.04	±0.03	±0.02
	Percent of K_2O						
15394	0.74	0.59	0.66	0.67	−0.15	−0.08	−0.07
15396	1.03	.89	1.02	1.05	− .14	− .01	+ .02
15482	0.48	.43	0.43	0.44	− .05	− .05	− .04
15559	.49	.44	.46	.48	− .05	− .03	− .01
15399	.57	.55	.55	.57	− .02	− .02	0
15591	.14	.10	.10	.10	− .04	− .04	− .04
15614	.28	.20	.24	.22	− .08	− .04	− .06
*43	.08	.08	.09	.08	0	+ .01	0
Averages	.....	.....	.....	.....	±0.07	±0.035	±0.03

[a] No. 43 PCA Long-Time Series [8].
[b] Beyond range of standard solutions; approximated by dilution.

[2] See below for a detailed description of the methods of preparation of the solutions.
[3] PCAF cement K5-382, Lot No. 14646.
[4] Gravimetric determinations on cements reported in tables 1, 3, 4, and 5 were made in the laboratory of the Portland Cement Association, Chicago. Some of these data have been published [8].

tion, would be reflected in all photometric determinations subsequently obtained by their use. Furthermore, if Li_2O is present, it will introduce an error in the gravimetric value for Na_2O as commonly determined, because the value determined for Na_2O includes any Li_2O that is present.

The use, as standard solutions, of water solutions of NaCl and KCl was found, as anticipated, to give less reliable analytical results than those just reported. A number of such data, making use of the internal-standard procedure, are shown in table 1, where the gravimetric and photometric determinations are set down for a series of cements in columns 2 and 3 respectively, and compared in column 6.

A series of standard solutions was then prepared so as to contain calcium ion and hydrochloric acid in approximately the same concentration as would occur in the solutions of portland cement to be analyzed. These were composed of 6,000 ppm CaO (using low-alkali $CaCO_3$[5]) and 50 ml of HCl per liter, to which pure NaCl and KCl were added in such amounts as to give both Na_2O and K_2O concentrations in the solutions ranging from 10 to 100 ppm (equivalent to 0.10 to 1.00% of Na_2O and K_2O in 1-g samples of the cements). The above concentration of CaO (equivalent to 60% of CaO in the cements to be analyzed) is believed to be as satisfactory as any other concentration since, at these high concentrations, a variation of a few percent in the CaO content of the cements has no significant effect on the analytical results for Na_2O and K_2O. The analytical values on a series of portland cements obtained with the use of these standard solutions are given in column 4 of table 1, and compared with the gravimetric values in column 7. The agreement with the latter values is seen to be practically as good as that obtained with the use of standard solutions prepared from the low-alkali cement.

From the results discussed above it was concluded that:

The use of a lithia-free low-alkali cement in the preparation of the standard solutions gives photometric values for Na_2O and K_2O that are in somewhat closer agreement with results obtained by gravimetric analysis than does the use of CaO–HCl standard solutions.

[5] The calcium carbonate should meet the specifications for the ACS low-alkali $CaCO_3$, which carries a limit of 0.020% of total alkalies as sulfate. The purchaser should assure himself that the material used meets the specification.

The general unavailability of accurately analyzed lithia-free low-alkali cements makes the use of commercial cements for the preparation of standard solutions of questionable merit.

The excellent agreement between values for Na_2O and K_2O obtained by gravimetric analysis, and values obtained with the flame photometer making use of CaO–HCl standard solutions, warrant the recommendation of such solutions as standards in the flame photometric determination of Na_2O and K_2O in portland cement.

2. Concentration of Internal Standard

The concentration of Li_2O as nitrate as the internal standard used in the above tests was 100 ppm, in accordance with the recommendation of the manufacturer [11]. A series of determinations was made to note if changes in the concentration level of this material, maintained identical of course in the standard and the unknown solutions, had any effect on the photometric results obtained for Na_2O and K_2O.[6] The standard solutions were prepared with the use of the low-alkali cement. The determinations were made by both procedures with lithia added to the standard solutions. The results are shown in table 2, where the concentration of Li_2O as nitrate varied between 50 and 200 ppm. No significant effects on the analytical values for either Na_2O or K_2O were observed due to this variation in the concentration of the lithia. As a result of this series of tests, it was concluded that the concentration of 100 ppm Li_2O as nitrate would be satisfactory.

3. Viscosity of Solutions

Since the light intensity emitted is a function of the amount of liquid projected into the flame at any moment, and the latter is a function of the viscosity of the solution, it was felt necessary to compare the viscosities of the solutions employed as standards with those of the cements to be analyzed. The time of flow was accordingly measured for 5 ml of such solutions through an Ostwald viscosimeter in a constant-temperature bath at 29° C. The solution of low-alkali cement required 163.2 sec; the CaO–HCl solution, containing 100 ppm each of Na_2O and K_2O as chlorides and Li_2O as nitrate, required 161.7 sec. As

[6] In the "Long-Time Series" [8] of portland cements examined in this study, the lithium content (as Li_2O) had been shown spectroscopically to be less than 0.05% [6].

843576—49——6

TABLE 2. *Effect of varying concentration of Li_2O (as nitrate), used as internal standard, on Na_2O and K_2O determined. Low-alkali cement used in preparation of standard solutions*

Cement No.	Gravimetric	Internal standard			Direct intensity		
Long-time series [8]	ASTM	Concentration of Li_2O			Concentration of Li_2O		
		50 ppm	100 ppm	200 ppm	50 ppm	100 ppm	200 ppm
	Percent of Na_2O						
11	0.21	0.21	0.21	0.21	0.22	0.23	0.22
23	.59	.60	.62	.63	.63	.57	.63
31	.23	.24	.23	.24	.26	.22	.26
43A	.33	.38	.33	.39	.39	.34	.37
51	.08	.08	.07	.07	.07	.07	.08
	Percent of K_2O						
11	0.51	0.49	0.57	0.50	0.54	0.52	0.54
23	.14	.13	.15	.12	.12	.13	.12
31	.22	.22	.26	.21	.23	.25	.23
43A	.01	.01	.02	.01	.01	.02	.01
51	.22	.27	.27	.25	.25	.26	.24

a basis of reference, distilled water was found to require 155.4 sec. The viscosity difference between the CaO–HCl solution and the cement solution appears to be so small as to be insignificant.

4. Flame Characteristics

It is essential that the gas employed for producing the flame in the photometer be of constant composition and pressure and free of materials that may cause interferences in the spectral emission. It is also desirable that the flame temperature be such that the alkali elements will be readily excited, whereas other elements that require higher temperatures for excitation will not be excited. Complete separation cannot be made of the alkali elements from the alkaline-earth elements present by such control of temperature as is possible with a selection of the gas, but some advantage can be expected from a judicious selection. Excitation of the other metallic elements can be almost entirely avoided [2].

Gas from the city mains was tried with the earlier (model 18) instrument but was found to give rise to a variable flame and erratic analytical results. The pressure also was inadequate for best performance in the burner. Of the gases commonly available in steel cylinders (bottled gas), acetylene and propane (under various trade names) have been used by various investigators. The flame temperature of acetylene burning in air is much higher than that of propane [14] and results in greater excitation of the nonalkali elements [2]. Propane appears to be nearly ideal for the purpose of exciting the alkali elements with a minimum of interference from other causes, and was employed in these studies.

III. Analytical Results

1. Precision of Flame-Photometric Method

A group of five cements was subjected to repeated analysis for Na_2O and K_2O by use of the

TABLE 3 *Flame-photometric values for Na_2O and K_2O in portland cements obtained by two operators over a period of several weeks, and employing varying concentrations of internal standard, to indicate reproducibility of the analytical results under average laboratory conditions*

Internal-standard procedure with low-alkali cement standard

Cement No.	Na_2O		K_2O	
Long-time series [8]	Value determined	Standard deviation	Value determined	Standard deviation
	%		%	
11	0.21, .21, .20, .21, .22, .22	0.007	0.50, .48, .49, .50, .54, .54	0.023
23	.62, .61, .59, .63, .63, .63	.015	.15, .12, .13, .12, .12, .12	.011
31	.23, .25, .23, .24, .26, .26	.013	.22, .22, .22, .21, .23, .23	.007
43A	.34, .38, .38, .39, .37, .39	.017	.01, .01, .01, .01, .01, .01	.000
51	.07, .08, .08, .07, .08, .07	.005	.26, .27, .27, .25, .24, .25	.011
Average	.....	0.012	.....	0.013

flame photometer over a period of several weeks, using the internal-standard procedure with the low-alkali-cement standard solutions. These tests represent the accumulated analytical values on these cements obtained by two operators using various concentrations of Li_2O as an internal standard. The data are set down in table 3 as an indication of the reproducibility of the photometric values even under conditions far from ideal. The standard deviation is seen to vary from 0.005 to 0.017 for Na_2O and from 0.000 to 0.023 for K_2O. The maximum spread for any cement was 0.05 percent for Na_2O and 0.06 percent for K_2O, based on the original sample.

A comparable series for study of the reproducibility of the alkali values by gravimetric methods is not known to be available, but it is believed that the photometric values given will compare favorably with any similar series of gravimetric determinations.

2. Reproducibility by Different Operators

The flame-photometric results on a series of cements obtained by three operators using two different units of the model 52–A instrument are shown in table 4. The agreement between operators (col. 10) is generally satisfactory, the average maximum variation from operator to operator being 0.03 percent for Na_2O and 0.04 percent for K_2O. The average of the differences between the values obtained by the photometric and the ASTM chemical method (col. 9) is only 0.02 percent for Na_2O and 0.01 percent for K_2O.

These results indicate that the personal factor in operating the flame photometer is small and that a high degree of training for an operator is not necessary. Operators *b* and *c* had less than 2 days previous experience with the instrument when the determinations were made.

3. Comparison of Photometric and Gravimetric Methods

There are also shown in table 4 gravimetric values on these cements by two different methods, the ASTM standard [1] and the modified Berk-Roller [3]. These two methods are given because the former is usually conceded to be more accurate, whereas the latter is more rapid. It will be noted

TABLE 4. *Analytical values for* Na_2O *and* K_2O *obtained by two gravimetric methods and by three operators using the flame photometer direct-intensity method,* CaO–HCl *standard*

1	2	3	4	5	6	7	8	9	10	11
Cement No.	Gravimetric			Flame photometer					Comparisons	
Long time series [8]	ASTM	Berk-Roller	Difference 3−2	Operator *			Avg. a, b, c	Difference 8−2	Maximum variation between a, b, and c	Maximum variation between 2 and a, b or c
				a	b	c				
Percent of Na_2O										
11	0.21	0.24	+0.03	0.21	0.22	0.18	0.20	−0.01	0.04	0.03
23	.59	.66	+.07	.62	.63	.65	.63	+.04	.03	.06
31	.23	.28	+.05	.24	.26	.23	.24	+.01	.03	.03
43A	.33	.38	+.05	.34	.38	.36	.36	+.03	.04	.05
51	.08	.08	0	.08	.08	.05	.07	−.01	.03	.03
Averages	.....	.....	+0.04	.....	.....	.....	.....	±0.02	0.03	0.04
Percent of K_2O										
11	0.51	0.59	+0.08	0.56	0.54	0.50	0.53	+0.02	0.06	0.05
23	.14	.15	+.01	.15	.12	.09	.12	−.02	.06	.05
31	.22	.26	+.04	.25	.23	.19	.22	0	.06	.03
43A	.01	.04	+.03	.02	.01	.01	.01	0	.01	.01
51	.22	.27	+.05	.26	.24	.23	.24	+0.02	.03	.04
Averages	.....	.....	+0.04	.....	.....	.....	.....	±0.01	0.04	0.04

* Operators a and b used the same instrument; operator c, a different instrument.

that the average of the differences obtained by the two gravimetric methods (col. 4) is 0.04 percent for both Na_2O and K_2O, with maximum individual differences of 0.07 percent for Na_2O and 0.08 percent for K_2O. The more rapid Berk-Roller method gives values for both Na_2O and K_2O that are consistently somewhat higher than those obtained by the ASTM method. The photometric results also agree closely with the gravimetric results and in general conform best with those obtained by the ASTM procedure. The average differences between the gravimetric and photometric values (col. 11) are 0.04 percent for both Na_2O and K_2O. It may here be noted that the gravimetric values, though serving as the basis of reference, cannot be considered as necessarily accurate. The outstanding advantage of the photometric procedure over either gravimetric method is found to lie in the greatly shortened time required for the determination.

4. Comparison of Direct-Intensity and Internal Standard Procedures

Values for Na_2O and K_2O obtained on 10 cements by both the internal-standard and direct-intensity procedures are given in table 5. The standard solutions for the former were prepared from the low-alkali cement and for the latter from the CaO–HCl solution. For comparison, gravimetric determinations by the ASTM standard method [1] are also included. Averages of the differences between the values thus obtained are given at the bottom of the table.

The average of the differences between the flame-photometric determinations using the internal standard and the ASTM gravimetric values (col. 5) is only 0.009 percent for Na_2O and 0.016 percent for K_2O. Using the direct-intensity procedure, the average of the differences (col. 6) is slightly greater, being 0.012 percent for Na_2O and 0.024 percent for K_2O. The average of the differences between the internal-standard and direct-intensity results (col. 7) is 0.005 percent for Na_2O and 0.012 percent for K_2O. Values obtained for Na_2O with the flame photometer by both procedures are in somewhat better agreement with gravimetric values than those for K_2O. In either case, the flame-photometric results compare favorably with the gravimetric values.

From these data, as also those shown in table 2, the results obtained by the internal-standard procedure are seen to be in slightly better agreement with the ASTM values than those obtained by the direct-intensity method. This difference is small and usually insignificant.

There is, however, an important reason for considering the direct-intensity method to be the more reliable for portland cements and cement raw materials. The internal-standard procedure involves the introduction to the standard and the unknown solutions of a fixed amount of some element by means of which intensity ratios of the alkali elements to the standard are measured. The characteristics of this element are severely restricted; it must be readily excited in the photometer flame, it must not emit spectral lines that would interfere with those of sodium and potassium, and it must not be a constituent of the cements used as stand-

TABLE 5. *Comparison of analytical results obtained by the internal-standard procedure, using low-alkali cement standard solutions, and by the direct-intensity procedure, using* CaO–HCl *Standard solutions*

1	2	3	4	5	6	7
Cement No.	Gravimetric	Flame photometer		Comparisons		
Long-time series [8]	ASTM	Internal standard	Direct intensity	3−2	4−2	4−3
			Percent of Na_2O			
11	0.21	0.21	0.21	0	0	0
13	.04	.05	.05	+0.01	+0.01	0
18	.12	.13	.13	+.01	+.01	0
23	.59	.62	.62	+.03	+.03	0
25	.21	.21	.22	0	+.01	+0.01
31	.23	.23	.24	0	+.01	+.01
34	.28	.28	.29	0	+.01	+.01
42	.16	.13	.13	−0.03	−.03	0
43A	.33	.33	.34	0	+.01	+.01
51	.08	.07	.08	−.01	0	+.01
Averages	.....	.....	.....	±0.009	±0.012	±0.005
			Percent of K_2O			
11	0.51	0.50	0.56	−0.01	+0.05	+0.06
13	.19	.19	.19	0	0	0
18	.13	.15	.14	+.02	+0.01	−.01
23	.14	.15	.15	+.01	+.01	0
25	.54	.56	.58	+.02	+.04	+0.02
31	.22	.22	.25	0	+.03	+.03
34	.28	.30	.30	+0.02	+.02	0
42	.26	.30	.30	+.04	+.04	0
43A	.01	.01	.01	0	0	0
51	.22	.26	.26	+.04	+.04	0
Averages	.....	.....	.....	±0.016	±0.024	±0.012

ards or to be analyzed. The only element thus far found partially to meet these requirements is lithium [4], but unfortunately lithium is present in some raw materials that may be used in cement manufacture. Since, in the internal-standard procedure, the measured ratio between the intensity of the lithium (added in a fixed concentration) and of the sodium and potassium (being determined) is the basis for the establishment of the concentration of the latter elements, it is obvious that the concentration of the lithium must be identical in the standard and the unknown solutions. And since the cements being tested may contain lithia in small but unknown concentration, the measurement of the above ratio will not, when lithia is present in the cements being tested, correctly indicate the Na_2O and K_2O concentrations. Because of this uncertainty, the internal-standard method is not recommended for the flame-photometric determination of the alkalies in portland cement or cement raw materials, and only the direct-intensity method will be included in the procedure outlined below.

IV. Application to Raw Materials

The principal differences between the flame-photometric analysis of a portland cement and of a raw material, such as a clay, are concerned with the increased difficulty of getting the latter into solution and of making a proper selection of materials to be used in preparing the standard solutions.

A flint clay, a plastic clay, and an argillaceous limestone were selected for photometric analysis. These were NBS standard samples for which complete gravimetric analyses were available. It should be pointed out, however, that cement raw materials vary considerably from location to location, and probably no individual material can be considered as representative of a type. Some modifications of the procedure followed here may be necessary for other materials.

An attempt was made to dissolve these materials by the Glaze method [5] using nitric, perchloric, and hydrofluoric acids. By this method, the minerals of the argillaceous limestone were completely dissolved, and the graphite and organic matter were burned off during ignition of the solid perchlorates. This procedure failed, however, to decompose the clays. The latter were accordingly subjected to sintering with NH_4Cl and $CaCO_3$ (J. Lawrence Smith procedure [1]), extracted several times with boiling distilled water and filtered. By this means the alkalies in these clays were brought into solution.

The standard solutions required for a particular type of raw material will depend on the chemicals employed to dissolve the material and the concentration range of the alkalies. Sometimes the resulting solution contains only water and the alkalies; in other cases interfering substances, such as CaO, may also be present. In case only sodium and potassium are in solution, standard solutions of the alkalies in water may be prepared of several concentrations up to the maximum amounts of the alkalies expected in the raw material. An alternative procedure in samples of high-alkali content (more than 1%), is to dilute the sample to the concentration range of the usual standard solutions (0 to 100 ppm).

When interfering substances occur in appreciable amounts in solution with the alkalies, it may be necessary to compensate for them in the standard solutions. This will depend on the accuracy required. As mentioned earlier, CaO and HCl have been found to constitute the chief interferences in these studies. In many cases it may be easier to treat the sample with HCl before filtering, and then add the amount of CaO occurring in the raw material, plus HCl, to the standard solution.

The data from a flame-photometric analysis of these materials for Na_2O and K_2O by the direct-intensity method using CaO-HCl standard solutions are given in table 6. Values obtained for the argillaceous limestone, which was the easiest to put in solution, checked closely, within 0.01 percent for both Na_2O and K_2O, with the average gravimetric determinations. Soda determina-

TABLE 6. *Gravimetric and flame-photometric determinations of Na_2O and K_2O in cement raw materials*

Gravimetric values as reported in certificates of National Bureau of Standards. Flame-photometric direct-intensity method; CaO–HCl standards

	Flint Clay NBS Std. 97		Plastic Clay NBS Std. 98		Argillaceous Limestone NBS Std. 1A	
	Na_2O	K_2O	Na_2O	K_2O	Na_2O	K_2O
Average value on certificate (a)	0.12	0.54	0.28	3.17	0.39	0.71
Flame-photometric value (b)	.10	.47	.25	3.04	.40	.70
(b)−(a)	−.02	−.07	−.03	−0.13	+.01	−.01

tions for both clays also checked closely with the gravimetric results, but the potash values showed, on the basis of the original sample, greater variation from the gravimetric results. This is seen to be related to the larger concentration of potassium present, and the percentage variations are not excessive. These results demonstrate the successful application of the flame-photometric method to the determination of Na_2O and K_2O in cement raw materials.

V. Recommended Procedure for the Determination of Na_2O and K_2O in Portland Cement

In employing flame photometry for the determination of the alkalies in cement, the instrument must first be calibrated with solutions of known concentration. It is convenient to prepare stock solutions of relatively high concentration in amounts sufficient to last for 3 or 4 weeks, and from these to prepare the standard solutions as required. These solutions should be stored in acid-resistant glass containers, such as Pyrex.

1. Stock Solutions

A lime-acid stock solution is prepared to contain 63,000 ppm (6.3 %) of CaO and 500 ml of HCl per liter:

Add 300 ml of water to 112.5 g of $CaCO_3$ (see footnote 5) in a 1,500 ml beaker. While stirring, slowly add 500 ml of HCl. Cool to room temperature, transfer to a 1-liter volumetric flask, dilute to 1 liter and mix thoroughly.

A second stock solution is required containing 1,000 ppm (0.1 %) of Na_2O and K_2O, both soda and potash being included in the same solution:

Dissolve 1.8858 g of NaCl and 1.5830 g of KCl (previously dried at 105° to 110° C for several hours) in water, dilute to 1 liter in a volumetric flask and mix thoroughly.

2. Standard Solutions

Standard solutions are required, for the calibration of the apparatus, which contain known amounts of the alkali oxides together with a concentration of CaO and acid approximating that which will be present in the unknown cement solutions. These are prepared by the proper dilution of portions of the stock solutions. Since 1 g of the cement to be analyzed is dissolved and made up to 100 ml of solution, a K_2O concentration in the cement of 1 percent would be equivalent in the solution to 100 ppm. And since very few cements contain more than 1 percent of either Na_2O or K_2O, the usual upper concentration of the alkali oxides in the standard solutions can be fixed at 100 ppm. In the few instances where higher concentrations are encountered, the upper concentration in the standard solutions can be raised as far as necessary, or the solution being analyzed can be further diluted.

In general, the range of 0 to 100 ppm of Na_2O and K_2O in the standard solutions will cover adequately the range of alkali concentrations (0 to 1%) in cements. Although higher sensitivity could be obtained by narrowing the alkali limits in the standard solutions (as between 25 and 75 ppm where the cements contain not less than 0.25 nor more than 0.75% of either alkali oxide), such dilution is not recommended. The likelihood of contamination and consequent erratic results would thereby be greatly increased.

The standard solutions recommended are as follows:

Alkali (as oxide)	Lime-acid solution	NaCl-KCl solution	Volume of final solution
ppm	*ml*	*ml*	*ml*
100	200	200	2, 000
75	100	75	1, 000
50	100	50	1, 000
25	100	25	1, 000
10	100	10	1, 000
0	100	0	1, 000
100	0	100	1, 000

The lime-free solution is for use only in establishing the correct position of the wavelength selector for maximum response to Na_2O and K_2O. Each alkali solution is measured out, as indicated above, in calibrated pipettes or burettes, but the lime-acid solution may be measured in a graduated cylinder.

3. Calibration of the Instrument

With the electric current turned on, the air pressure is adjusted to about 10 psi, the gas pressure to about 5 psi, and the burner lighted. The chimney should be adjusted with its bottom edge

about ⅛ to ¼ in. below the top of the burner. The gas and air pressures are further adjusted to give a flame 5 to 6 in. high and having uniform, quiet, greenish-blue cones over the grid of the burner. Under humid conditions, moisture condensation may be prevented by leaving the electrical circuit on continuously. The burner should be on for a half hour before commencing a run.

The internal-standard dial should be set and caused to remain at zero.

The correct position of the wavelength dial is established by pouring lime-free standard solution into the atomizer and moving the selector back and forth on each side of the indicated wavelength for the element until the point of maximum deflection of the meter is obtained. During this operation, the meter is caused to reach the range 90 to 100 by means of the coarse and fine gain controls.

The atomizer should be rinsed with each solution prior to taking readings on that solution.

The 100 ppm alkali lime-containing solution is then poured into the atomizer, and the coarse and fine gain controls adjusted until the meter reads 100. With the alkali-free solution in the atomizer, the zero-adjustment knob is turned until the meter reads zero. These steps should be repeated until the meter needle returns to 100 and 0, respectively, on going from one solution to the other.

The 75-ppm solution is then poured into the atomizer and the meter reading noted. Again the 0 and 100 ppm solutions are tested and the process repeated until consistent results are obtained. The meter reading for the 75-ppm solution is then recorded and the operation repeated with the other standard solutions.

The final recordings for the meter readings of all standard solutions are then plotted on cross-section paper, noting that 10-ppm standard solution represents 0.1 percent of Na_2O or K_2O in the cement solutions, 100 ppm represents 1.0 percent, etc.

4. Determination of Na_2O and K_2O

When the instrument has been checked against the standard solutions and the calibration curves drawn, the balance of the procedure for the determination of Na_2O and K_2O concentrations in the cements consists in placing the cements in solution and comparing meter readings obtained upon such solutions with the calibration curves.

1 g of cement is placed in a 150- to 250-ml beaker and dispersed with 10 to 25 ml of water. 5 ml of HCl is added all at once and diluted immediately with 50 ml of water. Any lumps are broken up with a flat-end stirring rod. After digesting for 15 min on a steam bath or hot plate, the solution is filtered into a calibrated 100-ml volumetric flask. The beaker and paper are washed thoroughly with water, the solution cooled and diluted to 100 ml, and this solution mixed thoroughly.

The apparatus is warmed up and adjusted, and the wavelength selector properly placed as in the procedure for calibration. The 100-ppm and alkali-free standard solutions are used for the proper setting of the meter by means of the coarse and fine gain controls, and of the zero-adjustment knob, as previously described.

The cement solution is then poured into the atomizer and the reading noted. The standard solution nearest this reading is then used and its reading noted. If the standard deviates more than one scale division from its former value, the original reading is reestablished by use of the fine gain control. These readings of unknown and nearest standard are repeated until consistent. The reading of the cement solution is then recorded and the Na_2O or K_2O concentration read from the appropriate calibration curve.

Each oxide should be reported to the nearest 0.01 percent. Where the combined oxides expressed as Na_2O are required, the Na_2O equivalent of the K_2O is obtained by multiplying the percentage of K_2O by 0.658, recording to nearest 0.01 percent, and adding to the Na_2O as determined.

VI. References

[1] ASTM (C 114–47) Section 22, Standard procedure; Section 46, Alternate procedure.

[2] R. B. Barnes, D. Richardson, J. W. Berry, and R. L. Hood, Ind. Eng. Chem. Anal. Ed. **17,** 605 (1945).

[3] A. A. Berk and P. S. Roller, Concrete (March 1935).

[4] J. W. Berry, D. G. Chappell, and R. B. Barnes, Ind. Eng. Chem. Anal. Ed. **18,** 19 (1946).

[5] F. W. Glaze, Rock Products (July 1941).

[6] A. W. Helz, J. Research NBS **34,** 129 (1945) RP1633; A. W. Helz and B. F. Scribner, J. Research NBS **38,** 439 (1947) RP1786.

[7] J. Heyes, Z. Angew Chem. **50,** 871 (1937).
[8] W. Lerch and C. L. Ford, J. Am. Concrete Inst. **19,** 745 (1948).
[9] H. Lundegårdh, Die quantitative specktralanalyse der elemente, Jena, Gustav Fischer, Part I, 1929, Part II, 1934.
[10] T. D. Parks, H. O. Johnson, and L. Lykken, Anal. Chem. **20,** 822 (1948).
[11] Perkin-Elmer Corp., Instruction Manual, Model 52–A Flame Photometer (Glenbrook, Conn., 1948).
[12] L. R. Pritchard, Pit and Quarry **41,** No. 1, 83 (1948).
[13] L. Schmitt and W. Breitweiser, Bodenkunde u. Pflanzenernahr **9–10,** 750 to 757 (1938).
[14] L. Shnidman, Gaseous Fuels, p. 34 and 129 (1948).

WASHINGTON, January 15, 1949.

U. S. GOVERNMENT PRINTING OFFICE: 1949